Evaluation of spasticity in experimental models of ischemic stroke

Inaugural Dissertation

zur

Erlangung des Doktorgrades
Dr. nat. med.

der Medizinischen Fakultät
und
der Mathematisch-Naturwissenschaftlichen Fakultät
der Universität zu Köln

vorgelegt von

Frederique Pascal Wieters

aus Bamberg

Meine Diplomarbeit drucken

2021

Evaluation of spasticity in experimental models of ischemic stroke

Inaugural Dissertation

zur

Erlangung des Doktorgrades
Dr. nat. med.

der Medizinischen Fakultät
und
der Mathematisch-Naturwissenschaftlichen Fakultät
der Universität zu Köln

vorgelegt von

Frederique Pascal Wieters

aus Bamberg

Meine Diplomarbeit drucken

2021

Betreuer:	Dr. rer. nat. Markus Aswendt
Referenten:	Prof. Dr. rer. nat. Ansgar Büschges
	Prof. Dr. rer. nat. Holger Grüll

Datum der mündlichen Prüfung: 06.10.2021

Contents

1 List of Publications **8**

2 Zusammenfassung **9**

3 Abstract **10**

4 Introduction **11**

4.1 Stroke . . . 11

4.1.1 Pathophysiology . . . 11

4.1.2 Neuro- and maladaptive plasticity . . . 13

4.2 Stroke and spasticity models in mice . . . 14

4.2.1 Photothrombosis . . . 16

4.2.2 White matter stroke . . . 16

4.2.3 Animal models of spasticity . . . 17

4.3 Motor Neuron Syndrome . . . 20

4.3.1 What is spasticity? . . . 20

4.3.2 Post-stroke spasticity . . . 21

4.3.3 Neural circuits of spasticity . . . 23

4.3.4 Clinical diagnosis and therapy of spasticity . . . 27

4.3.5 Hoffmann-reflex . . . 29

4.4 Aims of this thesis . . . 30

5 Material & Methods **31**

5.1 Consumables and materials . . . 31

5.2 Animal experiments . . . 34

5.2.1 Anesthesia and Analgesia . . . 35

5.2.2 Photothrombosis . . . 35

5.2.3 Internal capsule stroke . . . 37

5.2.4 Intracerebral injection . . . 38

5.2.5 Transcardial perfusion fixation . . . 39

5.3 Sensomotoric behavior tests . . . 39

5.3.1 Rotating beam . . . 40

5.3.2 Grid walk . . . 41

5.3.3 Cylinder test . . . 41
5.3.4 Grip strength . . . 42
5.4 Electrophysiology . . . 42
5.4.1 Transcutaneous electrophysiological measurement . . . 42
5.4.2 Direct nerve H-wave measurement . . . 43
5.4.3 Electrophysiological evaluation of spasticity . . . 44
5.5 Histology . . . 45
5.5.1 Tissue freezing and sectioning . . . 45
5.5.2 Immunohistochemistry . . . 45
5.5.3 Histochemistry . . . 45
5.5.4 Data evaluation . . . 46

6 Results **48**
6.1 Establishment of an electrophysiological method to measure post-stroke spasticity . . . 48
6.1.1 H-wave measurement improvement . . . 48
6.1.2 Validation of electrophysiological measurements . . . 50
6.2 Electrophysiological changes during post-stroke spasticity . . . 51
6.3 Behavioral changes after cortical and subcortical stroke . . . 61
6.3.1 Strokes in MOp and MOs show analogous sensorimotor changes . . . 61
6.3.2 Strokes within the internal capsule result in severe impairment of sensorimotor properties . . . 65
6.3.3 Comparison of test sensitivity for motor deficits . . . 67
6.3.4 Correlation between behavior and electrophysiology . . . 67
6.4 Structural changes after cortical and internal capsule stroke . . . 70

7 Discussion **82**
7.1 Mouse models of post-stroke spasticity . . . 82
7.1.1 Lesion location dependent post-stroke spasticity . . . 84
7.1.2 Electrophysiological validation of spasticity . . . 85
7.1.3 Evaluation of post-stroke spasticity . . . 86
7.2 Behavioral changes after cortical and internal capsule stroke . . . 88
7.2.1 Correlation of electrophysiological and behavioral changes during PSS 88
7.2.2 Limitations of PSS induction and evaluation . . . 89
7.3 Neural circuits of spasticity . . . 90
7.4 Pathophysiological changes after stroke . . . 92

8 Outlook **94**

9 Summary of projects and publications **96**

9.1 Published projects 96

9.1.1 Structural integrity and remodeling underlying functional recovery after stroke 96

9.1.2 A teaching tool about the fickle p value and other statistical principles based on real-life data 97

9.1.3 Introduction into spasticity and related mouse models 98

9.1.4 Graph theoretical quantification of white matter reorganization after cortical stroke in mice 99

9.1.5 Lesion Size- and Location-Dependent Recruitment of Contralesional Thalamus and Motor Cortex Facilitates Recovery after Stroke in Mice 100

9.1.6 Atlas-based imaging data analysis tool for quantitative mouse brain histology (AIDAhisto) 101

9.1.7 Processing Pipeline for Atlas-Based Imaging Data Analysis of Structural and Functional Mouse Brain MRI (AIDAmri) 102

9.1.8 Cloud-based relational database for multimodal animal data 103

9.2 Projects and publications in progress 104

9.2.1 Terminal Hoffmann-Reflex Measurement after Stroke in Mice 104

9.2.2 Longitudinal measurement of spasticity after cortical and subcortical stroke in mice 105

9.2.3 Long-term pathology and behavioral deficit after thrombin stroke in mice 106

9.2.4 Passive extending forces in mouse hip, knee, and ankle affect half of their joint angular ranges used in walking 107

9.2.5 Reactive astrocytes prevent maladaptive plasticity and facilitate recovery after ischemic stroke 108

9.2.6 The gut microbiota is required for physiological brain network connectivity 109

10 Supplemental figures **110**

11 Abbrevations **114**

12 Acknowledgement **117**

13 Erklärung **148**

1 List of Publications

1. Alawbathani S., Batool M., Fleckhaus J., Hamad S., Hassenrück F., Hou Y., Li X., Salmanton-Garcia J., Ullah S., **Wieters F.**, Michel M.C., "A teaching tool about the fickle p value and other statistical principles based on real-life data", *Naunyn-Schmiedeberg´s Archives of Pharmacology* (2021)

2. **Wieters F.** & Aswendt M. "Structural integrity and remodeling underlying functional recovery after stroke", *Neural Regeneration Research* (2020)

3. **Wieters F.**, Weiss Lucas C., Gruhn M., Büschges A., Fink G.R., Aswendt M., "Introduction into spasticity and related mouse models", *Exp. Neurology* (2020)

4. Pallast N., **Wieters F.**, Nill M., Fink G.R., Aswendt M. "Graph theoretical quantification of white matter reorganization after cortical stroke in mice", *Neuroimage* (2020)

5. Aswendt M., Pallast N., **Wieters F.**, Baues M., Hoehn M., Fink G.R., "Lesion Size- and Location-Dependent Recruitment of Contralesional Thalamus and Motor Cortex Facilitates Recovery after Stroke in Mice", *Translational Stroke Research* (2020)

6. Pallast N., **Wieters F.**, Fink G.R., Aswendt M., "Atlas-based imaging data analysis tool for quantitative mouse brain histology (AIDAhisto)", *Journal of Neuroscience Methods* (2019)

7. Pallast N., Diedenhofen M., Blaschke S., **Wieters F.**, Wiedermann D., Hoehn M., Fink G.R., Aswendt M., "Processing Pipeline for Atlas-Based Imaging Data Analysis of Structural and Functional Mouse Brain MRI (AIDAmri)", *Frontiers in Neuroinformatics* (2019)

8. Pallast N., **Wieters F.**, Nill M., Fink G.R., Aswendt M., "Cloud-based relational database for multimodal animal data", *The Journal of Biological Database and Curation* (2018)

9. Müller J., Greiner F.W.J., Zeuner M., Brotzmann V., Schafermann J. **Wieters F.**, Widera D., Sudhoff H.H., Kaltschmidt B., Kaltschmidt C., "1,8-Cineole potentiates IRF3-mediated antiviral response in human stem cells and in an ex vivo model of rhinosinusitis", *Clinical Science* (2016)

2 Zusammenfassung

Schlaganfälle sind eine der häufigsten Ursachen für lebenslange körperliche Beeinträchtigungen, wobei 35% der Patienten unter einer Post-Schlaganfall-Spastik (PSS) leiden. Im Gegensatz zur langen und erfolgreichen Geschichte des experimentellen Schlaganfalls sind die Nagetiermodelle der PSS unzureichend charakterisiert. Motiviert durch diese Wissenslücke, konzentriert sich diese Arbeit auf die Entwicklung eines PSS-Mausmodells und die Langzeiteffekte nach Schlaganfällen im primär-motorischen Areal (MOp), sekundärmotorischen Areal (MOs) und der Capsula interna.

Zur longitudinalen Bestimmung des PSS wurden Verhaltenstests und elektrophysiologische Messungen des Hoffmann-Reflex durchgeführt, wozu neben einer repetitiven subkutanen H-Wellen Messung eine neuartige Methode etabliert wurde, um die H-Welle direkt am Nerven zu messen. Zur quantitativen Bestimmung des PSS wurde das Verhältnis von H- und M-Welle, sowie die frequenzabhängige Depression gemessen.

Dabei zeigte sich, dass eine Läsion innerhalb des MOp zwar zu motorischen Defiziten führt, aber kein PSS ausgelöst wird, während eine Läsion innerhalb des MOs bzw. der Capsula interna nach 56 Tagen in einer milden bzw. starken PSS resultiert. In dem hier erstmals in der Maus gezeigten PSS-Modell konnte ein Beginn von PSS bereits nach 14 Tagen elektrophysiologisch nachgewiesen werden. Der sensomotorische Defizit-Score korrelierte dabei mit der PSS-Messung, d.h. Tiere mit einer PSS wiesen eine geringere spontane Verbesserung des motorischen Defizits. Es konnte gezeigt werden, dass neben dem Grid Walk auch der Zylinder Test Methoden sind, die noch 56 Tage nach einer Läsion ein motorisches Defizit nachweisen und sensitiv für die bei PSS auftretenden motorischen Defizite sind. Zusätzlich zu den elektrophysiolgischen und sensomotorischen Veränderungen wurden auch strukturelle Veränderungen analysiert, was neben der Läsionsbeschreibung auch die Untersuchung der sekundären Neurodegeneration einschloss. Innerhalb von 28 Tage nach Läsion im MOp konnten Mikroglia/Makrophagen vor allem in der ipsilesionalen Hemisphere in Teilregionen des Thalamus als Zeichen einer sekundären Neurodegeneration nachgewiesen werden. Innerhalb des Rückenmarks war diese Aggregation besonders im dorsalen corticospinalen Trakt, einer wichtigen absteigenden motorischen Bahn, zu beobachten.

Das neue PSS Mausmodell und die gewonnenen Erkenntnisse dienen als Grundlage für weitere Studien zur Charakterisierung welche absteigenden Bahnen kausal mit PSS im Zusammenhang stehen und inwieweit sekundären Neurodegeneration in den Relay- und Projektionsstellen im Hirnstamm und auf Rückenmarksebene dabei eine Rolle spielt.

3 Abstract

Strokes are one of the most common causes of lifelong physical impairment, with about 35% of the patients suffering from post-stroke spasticity (PSS). In contrast to the long and successful history of experimental stroke, rodent models of PSS are sparse and insufficiently characterized [275]. Motivated by this gap in stroke studies, this thesis focused on the development of a PSS mouse model and the long-term effects after strokes within the primary motor area (MOp), secondary motor area (MOs), and internal capsule.
For longitudinal determination of PSS, sensorimotor behavioral tests, and equivalent to the measurement in the patient, electrophysiological measurements of the Hoffman reflex were performed. For this purpose, in addition to a longitudinal H-wave measurement, a novel direct nerve H-wave measurement was established in the mouse. For the quantitative determination of the PSS, the ratio of H- and M-wave as well as the rate-dependent depression were measured, which allow an objective measurement of PSS.
The experiments revealed that a lesion within the MOp leads to motor deficits, without development of PSS, whereas a lesion within the MOs and internal capsule leads to mild and strong PSS, respectively, after 56 days. In the established internal capsule stroke model for the induction of PSS, an onset of PSS was detected electrophysiologically after 14 days. The sensorimotor deficit score correlated with the PSS measurement, i.e. animals with a PSS showed a reduced recovery of motor function. It was demonstrated that, in addition to the grid walk test, the cylinder test represents behavioral tests that still detect a motor deficit 56 days after a lesion and are sensitive to the motor deficits that occur in PSS.
In addition to electrophysiolgical and sensorimotor changes, structural changes were also analyzed, which included examination of secondary neurodegeneration in addition to lesion description. Within the first 28 days after lesion within the MOp microglia/-macrophages were found mainly in the ipsilesional in subregions of the thalamus, which suggested a secondary neurodegeneration. Within the spinal cord, this aggregation of microglia/macrophages and thus evidence of selective secondary degeneration was particularly evident in the dorsal corticospinal tract, an important descending motor pathway. The knowledge gained will serve as a basis for further studies, which will include a precise characterization of secondary neurodegeneration at the spinal cord level and neuronal tracing to evaluate the influence of the cortico- as well as reticolospinal tracts.

4 Introduction

4.1 Stroke

Strokes remain one of the leading causes of death worldwide and result in an increasing number of patients with physical disabilities each year [256]. The occlusion of an intracranial artery interrupting blood supply and subsequent cell death accounts for approximately 80% of strokes (ischemic strokes) [255], which, depending on size and location, can result in permanent disability in 36-45% [109, 282]. Depending on the location of the ischemia, about 80% of patients suffer from motor impairments, mainly affecting control of the arms, face or legs [31], and may end in spasticity as the disease progresses, which will be considered in more detail later in this thesis. The rehabilitation of motor control that patients go through is based on recovery processes [26, 162, 63]. Worldwide, stroke consumes around 2-4% of total healthcare costs [184] and the age of the population will result in more demands on the healthcare system because stroke in older people often occurs. According to a statement by the American Heart Association it was stated, that the stroke-related medical costs will rise from 71 billion US$ in 2021 to 183 billion US$ in 2030 [192] and will continue to place a heavy burden on the world's health insurers [99].

4.1.1 Pathophysiology

Stroke can be understood as local cell death surrounded by tissue with reduced perfusion, the so-called penumbra, in which cells can survive, whereas cells in the ischemic core will die definitively. Ischemic stroke begins as an acute loss of blood flow (CBF) resulting in a cascade of damage to blood vessels, neurons, astrocytes, and other cell types whose damage begins as early as 2 minutes after the onset of ischemia [34]. If the CBF is reduced under 15% it can result in terminal depolarization and metabolism fails of the energetically expensive neuronal function resulting in loss of membrane potentials [124]. The loss of connections to distant areas results in reorganization (Figure 1) and on the other hand in degradation of the axons the so-called wallerian degeneration.
The effects of focal stroke are relayed to distant brain sites through the loss of connections, secondary axonal degeneration, and microglial/astrocyte activation [14]. The pathophysiological processes that occur during and after stroke result not only in cellular changes but also lead to motor impairments influenced by neuro- and maladaptive plasticity.

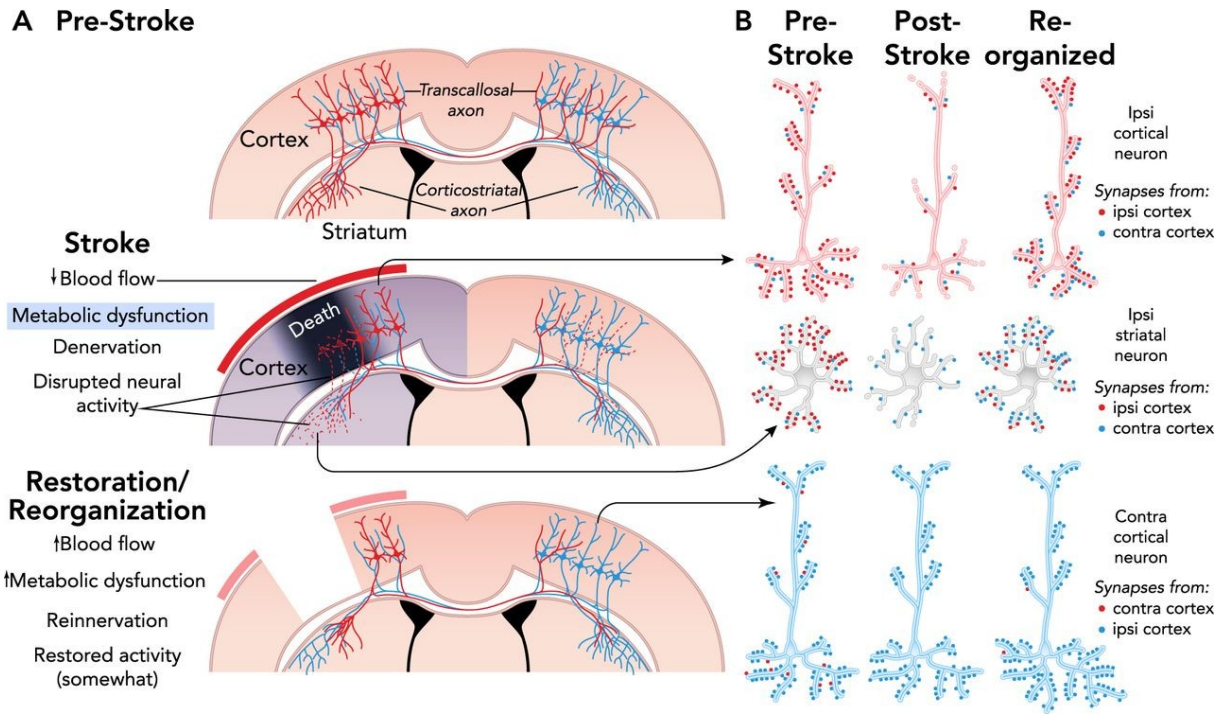

Figure 1 Mechanisms during spontaneous recovery after stroke. (**A**) Representation of coronal sections and the axonal projections of cortical pyramidal neurons. The death of neurons due to reduced local blood flow and metabolic dysfunction during ischemic stroke leads to denervation and disrupted neural activity within the ischemic core, resulting in the death of connections to the striatum and contralateral cortex. After the restoration of blood flow and metabolic functions, reinnervation occurs through axonal sprouting and synaptogenesis. (**B**) Due to stroke, neural connectivity is altered by reinnervation of ipsi- and contralateral neurons. Adapted from [139]

A unilateral lesion to the motor cortex results in the degeneration of interhemispheric projection, which propagates axonal sprouting of layer 5 pyramidal neurons of the contralesional cortex [140] with more dendrites [199]. The remaining neurons, which are responsible for limb control and surrounding the motor cortex can contribute to reinnveration of the unilateral lesion. Motor recovery can be further supported by rehabilitation training [78] as well as by robotic training [242]. To be able to treat the impairments after stroke, some therapies have been discovered by experimental animal models and clinical research. In order to reduce the load on the penumbra [157] and alleviate the effects of stroke, hypothermia can be used to suppress depolarization, reduce metabolism of the brain [272], and improve CBF through collaterals of the ischemic territory [165]. Effective therapies have been shown with the thrombus removal by thrombolysis within the first 3-4.5h [266] and up to 16 h after stroke by thrombectomy [7], but due to risk of hemorrhage and short treatment window, not every stroke patients receive this therapy.

4.1.2 Neuro- and maladaptive plasticity

Due to neuroplasticity the brain is capable of structural and functional reorganization after damage to the central nervous system (CNS) even in the adult state [89]. These mechanisms include axonal sprouting [49], functional re-mapping, intra- and interhemispheric remodeling of neural networks [279], and restoration of brainstem-spinal tracts [15]. This remodeling after stroke results in altered connectivity [71], which at the same time, has a positive effect on recovery [43]. In contrast, dysregulation of these mechanisms can lead to maladaptive plasticity, which results in epilepsy, compensatory movements, neuropathic pain [86, 33], and spasticity [169]. The resulting posture of the affected extremities can lead to muscle shortening [127], which is associated with further motor impairments [265]. The severity of these motor impairments depends on the location and size of the cortical injury [235]. Studies indicate that hyperexcitability and spasticity occur due to maladaptive plasticity [164]. How positive and detrimental effects of neuroplasticity are regulated and potentially can be used for novel therapies remains understudied [84]. The pathophysiological mechanisms that are induced after a stroke are still not fully understood. In the last decades, a broad range of animal models has been established, which made it possible to better understand the molecular mechanisms after a stroke.

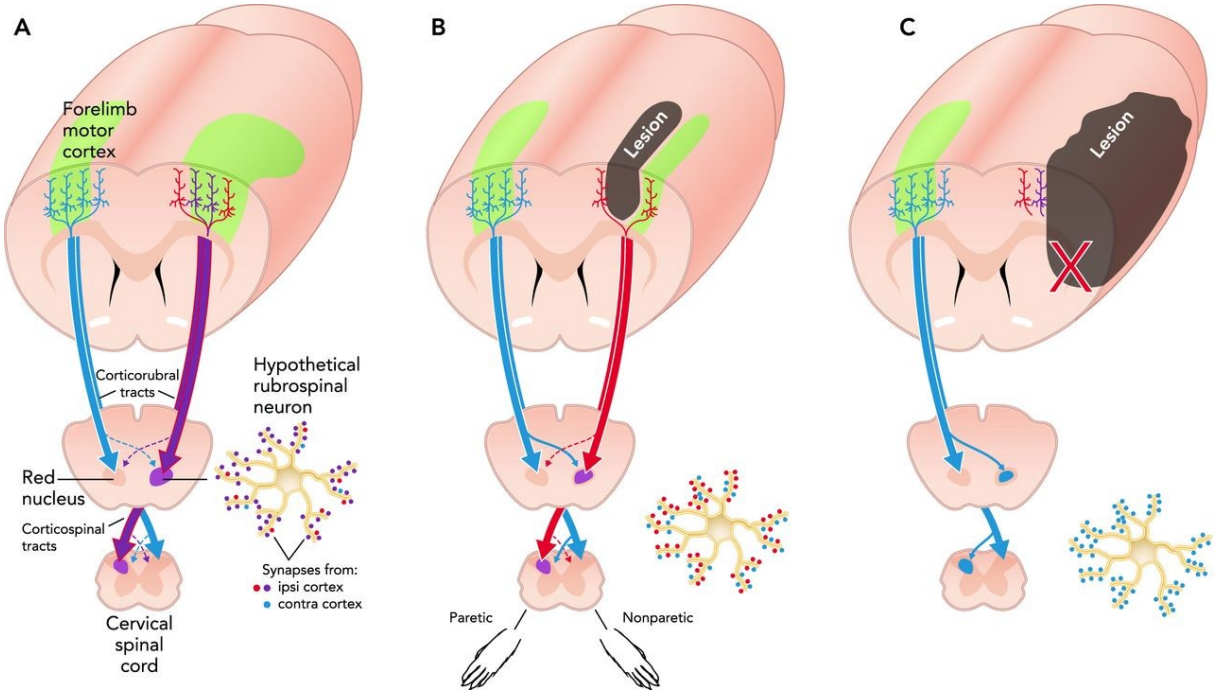

Figure 2 Neuroanatomical reorganization after stroke. (**A**) Coronal illustration of forelimb motor cortex representation (green), with their corticorubral and corticospinal tract projections. (**B**) After cortical stroke within the motor cortex, the remaining ipsilateral motor cortex can contribute to reinnervation. (**C**) Stroke damaging cortical/striatal regions can destroy descending projections of the motor cortex and leaving only crossed collaterals of the contralesional projections as a source of reinnervation. Adapted from [139].

4.2 Stroke and spasticity models in mice

A variety of different animal models have been developed [47], to study the pathologically alterations after stroke [170]. The mouse model has proven to be the most promising animal model, as mice are well suited for the study of diseases such as stroke due to their high reproduction rate, genetic modifiability, low costs, and restricted research use of higher mammals [88]. Some stroke models were initially developed for cats or rats and later transferred to mice [53]. The increasing importance of animal experiments has been recognized by society, and therefore the 3R principles [12] has also been adapted to stroke research [48]. Guidelines like ARRIVE [146] and IMPROVE [75], improve animal welfare, the informative value of these experiments, and make them more comparable [63]. Animal models have been developed, which are able to decipher mechanisms underlying rehabilitation and plasticity [43, 131], which form the basis for further clinical studies [73, 44].

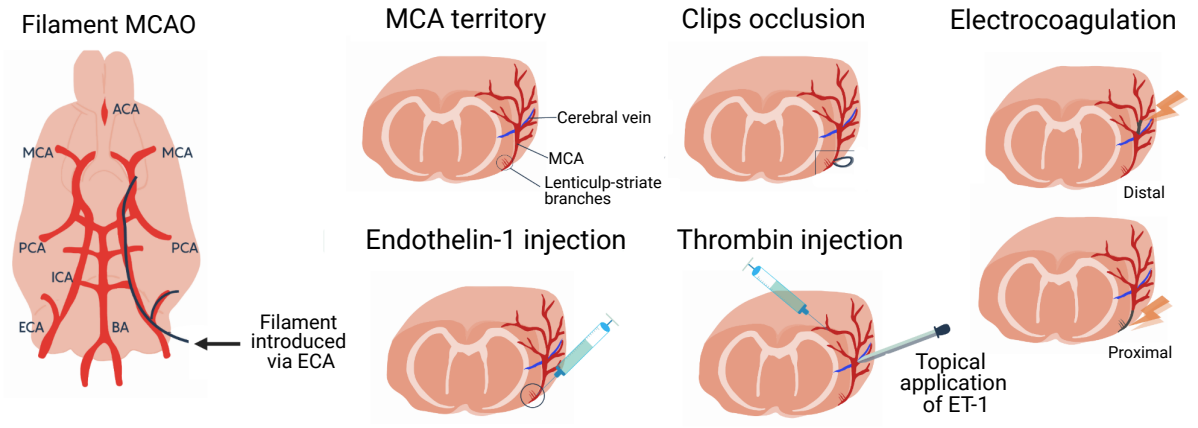

Figure 3 Commonly used mouse models of stroke. Insertion of a filament over the external carotid artery leads to occlusion of the middle cerebral artery (MCA) and ischemia can be varied over the occlusion time. The MCA can also be occluded with vascular clips or injection of endothelin-1 and intraluminal injection of thrombin. Permanent occlusion can be achieved via electrocoagulation of the distal or proximal MCA. (Adapted from Neuroscience: Canadian 2nd Edition by William Ju, under CC BY 4.0 licence)

With one stroke model, it is impossible to reproduce the heterogeneity of strokes in humans in terms of lesion size, location, and most importantly age and comorbidities. One of the most common stroke models is the filament middle cerebral artery occlusion model (MCAO, [81]), in which a filament is passed through the external carotid artery (ECA) to the middle cerebral artery (MCA), and occluded for a defined time. Due to the high incidence of MCA occlusion in patients, this model has become the gold standard but continues to generate controversy due to its outcome variability and comparably large lesions [166]. As an alternative, an aneurysm clip can be used [152]. In addition to mechanical occlusion, the MCA can also be chemically occluded by injection of endothelin-1 (ET-1, [189]) into the MCA, by topical application to the MCA [171], as well as by intracerebral injection into any desired region [122]. Another model established by Orset and colleagues [191] is based on local injection of thrombin into a bifurcation of the MCA, which leads to ischemia of surrounding regions. An advantage of this thrombin model is the possible thrombolysis by recombinant tissue-specific plasminogen activator (rtPA), in the same way as it is performed in the patient during thrombolysis [106]. If reperfusion is not necessary for the research topic, distal [182] or proximal [61] electrocoagulation of the MCA can be an additional alternative (Figure 3).
The most established model of cortical stroke without subsequent reperfusion is photothrombosis, which is described in more detail below.

4.2.1 Photothrombosis

The concept of photothrombosis was initially proposed by Rosenblum and El-Sabban in 1977 [216] and became renowned by its application in the rat brain by Watson in 1985 [270]. The cortical infarction is induced by activation of the photosensitive dye Rose Bengal using cold light or laser light with a wave length of 559 nm (Figure 9). When the circulating dye is illuminated through the intact skull of the mouse, free oxygen radicals and reactive oxygen species (ROS) are generated [153]. The result of the endothelial damage is the activation of platelets and platelet-rich thrombi formed, which results in the occlusion of the microvessel lumina by thrombi formation, which determines the interruption of local blood flow and results in ischemic cell death in the illuminated brain area (Figure 9). Photothrombosis induces a simultaneous development of vascular and cytotoxic edema with a rapid breakdown of the blood-brain barrier [273]. This model, however, causes only minimal ischemic penumbra, which limits its use for studying the progression of ischemic injury. Still, it allows the examination of structural and functional remapping after stroke [60]. This is because photothrombosis is also capable to trigger neuroplasticity of the peri-lesional and contralesional hemisphere [274] and was therefore modified to achieve an artificial penumbra, by using a ring photothrombosis [273].

4.2.2 White matter stroke

Axons and glia cells build the white matter (WM), permitting fast communication between peripheral to central regions. This rapid conduction is made possible enabled by myelin sheath-forming oligodendrocytes that allow action potentials to move rapidly by saltatory propagation. Small vessel infarcts within the WM account for approximately 25% of all stroke subtypes and are the second leading cause of vascular dementia [129]. Within the WM there is only a small amount of lateral blood supply, making the WM more vulnerable to small vessel disease such as diabetes type II than other brain regions. Strokes within the internal capsule (IC) are particularly common, for which reason they have become the focus of investigations into functional network changes during recovery [271]. Damage to the IC can lead to degeneration of descending fibers from the motor cortex and ascending fibers to the somatosensory cortex. To date, no therapy exists to promote tissue repair and recovery after a WM stroke [268]. Lesions within the WM result in motor impairment [113] which makes the integrity of the WM critical for subsequent motor recovery [227]. After stroke within the WM demyelination, axonal damage, loss of oligodendrocytes, local activation of microglia/macrophages and astrocytes can be observed [85].

However, most studies using pre-clinical models focus on ischemia within the gray matter, which is why the biological understanding of inflammation and reorganization after WM strokes is still incomplete [218]. This knowledge gap is due to the difficulty of inducing ischemia specifically within the WM in animal models.
In addition to the study of cortical strokes induced by photothrombosis, there are also animal models for the induction of lesions within the WM [240]. Compared to lesions within the cortical gray matter, methods for the induction of WM strokes, the recovery and its mechanisms differ [218]. One of the most commonly used WM stroke models is the local injection of the peptide endothelin-1 (ET-1), which is naturally produced by endothelial cells and has vasoconstrictive or vasodilatory activity by binding to endothelin receptors [123]. Intracerebral injection of ET-1 into the parenchyma results in a local reduced CBF of approximately 3h [128] without disruption of the blood-brain barrier (BBB, [128]). The injection of ET-1 leads to a reduction of myelin basic protein and neuronal loss [128, 238], as well as local necrosis [92]. Furthermore, axonal injury can also be detected after ET-1 injection, as indicated by the detection of amyloid precursor protein (APP, [188]). The ET-1 injection model leads to a site-dependent early activation of microglia/macrophages infiltration [241] and to a later activation of astrocytes after about 24h [128]. Sozmen and colleagues demonstrated that white matter strokes form a niche for oligodendrocytes and astrocytes, which prevents recovery and thus could be a potential target for future therapy [239].

4.2.3 Animal models of spasticity

The induction of stroke in animal models not necessarily results in spasticity due to different size and localization. In addition to the induction of spasticity by strokes, genetic models, spinal cord injury, and inflammatory models for multiple sclerosis or amyotrophic lateral sclerosis have been developed, which can result in spasticity [275].

The spastic mouse

The spastic mouse was discovered by random breeding and develops a tremor, abnormal gait, and reflexes [54] as a result of aberrant splicing of glycine receptor beta-subunit mRNA [186]. Additional studies suggest that the spasticity in the spastic mouse is due to a deficit of a single gene that codes for GABA receptors in the spinal cord and brain.

Ziv and his colleges compared the different muscle growth of genetically spastic mice to wild types, and found that the spastic muscle grew only 55% as fast as the bone, which led to the development of contractures in this mouse model [288]. They assume that these changes may be due to altered posture (resulting in secondary muscle shortening), abnormal nerve activation of the the muscle, or muscle spasms, resulting in shortening. Drugs that enhance GABA synaptic action reduce spastic symptoms [27, 55] in the spastic mouse, suggesting that they result from an imbalance in of inhibitory and excitatory signals [112, 278].

Spinal cord injury

Spinal cord injury (SCI) is one of the most common causes of spasticity, for which reason a variety of different SCI models have been developed [76]. In rare cases, the transection model is used, but in many cases, an experimental contusion model is used, because this model corresponds more to the situation in humans [116]. Based on SCI models, in addition to improved therapy with botulinum toxin [221, 284], treatment with repeated anodal trans-spinal direct current stimulation [179] and nimodipine, an FDA-approved calcium channel blocker, were developed [173].

Amyotrophic lateral sclerosis

Amyotrophic lateral sclerosis (ALS) is a neurodegenerative disease, caused by the loss of motor neurons, and results in progressive weakness of skeletal muscles, atrophy, and death as the result of respiratory muscle paralysis up to 5 years after the onset of the disease [251]. The Cu/Zn superoxide dismutase 1 (SOD1) has been identified as the most frequent cause of inherited ALS [97]. Beside the SOD1 the TAR DNA binding protein 43 (TDP-43, [276]), ubiquilin-2 (UBQLN2, [213]), and the ALS2 gene [281] seems to be responsible for ALS and were therefore modified to mimic ALS in mice models.

Multiple sclerosis

Multiple sclerosis (MS) is a neuroimmunological disease whose exact etiology is still not fully elucidated. MS is one of the most common causes of non-traumatic disability in young adults due to progressive demyelination of the CNS and neurodegeneration in later stages. Besides muscle spasm and depression, in severe cases spasticity is one of the most common symptoms of MS (80%, [200]). In mouse models, spasticity can be induced by MS using experimental autoimmune encephalomyelitis (EAE, [39]). The EAE model is a T-helper cell-mediated autoimmune disease where T-cells and monocytes infiltrate the CNS, which results in demyelination of axons, impaired axonal conductivity, and ultimately paralysis [214].

Stroke

A cerebral lesion can lead to an imbalance of excitatory and inhibitory neural circuits, and result in post-stroke spasticity (PSS, [247]). To date, there are only two studies that have been able to induce spasticity after a cortical lesion using photothrombosis in a mouse model [257, 160]. In this model, spasticity was measured using rate-dependent depression over 8 weeks after cortical lesion. The spasticity induced by photothrombosis could be attenuated by administration of the anti-spastic GABA-B agonist baclofen one week after stroke, but could not show any improvement in behavior tests. Depending on the stroke model and the localization of ischemia, PSS may occur as a symptom of upper motor neuron syndrome in addition to cognitive and motor deficits.

4.3 Motor Neuron Syndrome

The upper motor neurons (UMN) are responsible for carrying the neuronal information, which initiates and modifies movements, and originate in lamina 5 (pyramidal layer) of the primary motor, supplementary motor, and primary somatosensory cortex [220]. Most UMN originate from the primary motor cortex and are associated with the voluntary movements of the skeletal muscles. Posterior and caudal to the primary motor cortex, the premotor cortex is located, which is associated with learned, planned, and repetitive movements. Posterior to the premotor cortex, is the the supplementary motor located, which is associated with the planning of more complex movements. In contrast to these regions, the primary somatosensory cortex is associated with conscious sensations, and up to 30% of all UMN originate from this area. Lesion to the UMN, especially to the supplementary and premotor motor cortex are associated with an increased stretch reflex, while damage to regions like the primary somatosensory cortex and primary motor cortex results in paralysis and weakness in the corresponding muscles. UMN lesions can lead to clinical symptoms, known as upper motor neuron syndrome (UMNS), and occur immediately after stroke or traumatic brain injury (TBI) with symptoms like weakness, impairments of the affected extremities, hypotonia, and loss or reduction of deep tendon reflexes. Depending on the location of the UMN lesion, pathological reflexes (Gordon, Babinski), foreign/mass reflexes, clonus (characterized by involuntary jerks of the limbs), clasp-knife phenomena as well as swallowing difficulties, and dysfunction of the automatic nervous system occur [229]. Later in the course of UMNS, muscle overreaction occurs, including increased deep tendon reflexes (tendon jerks), spasms, co-contraction, spastic dystonia, and spasticity (Figure 4, [79]).

4.3.1 What is spasticity?

Even after decades of research, the definition still proves to be challenging. One of the most common definitions was made by Lance in 1990 [155]:

"Spasticity is a disorder of the sensorimotor system characterized by a velocity-dependent increase in tonic stretch reflex ("muscle tone") with exaggerated tendon jerks, resulting from hyperexcitability of the stretch reflex, as one component of the upper motor neuron syndrome that does not include impaired voluntary movement and an abnormal posture".

The definition of spasticity was further refined by the Support Programme for Assembly of a database for Spasticity Measurement (SPASM), which concluded that spasticity is "a sensorimotor control disorder that emerges as a result of an upper motor neuron syndrome and in the form of muscles involuntary intermittent or permanent activation" [38]. Spasticity can develop over weeks and months, depending on the type of injury, largely due to loss of inhibitory circuits [77]. Spinal cord injuries lead to the development of spasticity [121] in a relatively short time, whereas cortical injury results more slowly and in a weaker time course [151]. Worldwide, around 12 million patients suffer under spasticity, whereby 17-38% of the patients develop spasticity after stroke, 50% with traumatic brain injury, 34% with spinal cord injury, 40-78% with multiple sclerosis [83]. The symptoms of spasticity result in an economic burden for the society and health care system of approximately 111,500€ per year and patient [248], additional to the loss of productivity, and costs for the family home care [96, 98].
As one sign of the upper motor neuron syndrome, post-stroke spasticity occurs in 17-38% of patients with a cortical or subcortical lesion [83] and is described in more detail in the next chapter.

4.3.2 Post-stroke spasticity

After stroke, up to 35% of the patients develop post-stroke spasticity (PSS) with symptoms like hypertonia and rigidity in the corresponding muscles, non-voluntary rapid muscle contractions (clonus), and pathologically augmented stretch reflexes, causing abnormal flexion (Figure 4). Among other symptoms of post-stroke motor disorders, PSS is a ubiquitous symptom with a prevalence depending on the location ranging from 4-8% in the first 4 weeks to 17-43% after 3 months [37, 244], 37-40% after 12 months [178]) up to 34% 18 months after stroke [277]. PSS is observed more frequently in the upper than in the lower extremities (Figure 4, [145]) and additional include symptoms like urinary incontinence, impairment of the gait, standing, and sitting, but also the impairment of tasks of daily life [237, 90].

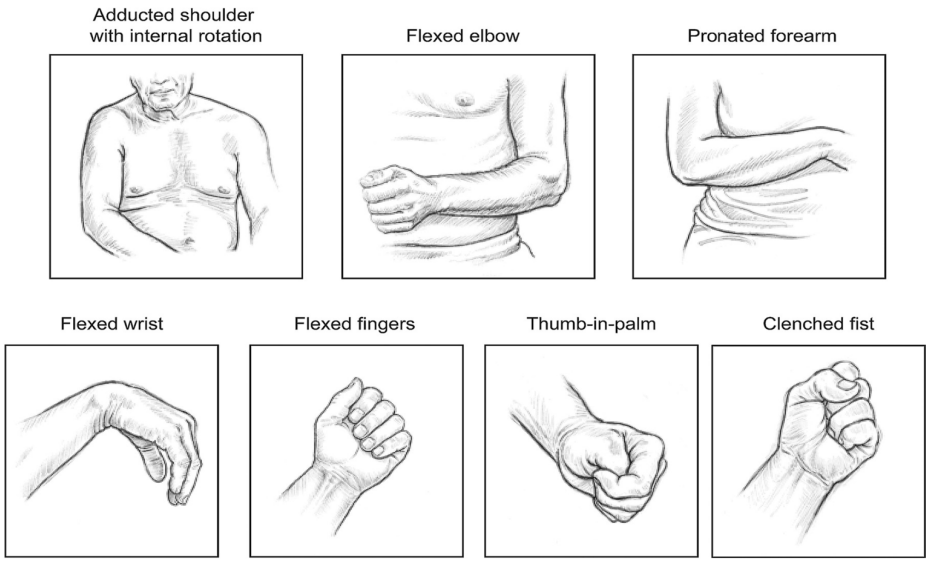

Figure 4 Symptoms of an upper motor neuron lesion resulting in spasticity. Common symptoms are clenched fists, fingers, elbow and wrist, but also pronated forearm and abducted shoulders. (Adapted from [235])

The development of PSS can be described using the interhemispheric competition model standing in addition to the disinhibition hypothesis. The disinhibition model postulates that each brain hemisphere inhibits the other hemisphere and thus maintains a balance [232, 279]. TBI or stroke leads to an overreaction of the contralateral hemisphere, which can lead to further functional dysregulation or over activity [103]. In contrast, some studies support the assumption that initial transient activation of both hemispheres has a positive effect on recovery and that further activation of the contralateral cortex leads to a deterioration [167, 65]. In the interhemispheric competition model, disruption of the interhemispheric connections by stroke or TBI results in loss of inhibition of the contralesional cortex. Intense inhibition of the contralesional cortex by the ipsilesional cortex through transcallosal fibers leads to the reduced motor output of the affected limb and worsening recovery processes [40, 250, 190]. In this model, activation of the contralesional hemisphere is considered to be negative for recovery, as demonstrated by the use of repetitive transcranial magnetic stimulation, in which motor function was improved after the suppression of the contralesional cortex [102, 101].

4.3.3 Neural circuits of spasticity

Based on risk factors [247] and the location of the brain damage, studies have shown that it is possible to predict if and how severe spasticity will occur [204], or the extent to which patients recover after a stroke [230, 209]. Thereby the insula, pallidum, thalamus, corona radiate, and the external/internal capsule are brain regions associated with severe upper limb spasticity [204]. The vulnerable structures, which are associated with PSS consist of the descending pyramidal cell axons build a fan shaped, ascending and descending myelinated structure, the corona radiata. Ascending tracts within the internal capsule (IC) originate predominantly from the thalamus and descending fibers from the various cortex areas. Because of the tight compression of the ascending and descending axons, the IC is especially vulnerable to strokes, whereby the IC is often damaged in stroke because it is supplied by a branch of the arteria centralis anterolateralis, deriving from the middle cerebral artery, which is commonly blocked in stroke. Especially lesions within the posterior limb of the IC are associated with spasticity because fibers from the premotor area descending there, which are responsible for the inhibition of the stretch reflex [259].
In addition to the primary lesion, e.g. stroke, TBI or SCI, neural and plasticity reorganization contribute to the adaption of inhibitory mechanisms [269] and to the time course of spasticity [156]. Lesions of the IC including both, the (pyramidal) corticospinal tract (CST) and the (extrapyramidal) corticoreticular input to the medulla, result in less inhibition through the dorsal reticulospinal tract (RST) and pronounced facilitatory input from the medial RST and the vestibulospinal (VST) tract (Figure 5). The lesion of these descending tracts leads to an exaggeration of the stretch reflex and subsequently spasticity [259]. The underlying mechanisms of the irreversible spasticity signs include the decreased inhibition of the spinal network [69, 176], the increased excitatory synaptic inputs associated with Ia afferent fibers [252, 25], and the increased motorneuron excitability [25]. Plasticity and neural remodeling processes, triggered by the initial damage, contribute to the time course of spasticity [156, 37, 185] and the adaptation of spinal inhibitory mechanisms [269]. Moreover, they can lead to muscle shortening, which further contributes to the motor impairments [265] and restricts mobility [127].
Cortical and internal capsular lesions such as in stroke, for example, damage not only the CST, but also the corticoreticular excitatory input to the medulla, with results in reduced inhibition from dorsal RST and pronounced faciliatory input from medial RST and VST.

Spasticity must be distinguished from rigor since spasticity leads to an increase in muscle tone with an increase in the passive speed of movement. Damage of the extrapyramidal motor system primarily causes rigor through omission of the calming input to the muscle that usually regulates tone and self-reflex. If this input is missing, the respective muscles become cramped. If, on the other hand, there is only damage to the pyramidal system, this results in flaccid paralysis. In contrast to rigidity, spasticity is a type of hypertonia that depends on both the velocity and the direction of movement and is most prominent during the fast, passive stretch. In severe cases, hypertonia can also be present at rest and result in the impairment of quality of life and activities of daily living (ADLs) such as walking, sitting, and standing [20].

Primary and secondary motor cortex

The primary motor cortex (also known as M1 [201] or MOp [267]) has a direct connection to the motor neurons of the spinal cord via the corticospinal tract (CST), which arise from the cortex layer 5. The MOp is responsible for the initiation of complex movement patterns, which are executed together with the premotor and supplementary motor cortex and receive their input mainly from other cortex areas and the thalamus. Otherwise, the MOp lacks direct projections to cortical targets, including retrospinal, parietal, insular, and orbital regions [134]. More projections arise from the secondary motor area (MOs), project through the CST to the spinal cord [94] and receive inputs from cortical and thalamic sources [210] allowing the control of motor units and initiating of complex movements together with the basal ganglia and cerebellum. The UMN originating from the MOs and MOp project through the IC as the CST down toward the brainstem and further into the spinal cord. In the spinal cord, the UMN forms connections with the lower motor neurons (LMN) or interneurons located there, allowing it to control the activity of specific motor units. The pyramidal cells localized in the MOs, are connected to the nuclei of the pons, and also relate to the extrapyramidal motor centers (nucleus ruber), MOp, and anterior horn cells of the spinal cord to inhibit reflexes and initiate movements of the proximal extremities.
Experiments in animal models have shown that there are two balancing descending systems controlling the stretch reflex, the inhibitory medial reticulospinal and the vestibulospinal tract. However, only the ventromedial bulbar reticular formation, the origin of the dorsal reticulospinal tract, is under cortical control. These circuits are also classified as postsynaptic inhibitory circuits and their effect as postsynaptic inhibition [69, 66, 176].

In patients suffering from spasticity, these mechanisms were each reduced, confirming the hypothesis that a reduction in postsynaptic inhibition is involved in the hyperexcitability of the stretch reflex.

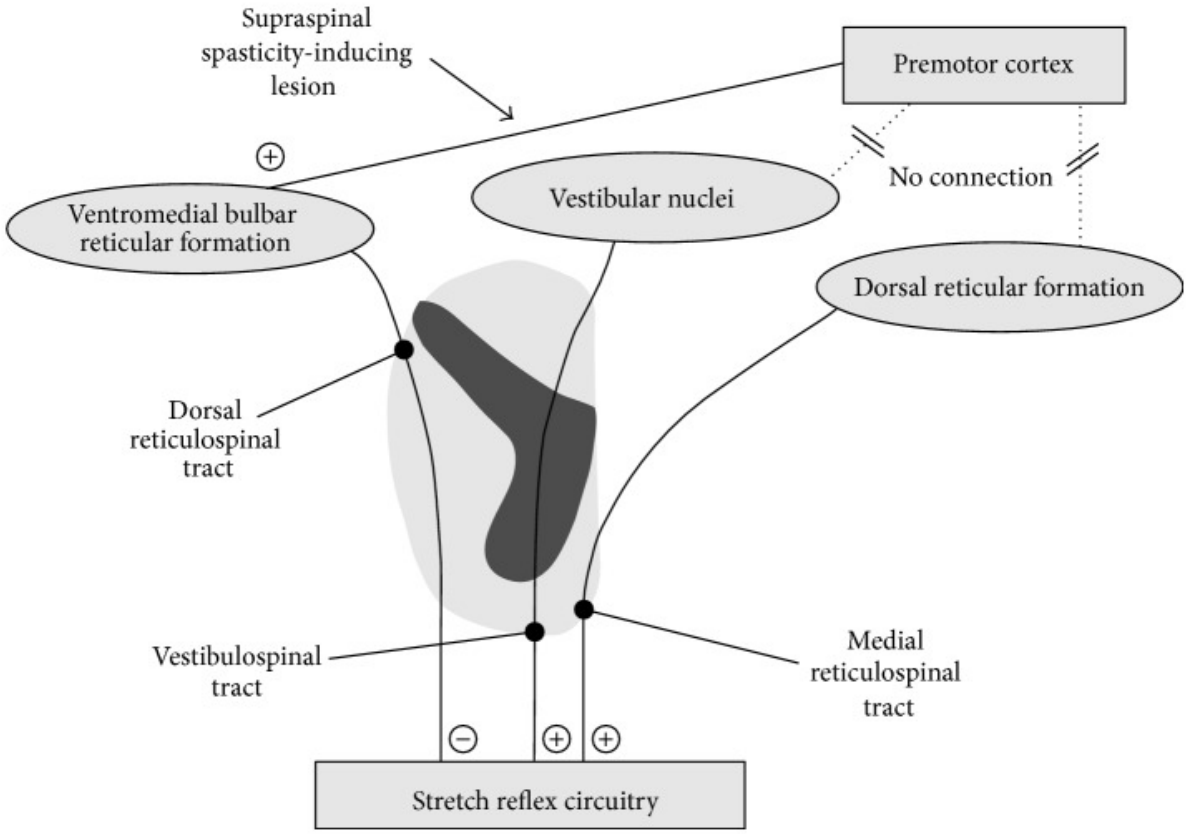

Figure 5 Descending pathways modulating the stretch reflex circuitry. Humans have two major descending pathways, the faciliatory medial reticulospinal/vestibulospinal tract and the inhibitory dorsal reticulospinal tract. The ventromedial bulbar reticular formation is under the control of the premotor cortex, in contrast to the dorsal reticular formation, which has no connection to the cortical premotor cortex. (Adapted from [259])

Cortico- and reticospinal tract

The CST originates in the motor cortex, passes through the basal ganglia in the IC, and terminates in the spinal cord [10], where the CST modulates the activities of the LMN resulting in the control of voluntary movement, and is also most responsible for the loss of function after SCI or stroke. Thereby the CST can be separated into three parts: the crossed lateral, uncrossed lateral, and the uncrossed ventral CST [283]. Besides the anatomical separation of the CST, a functional separation is also possible.

Distal muscles for the ankles and fingers are mainly controlled by the lateral CST and more proximal muscles are primarily controlled by the cortico-reticulospinal tract and the anterior CST. Additionally, the lateral CST is more involved in motor functions of the upper extremities than in the lower extremities, whereby the association of walking with the lateral CST is not as strong as for hand function [223, 236]. The CST is essential for voluntary movement and, in higher primates necessary for the hand dexterity control [258].

The CST in higher primates descends in the lateral and ventral part of the spinal cord, whereas in adult mice the CST descends only in the dorsal part of the spinal cord, the dorsolateral corticospinal tract (DLCST, [245, 272]). The CST crosses the midline of the spinal cord in the majority of mammals, in rodents at the level of the most ventral part of the funiculus, and in humans the crossed part of the CST is located in the dorsolateral funiculus of the spinal cord, contralateral to the hemisphere of origin. In contrast to higher primates, adult rodents show no monosynaptic connections between the motor cortex and motor neurons [135]. Gu and his colleagues demonstrated a monosynaptic connection between motor cortex and forelimb muscles using rabies virus-mediated tracing in postnatal mice only until postnatal day 14 [104]. The amount of CST axons, that cross the midline varies across species, ranging from 80-95% in rodents [141], 90% in cats [11], 85-90% in macaque and rhesus monkeys [217], to 75-90% in humans with high amount of interindividual differences [132]. The remaining uncrossed part of the CST (5-15%) plays a clinical role for motor recovery after stroke [91, 144, 46]. The structural changes of the CST after stroke was demonstrated in patients by neuroimaging and can be correlated with motor recovery [262]. An unilateral absence of the CST input, caused by stroke, can lead to downstream functional and morphological changes at the level of the spinal cord [144], which are associated with greater motor deficits [208] and recovery [136, 132]. The spontaneous motor recovery after stroke is mediated by the plasticity of uninjured CST circuits, but injured-dependent CST sprouting induced by plasticity is insufficient to regain complete motor function after larger injuries (Figure 2).

Descending projections from the reticular formation are involved in the control of posture and movement and mainly found in the reticulospinal tract (RST). The lateral RST and ventral RST belong to the descending tracts and have their origins in the reticular formation of the brainstem, and modulate motor and sensory functions of the spinal cord. The axons of some interneurons project to alpha motor in the spinal cord, whose axons in turn terminate at motor terminal plates of extrafusal skeletal muscle fibers as effectors.

As in the ventral reticospinal tract, these interneurons project to both alpha or gamma motor neurons and are innervated by multiple cortico-and/or subcorticospinal tracts (tractus rebrospinalis and vestibulospinalis). The brainstem reticular formation exerts both excitatory and inhibitory effects on muscle activity and tone, influences respiration and the cardiovascular system, and is involved in the transmission of sensory impulses to higher brain centers.

4.3.4 Clinical diagnosis and therapy of spasticity

As summarized above, the particular symptoms depend on the underlying cause of spasticity, which makes it difficult to apply common clinical measures [114, 158, 21]. The basic clinical evaluation of spasticity includes the assessment of patient-reported clinical findings, medication, physical examination, and is completed by a series of neurophysiological tests [114]. The physical examination measures the presence and frequency of flexor, extensor spasms or muscle tone, and tendon reflexes [37]. Besides voluntary muscle strength, contractures, functional loss, passive and active joint range of motion, sole skin reflex, triple flexion reflex, and clonus can be analyzed to diagnose spasticity. The quantitative evaluation of spasticity over time using biomechanical methods (isokinetic dynamometers, pendulum test), walking analysis (e.g., kinematic and kinetic registration, dynamic EMG), neurophysiological methods (Hoffmann-reflex), tendon reflex latency, and clinical scales (Penn Spasm Frequency Scale, Tardieu Scale, Barthel Index, Ashworth Scale) [17, 228, 38, 9] are necessary to measure the response to treatments.

One of the most in-clinic used ways to characterize spasticity in patients is the modified Ashworth scale (MAS). The MAS was initially established to measure the effect of therapies on the intensity of spasticity [172] for the situation after traumas like stroke [16], TBI [8], SCI [6] or inflammatory diseases like multiple sclerosis [110], and amyotrophic lateral sclerosis [74]. The MAS has been criticized [87] because of its nominal levels of the scale [2] and for its only moderately inter-rater reliability [180]. In mild cases of PSS, patients may recover, which Brunstrom et al. describes as 6 steps [35]:

1. Flaccidity
2. Appearance of spasticity
3. Increased spasticity with synergistic voluntary movement
4. Movement patterns out of synergy and spasticity begins to decrease
5. More complex movements and spasticity continues to decrease
6. Spasticity disappears
7. Full recovery of normal function with coordinated voluntary movements

Novel therapies focus on cortical plasticity and the hyperexcitability of the reticulospinal tract because this tract could be the main reason for PSS [163]. One of the most effective therapies of PSS is the automatic EMG-guided [30] or manual injection of botulinum toxin (BTX) into the affected extremities [105, 193, 30] resulting in improved walking and quality of life. The injection of BTX creates a transient plastic state of the motorneuron system and allows the re-learning and recovery, even if the patient are already in the chronic stage of spasticity. In addition to BTX injections, cannabinoids can also be used to treat spasticity, because cannabinoids inhibit neurodegeneration in multiple sclerosis models [206] and represent a promising therapy option [72, 207]. Besides pharmacotherapy, transcutaneous electrical and magnetic stimulation has been developed as two alternative methods that can be used to treat spasticity [149]. Trans-spinal direct current stimulation in mice with spinal cord injury results in improved functional outcome [4], which has thus also been shown in patients [119]. Noninvasive repetitive treatment using transcranial magnetic and transcranial direct current stimulation show promising motor recovery [249]. But intensive treatment of patients with incipient spasticity is crucial because compensatory movement strategies can lead to a worsening motor ability [138]. In order to determine the motor impairment that may be caused by spasticity, electrophysiological measurements such as quantification of the Hoffmann-reflex are performed in addition to the scoring systems described above.

4.3.5 Hoffmann-reflex

The Hoffmann-reflex (H-wave), named after the physiologist Paul Hoffmann, can be induced by electrical stimulation of peripheral nerves (Figure 6) and represents an electrically induce analog to the monosynaptic stretch reflex [117, 118]. It is elucidated using implanted electrodes or transcutaneous stimulation of large nerves, such as the tibial nerve, through which efferent motor neurons (MNs) innervate the gastrocnemius muscle [5].

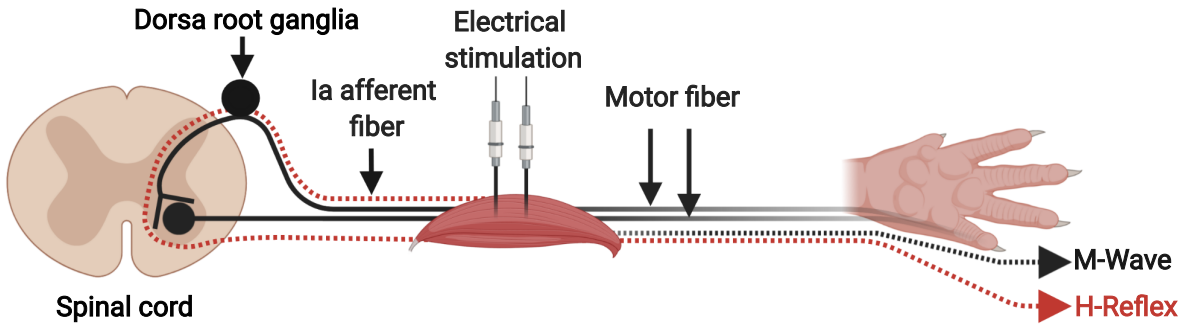

Figure 6 Hoffmann-reflex as electrophysiological sign for the CNS integrity. For verification of the integrity of neural circuits, both the M-wave (direct muscular response) and the Hoffmann-reflex (H-wave) can be used by electrical stimulation. The H-wave is induced by transcutaneous stimulation of afferent Ia neurons, which in turn monosynaptically activates corresponding alpha-MNs in the spinal cord and is then recorded in the muscle.

The physiological response can then be measured directly in the innervated skeletal muscle as an electromyographic (EMG) action potential. The stimulus response shows itself as a so called M-wave, which represents the action potential caused by direct orthodromic MN stimulation, and the indirectly elicited H-wave, which represents the delayed indirect activation of a subset of MNs through stimulation of Ia afferents and subsequent activation of their follower MNs. The M- and H-waves are the responses of different subsets of MNs, the M-wave that of directly activated MNs with larger axon diameters, the H-wave that of smaller MNs. The latter are the first ones to be recruited through Ia afferents in the monosynaptic connections on the spinal cord but lead to a smaller size response in the EMG recording. Depending on the organism, either M- or H-wave can appear at the lower stimulus threshold, the reason for which remains unresolved [161].

A stimulation strength is increased, the amplitude of the H-wave also increases until the short-latency M-wave is elicited. A further increase in stimulation intensity increases the M-wave but decreases the H-wave amplitude. If the stimulation amplitude is large enough the M-wave reaches a maximum through recruitment of all recorded motor units, while the H-wave may be completely absent. This is due to antidromic back propagation of action potentials which collide the the Action potentials elicited by Ia afferent stimulation. The observation of the ratio of the H-wave and M-wave (H/M ratio) allows a insight into the electrophysiological changes after SCI or stroke. In patients developing PSS an increase of the H-wave can be observed, whereas the M-response remains unchanged. In addition, the EMG shows a reduced rate-dependent depression (RDD), i.e. a reduced decrease in the amplitude of the H-wave over successive stimulations [154]. The reduction in the RDD is the result of reduced inhibition of the spinal cord after cortical or spinal lesions. RDD is an electrophysiological phenomenon that can validate the activation of spinal inhibitory circuits, whose interruption may result in spasticity [160].

4.4 Aims of this thesis

Cortical strokes, as well as strokes within the white matter, may lead to structural and functional disturbances of affected, but also more distant areas. In some cases post-stroke spasticity can develop after a stroke, however, a reliable mouse model does not exist and the basic mechanism of post-stroke spasticity are not well understood. In order to better investigate the mechanisms of post-stroke spasticity, this work aimed to:

1. Identify a reliable mouse model to study post-stroke spasticity
2. Optimize the electrophysiological measurement of post-stroke spasticity in mice
3. Analyse sensorimotor behavior tests for signs of post-stroke spasticity
4. Analyse the longitudinal development of electrophysiological and behavioral changes related to post-stroke spasticity
5. Structural changes after cortical and internal capsule stroke

5 Material & Methods

5.1 Consumables and materials

Table 1 Consumables and materials for animal experiments, histology, virus/dyes, and mouse lines.

Name	Product no.	Supplier
Animal experiments		
Micro driller	OmniDrill35	WPI
Digital stereotact	502300 Series, 61810	WPI
Heating pad	61840 Heating pad	WPI
Gas anesthesia mask	502053	WPI
Temperature controller	ATC200	WPI
Digital navigator	UMP3	WPI
Digital injection	Micro4 controller	WPI
Hamilton syringe	Nanofil 35G needle	WPI
651 nm laser	MGL-FN-561-100mW	PhotonTec
Fiber optic	FMC22L10	ThorLabs
Heating box	MediHeat V1200	MediHeat
Stimulator	Iworx-214	Iworx
Stimulator amplifier	WPI-A395	WPI
Digital stimulator	MS 501	Zoological Institute, UoC
Stimulator isolator	MI 401	Zoological Institute, UoC
Stimulation electrodes	C-ISO-PN3	iWorx
Hook electrodes		Zoological Institute, UoC
Peristaltic pump	Peripro-2Hs	WPI
Video camera	Brio	Logitech
Germinator	Germinator 500	CellPoint
Stereotactic adapter	XC5	Thorlabs
Rectal probe	RET-3	WPI
Vaporizer	Sigma delta	UNO
Flowmeter	CM2	UNO
Induction chamber	Induction box	UNO
Xylazine	Rompun	Bayer

Ketamine	Ketavet	Pfizer
Isoflurane	Isoflurane	Piramal Care
Carprofen	Rimadyl	Pfizer
Suture	HR 17 Silk	Resorba
Povidon Iod	Betaisodona	Mundipharama
Absorbent underpad	115-0684	VWR
Histology		
Cyromold	4566	Sakura Finetek
2-Methylbutane	3927.2	Carl Roth
Object slides	J1800AMNZ	Thermo Fischer
Embedding media	1825902829	Sakura Finetek
Black & Gold	AG105	Merck
Donkey serum	1540097	Linaris
Triton-X	T8787	Sigma Aldrich
Sodiumcitrate	567446	Calbiochem
Cover medium	HP20.1	Carl-Roth
GFAP	Z0334	Agilent Technologies
Iba1	019-19741	Wako Chemicals
Cy3-AffiniPure	711-165-152	Jackson Immuno Research
Cy2-Streptavidin	016-220-084	Jackson Immuno Research
DAPI	HP20.1	Carl Roth
Viruses and Dyes		
AAV1.CAG.Flex. tdTomato .WPRE.bGH	51503	Addgene
AAV1.EF1a.DIO. hChR2(H134R) -eYFP.WPRE.hGH	20298-AAV1	Addgene
AAV1.EF1a.DIO. eNpHR3.0 -eYFP.WPRE.hGH	26966-AAV1	Addgene
AAV1.hSyn.CaMPARI. WPRE.SV40	100832-AAV1	Addgene

pAAV.hSyn.eGFP.		
WPRE.bGH	105539-AAV5	Addgene
pAAV-CAG-GFP	37825-AAV1	Addgene
pAAV.CAG.LSL.		
tdTomato	10048	Addgene
CTB-488	C34775	Thermo Fisher
CTB-568	Z25006	Thermo Fisher
Mouse lines		
Emx1-Cre	B6.129S2-Emx1tm1(cre)Krj/J	MMRC
Rbp4-Cre	Tg(Rbp4-cre)KL100Gsat/Mmucd	MMRC
Wildtype	C57BL/6J	Jackson Laboratory

All experiments were performed in the animal facility of the department of pharmacology at the university hospital cologne in rooms dedicated for surgeries and behavior tests.

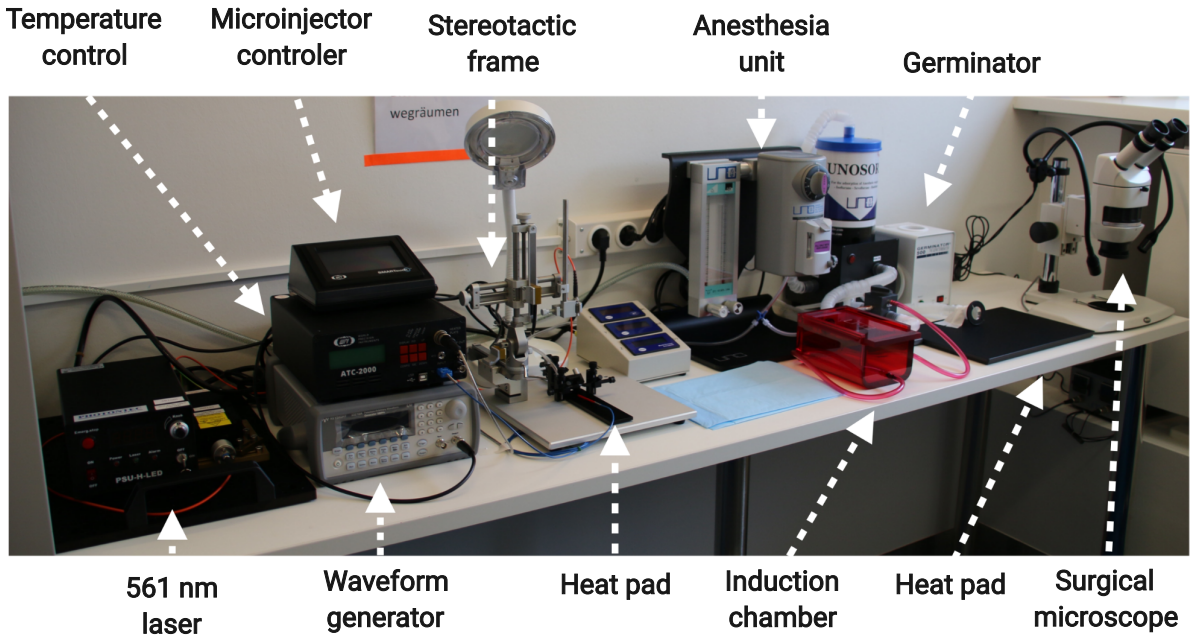

Figure 7 Technical setup for surgeries (photothrombosis, internal capsule stroke, intracerebral injection) and electrophysiological measurements.

5.2 Animal experiments

For the animal experiments, the rotating beam and cylinder test were used based on the expertise of Markus Aswendt, who had already established these behavioral tests at the MPI for Metabolic Research in cologne. With the help of Michael Dübbert from the Biozentrum Köln, a combined setup of the grid walk and a cylinder test was built. Expertise was archived during my master thesis and brought to the Aswendt Labt for the grid walk from the AG Minnerup at the University Hospital Münster. In addition, the grip strength was introduced by myself in the Aswendt Lab. All experimental methods and setups, except for the terminal H-wave measurement, were reviewed, ordered and set up in the lab by myself. For the improvement of the H-wave measurement Matthias Gruhn and Michael Dübbert from the group of Ansgar Büschges helped during the establishment. The animal experiment proposal, on which a large part of these experiments is based (81-02.04.2019.A309) was mostly developed and formulated by me in cooperation with Markus Aswendt. All animal experiments were carried out in accordance with our animal experiment licenses

- 81-02.04.2019.A309
- 81-02.04.2017.A404
- 84-02.04.2014.A305

approved by the Landesamt für Umwelt, Naturschtz und Verbraucherschutz NRW (LANUV). To increase animal welfare during the experiments and to follow the 3R principles (reduce, refine, replace; [264, 12], all experiments were conducted according to ARRIVE [146] and IMPROVE [75] guidelines. To prevent a possible influence of the experiments, as well as evaluation by influenced experimenters, the respective experimenters were blinded during the experiments [120, 24]. In the conducted experiments with viral tracing experiments the transgenic mouse lines Emx1-Cre [100] and Rbp4-Cre [134] were used. For animal experiments without viral tracing the wild-type mouse line, C57BL/6J (Charles River, Sulzfeld, Germany) was used.

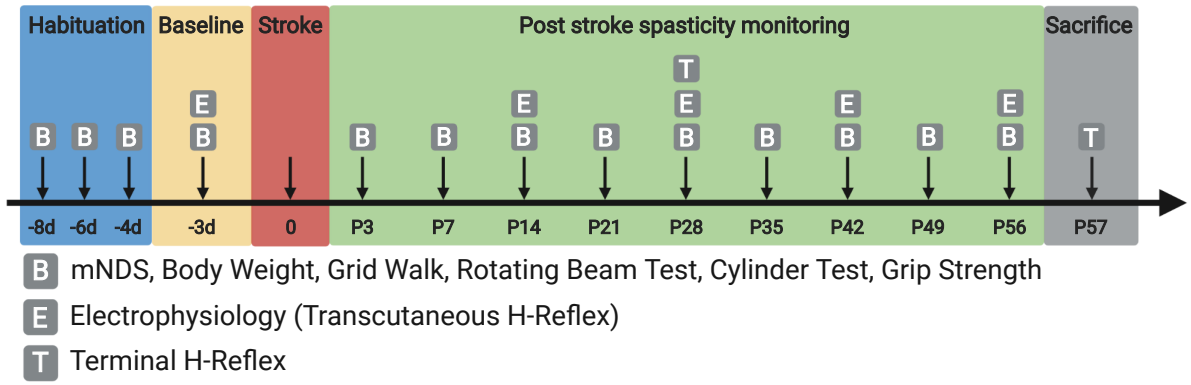

Figure 8 Schedule for post-stroke spasticity monitoring. Transcutaneous electrophysiological (E) and sensorimotor (B) baseline measurements were performed after three-time habituation. The induction of stroke (cortical photothrombosis or internal capsule stroke) is defined as time point 0. Sensorimotor testing was performed at P3, P7, P14, P21, P28, P35, P42, P49, and P56 days after stroke. Transcutaneous electrophysiological measurements were performed on days P14, P28, P42, and P56 after stroke. 57 days after stroke, terminal direct nerve measurement of the H-wave (T) followed by transcardiac perfusion were performed.

5.2.1 Anesthesia and Analgesia

Following with the recommendations of the GV-SOLAS (Pain Management in Laboratory Animals, 2015) and the publication of Krischak et al. [150] the animals received 1 mg/ml of the opioid tramadol via drinking water 3 days before each surgical procedure until 3 days after this procedure. The tramadol in the drinking bottles was renewed every day and care was taken to ensure sufficient fluid intake. 30 min before the surgery the animals received s.c. injections of carprofen (4 mg/kg).

5.2.2 Photothrombosis

The mice are initially anesthetized in an induction chamber with 4% isoflurane and then maintained under 2% isoflurane in a stereotactic frame (Figure 9). Control and maintenance of temperature were performed by a rectal sample coupled to a heating pad. After shaving and disinfection with povidone iodine, a 1.5 cm long incision was made into the skin from the height of the eyes to the neck. If necessary, the skin was fixed with skin retractors. The periosteum was removed and the surface of the exposed skull was cleaned with PBS and a cotton swab. A 561 nm laser coupled to the stereotactic frame via an optical light guide was aligned to point bregma and moved to the coordinates for the different lesion locations (Table 2 & Figure 10).

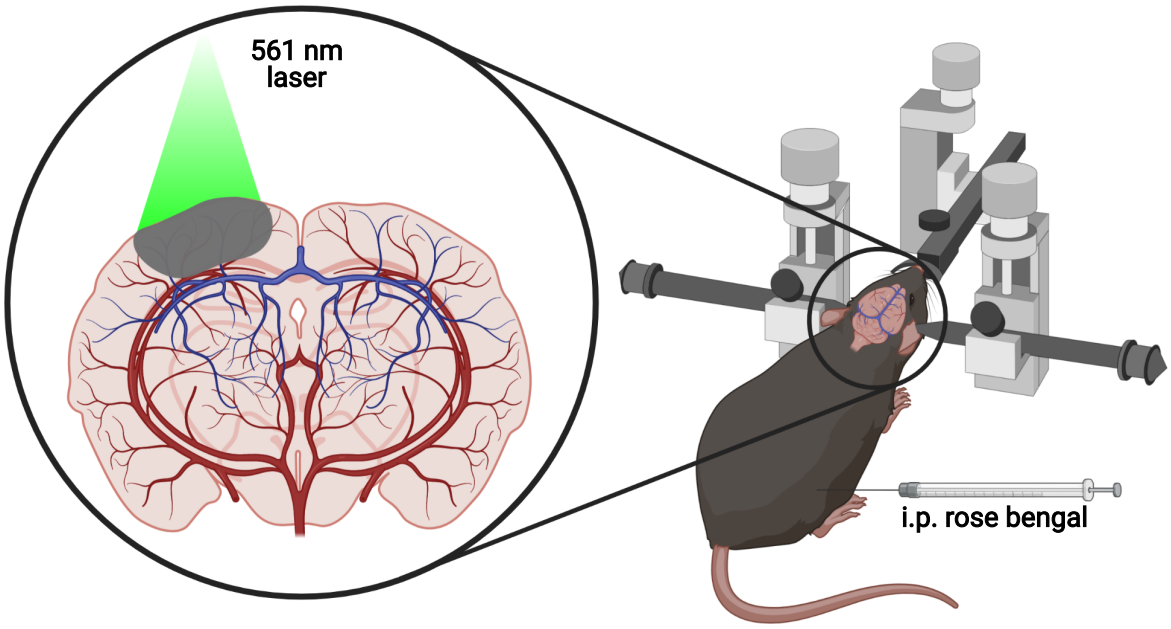

Figure 9 Cortical photothrombosis for focal ischemic stroke induction in the mouse. After i.p. injection of Rose Bengal, the cortical area was illuminated with a stereotactic mounted laser through the intact skull. The interaction of Rose Bengal and the 561 nm laser light results in local artery occlusion.

Table 2 Different photothrombosis protocols for small & large stroke, and stroke within the primary motor area (MOp) or secondary motor area (MOs).

	Laser intensity	Rose bengal	Coordinates [mm]	
	[mW]	[µg]	M/L	A/P
Small PT	35	1000	-2.0	0.0
Large PT	50	1500	-2.5	+0.5
PT (MOp)	50	1500	-2.5	+0.5
PT (MOs)	50	1500	-1.25	+1.0
	50	1500	-1.25	-0.5

For small cortical lesions, the laser was aligned with 35 mW to M/L: 2.00 mm and A/P: 0.00 mm and 1000 µg of the photosensitive dye Rose Bengal, dissolved in PBS, was injected i.p. (Table 2). For the large cortical lesion/primary motor cortex stroke the laser was aligned with 50 mW to M/L: 2.50 mm and A/P: 0.50 mm, and 1500 µg of the photosensitive dye Rose Bengal was injected i.p..

For cortical lesion of the secondary motor cortex, the laser was focused with 50 mW on two points, M/L: 1.25 mm, 1.00 mm and M/L: 1.25 mm, and -0.5 mm after i.p. injection of 1500 µg Rose Bengal (Figure 10). After injection of the Rose Bengal, 5 min was waited, during which time the dye was distributed throughout the body before the laser was activated. The sham-operated animals undergo the same procedure, including the skin incision and the injection of the Rose Bengal, but without laser radiation, so no ischemia occurs. After the successful induction of ischemia or sham-procedure, respectively, the wound was sutured and the animals were transferred to a preheated warming box where they could recover for 1h.

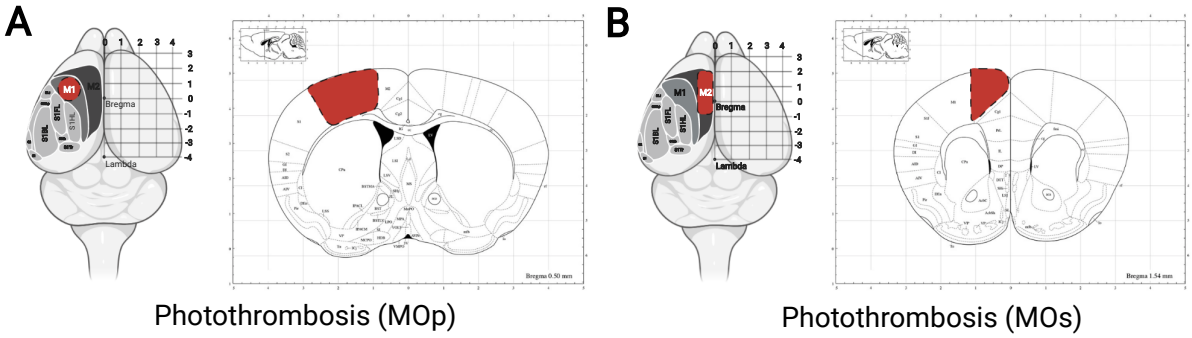

Figure 10 Cortical photothrombosis lesion location within the primary motor area (MOp) and secondary motor area (MOs). Induction of a lesion within the primary motor cortex (**A**) and secondary motor area (**B**) by photothrombosis. Photothrombosis affects only the cortical areas without destroying deeper striatal areas.

5.2.3 Internal capsule stroke

To create a lesion selectively in the internal capsule, a modification of the photothrombosis stroke model was established using a fiber optic to deliver the light localized deep into the brain (Figure 11). The animals were initially anesthetized with 4% isoflurane and shaved along with the incision site and anesthesia was maintained with 2% isoflurane. After craniotomy, a fiber optic (105 µm, 0.22 NA) was injected to the corresponding coordinates for the internal capsule (M/L: 1.8 mm; A/P: -1.06 mm; D/V: -3.5 mm) and hold there stereotactically with a cannula holder. After injection of 2 mg Rose Bengal i.p., dissolved in PBS, the Rose Bengal could be distributed for 5 min and a 10 min radiation with 5 mW of a 561 nm laser, which was coupled to the optic fiber (200 µm, 0.22 NA, SMA). After the surgery, the fiber optic was removed, the wound was sutured and the animals could recover from the surgery in a preheated heat box.

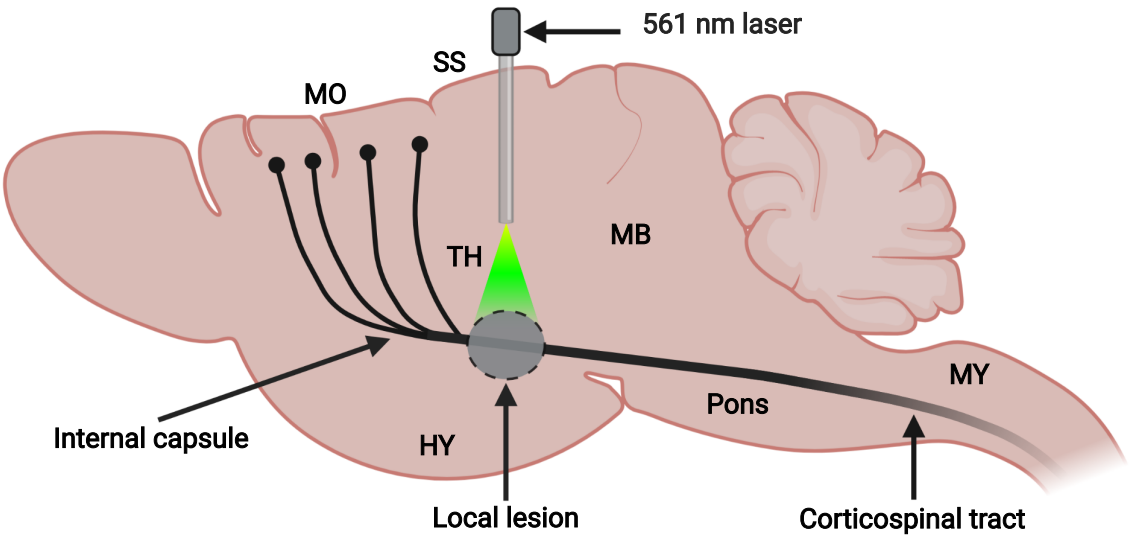

Figure 11 Internal capsule stroke as model for PSS. In the height between the thalamus (TH) and hypothalamus (HY). The descending fibers arise from the somatomotor (MO) and somatosensory (SS) areas continue between the TH and hypothalamus (HY) and further through the midbrain (MB). In the height of the pons, the internal capsule continues as corticospinal tract through the pons, and medulla (MY) into the spinal cord.

5.2.4 Intracerebral injection

Viral tracing is based on the natural ability of viruses to infect post-mitotic neurons. Especially the use of recombinant adeno-associated viral vectors (rAAV) for axonal tract-tracing in transgenic Cre driver mice has many advantages [1]. In the opposite to antero-grade tracers, such as biotin dextran amine (BDA), tracing with rAAV´s allow cell-type-specific mapping and modification of neural circuitry. Another sensitive neuroanatomical tracer that transports retrogradely in the nervous system is the cholera toxin subunit B (CTB-B, [62]). The injection of BDA or CTB in the region of interest allows multiple neuroanatomical and monosynaptic mapping in the same animal. For intracerebral injections, the animals were initially anesthetized with 4% isoflurane and then fixed in a stereotactic frame at 2% isoflurane. After reaching surgical tolerance, the incision site was shaved and cleaned with povidone iodine. The incision was made approx. 1.5 cm centrally along the skull bone and the craniotomy was performed above the target region. The injection by using a micro-injector was performed at 100 nl/min and a target volume of 1 µl. For the virus/dye to spread sufficiently in the target region, the cannula remains at the injection site for another 5 min. After removal of the cannula, the wound was sutured and the animals can recover from the operation in a heat box.

5.2.5 Transcardial perfusion fixation

The goal of fixation is rapid and uniform preservation in a life-like state. The advantage of directly perfusing fixative through the circulatory system is that the chemical can quickly reach every tissue of the organism using the natural vascular network [95]. The animals were perfused transcardially under ketamine / xylazine anesthesia and analgesia (120 mg/kg / 20 mg/kg i.p.). For this purpose, the thorax was opened and a perfusion needle was inserted into the left ventricle, the right atrium was cut with a scissor and the perfusion by a peristaltic pump with 20 ml phosphate buffered saline (PBS) was followed by 20 ml paraformaldehyde (PFA), both with a flow rate of 4 ml/min. After perfusion brain and spinal cord were extracted and post-fixated in 4% PFA O/N and transferred in 30% sucrose solution in PBS for long-term storage at 4°C.

5.3 Sensomotoric behavior tests

The combination of sensomotoric behavior tests allows to evaluate different functional impairments during recovery after brain lesions [19]. Here, the tests were selected to cover a broad range of sensorimotor deficits in the acute and chronic phase of cortical and subcortical strokes ([222, 67, 18, 125], Figure 12). The cylinder-, grid walk, and rotating beam test were video taped and later analyzed by an experimenter, who was blinded to the experimental design.

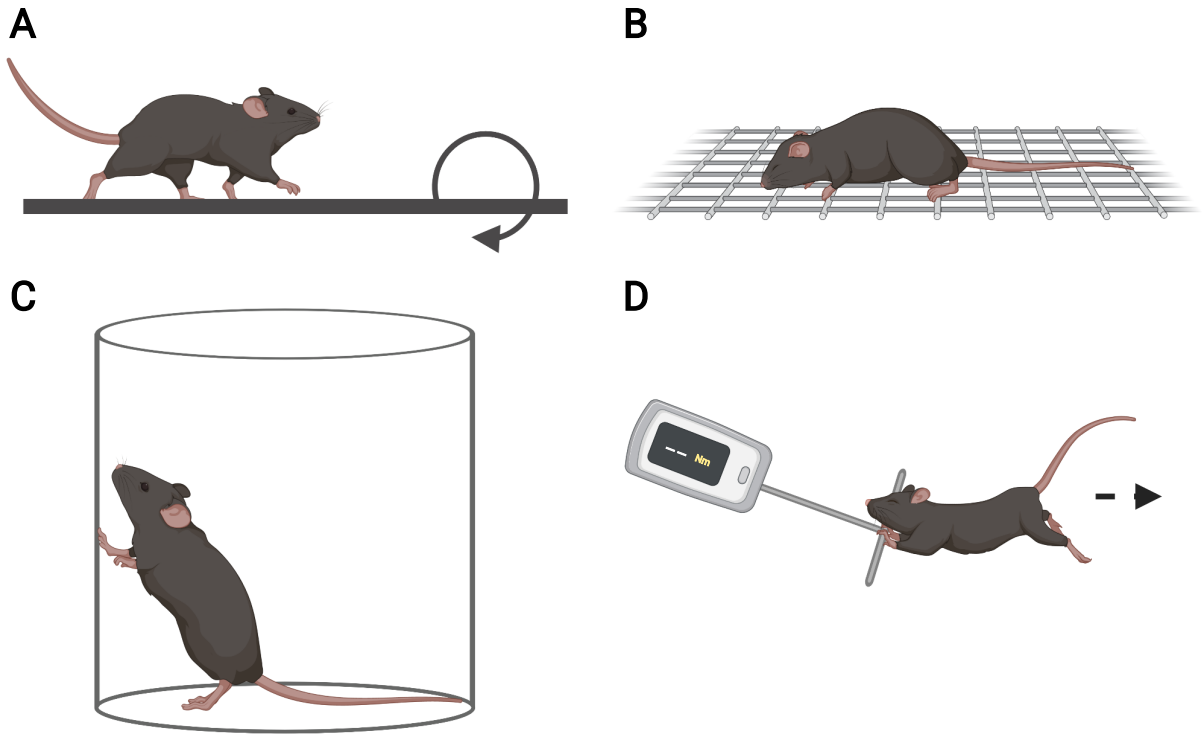

Figure 12 Behavior tests to determine sensorimotor deficits after brain lesion. (**A**) Rotating beam test evaluate the distance, speed, and hindlimb drops during the mice walks along the 120 cm long rotating beam. (**B**) In the grid walk test, the percentage of foot faults was counted during the mouse walks on a grid. (**C**) With the cylinder test the amount of paw drags, the asymmetry score, and activity score was quantified. (**D**) The grip strength tests give information about the muscle strength of the forepaw.

5.3.1 Rotating beam

The rotating beam test is a modification of the balance beam [52] and detects motor dysfunction of the fore- and hindlimb after stroke over several weeks [58]. The rotating beam is a 120 cm long rod with a diameter of 13 mm, which rotates at a speed of 6 RPM at a height of 60 cm (Figure 12 A). The animals are accustomed to the rotating beam three times before the baseline measurement. All four runs per session were recorded on video and the speed, how often the hind paws slip away (hind limb drops), and whether the mouse fell from the rotating beam were evaluated. If the mice did not reach the whole distance of 120 cm or the speed was <5 cm/s the mouse was excluded. The animals, which performed >55% of the baseline speed (baseline speed – day 3 speed / baseline speed) were also excluded. Mice were motivated to perform the test by placing the home cage at the end of the beam and by the resetting into the cage after a successful run.

5.3.2 Grid walk

The grid walk is a sensorimotor test for long-term dysfunction after stroke and was developed to evaluate the coordination of the limbs in the rat model and was later modified for mice [23, 56]. The setup consists of a grid with a mesh width of 12.7 X 12.7 mm, which is mounted at a height of 50 cm. The entire grid walk test is filmed with a camera mounted under the grid in a 45° angle and evaluated afterwards (Figure 12 B). In the grid walk test, the number of steps taken with the affected paw was related to the number of slip-throughs of the affected paw through the grid. For the analysis of the video, the blinded raters counted the number of foot faults of the impaired limb and non-foot fault steps. A step was considered as a foot fault if it was not providing support and the foot went through the grid hole. Further, if an animal was resting with the grid at the level of the wrist, this was also considered a fault. If the grid was anywhere forward of the wrist area then this is considered a normal step. A ratio between foot faults and totals steps were used to considered differences in the degree of locomotion between animals and trials. The percent of foot faults was calculated by:

$$\frac{footfaults}{footfaults+totalsteps} \times 100$$

5.3.3 Cylinder test

The cylinder test detects long-term sensorimotor dysfunction after stroke and was developed by Hua et al in 2002 for rats [126] and later modified for mice by Roome et al. [215]. The setup consists of a 15 cm high and 10 cm in diameter transparent cylinder, which was placed on a transparent plate and a camera was placed at a 90° angle below. Due to the natural exploratory behavior of mice the animal initiates exploratory scanning of the plexi glass cylinder wall by touching it with the right and left forelimb (Figure 12 C). To habituate the animals to the cylinder test animals were placed in the cylinder for 5 min on days 7, 5, and 2 before the stroke. The mouse was placed into the cylinder and the spontaneous movements were recorded for 5 min. For the evaluation of the cylinder test the protocol by Roome [215] was used to quantify the total number of paw touches and paw drags. After a stroke, there is a force reduction of the impaired forelimb and the animals are not able to induce pressure in a proper way to brace their weight drag down with their contralesional paw.

5.3.4 Grip strength

The strength and functionality of the front paws were measured with a strength meter (Figure 12 D). The mice were held by their tails and were allowed to hold on to a pole connected to the strength meter. The mice were then carefully pulled horizontally away from the strength meter until they released the pole. The test was performed 4 times and the respective average was determined. To better compare the grip strength of the individual mice, the individual force was normalized to the baseline.

5.4 Electrophysiology

In order to quantify a longitudinal measurement of the electrophysiological changes, the H-wave was measured at different time points (baseline, P14, P28, P42, P56) using transcutaneous measurement. At the end of the experiments (P28 and P56, respectively), the animals were measured by terminal measurement in addition to the transcutaneous measurement to evaluate the longitudinal H-wave measurements with higher accuracy. These measurements were established together with Matthias Gruhn (University of Cologne).

5.4.1 Transcutaneous electrophysiological measurement

For anesthesia, the mouse was injected i.p. with a mixture of ketamine (100 mg/kg) / xylazine (10 mg/kg), and placed in a preheated warming box until the anesthetics reached their effect. For stimulation, a pair of stainless needle electrodes were inserted into the chest muscle to stimulate nerve bundles, including the ulnar nerve at the axilla (Figure 13). The reference electrode was placed subcutaneously in the axilla between stimulation and recording electrodes. The measuring electrodes were placed subcutaneously in the abductor digiti minimi of the paw to be measured. The sample rate was set to 20,000/sec (Notch filter, 50 Hz), and recording was performed with a delay of 0.65 ms 15 times after a stimulus duration of 0.2 ms with 3 mA, because this current strength leads to the induction of a maximum H-wave in our hands. The stimulation was performed at different frequencies (0.1, 0.5, 1, 2, 5 Hz; [257]) to be able to determine the rate-dependent depression in a further step, and pauses of 2 min between stimulation at the individual frequencies. The surgical tolerance was repeatedly checked and if necessary a required amount of the ketamine / xylazine solution was injected. After measurement, the electrodes were removed and the mouse was allowed to recover in a preheated warming box.

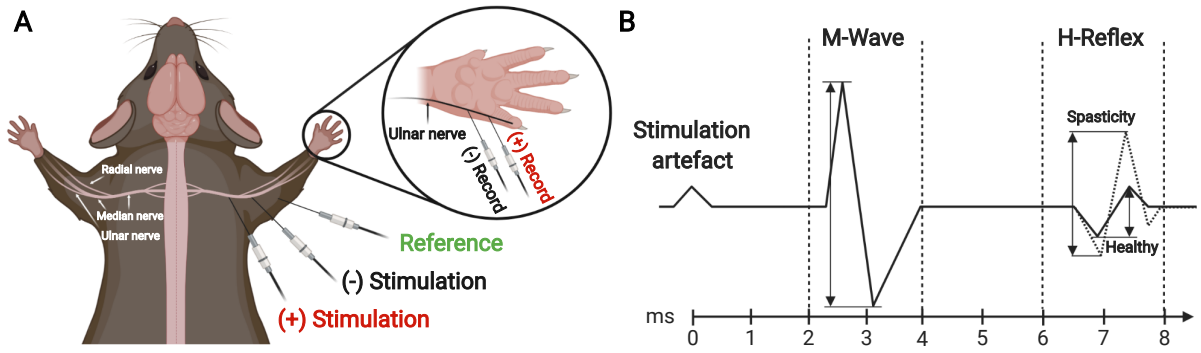

Figure 13 Measurement of the M-wave and H-wave at the forepaw using transcutaneous stimulation. (A) Measurement of the M-wave as well as the H-wave by electrical stimulation of the ulnar nerve at the level of the axilla and recording at the abductor digiti minimi. **(B)** Stimulation artifact followed by M-Wave (2-4 ms) and H-wave (6-8 ms) after electrical stimulation.

5.4.2 Direct nerve H-wave measurement

The animals received i.p. a mixture of ketamine (100 mg/kg) / xylazine (10 mg/kg) and placed on a heating plate. Initially, the protocol for direct nerve measurement were tested by the hind paw based on previous experience by Matthias Gruhn (Figure 14 B & C). In the course of the study, however, due to the better correlation to the performed sensorimotor behavior tests (which primarily measures the sensorimotor function of the forepaw), the protocol was adapted accordingly (Figure 14 D & E). For this purpose, the skin was opened along the axilla and the pectoralis profundus muscle was dissected away to reveal the median nerve (Figure 14 D). The median nerve was separated from the radial and ulnar nerve with a curved glass pipette. The ulnar nerve, which innervates the little finger (abductor digiti minimi) was chosen because of its easily accessible for electrophysiological measurement and was lifted out onto a stainless steel double-hook stimulation electrode with two curved electrodes (Figure 14 E). Warm vaseline was placed between the ulnar nerve and the surrounding nerve to insulate the electrodes from each other to the surrounding tissue. Insulated copper wires with a diameter of 100 µm were used for EMG recordings in the forepaw (10k amplification, 50 Hz filtered). The reference electrode was inserted s.c. into the femur (Figure 14 A). Stimulation of the ulnar nerve was performed 15 times at 70 µA for 0.2 ms each at increasing frequencies (0.1, 0.5, 1, 2, and 5 Hz), waiting 2 min between each stimulation. The stimulation electrodes was connected to a stimulation unit that was triggered by a pulse generator and recording / analysis of the data were performed with Spike2 (version 7.19).

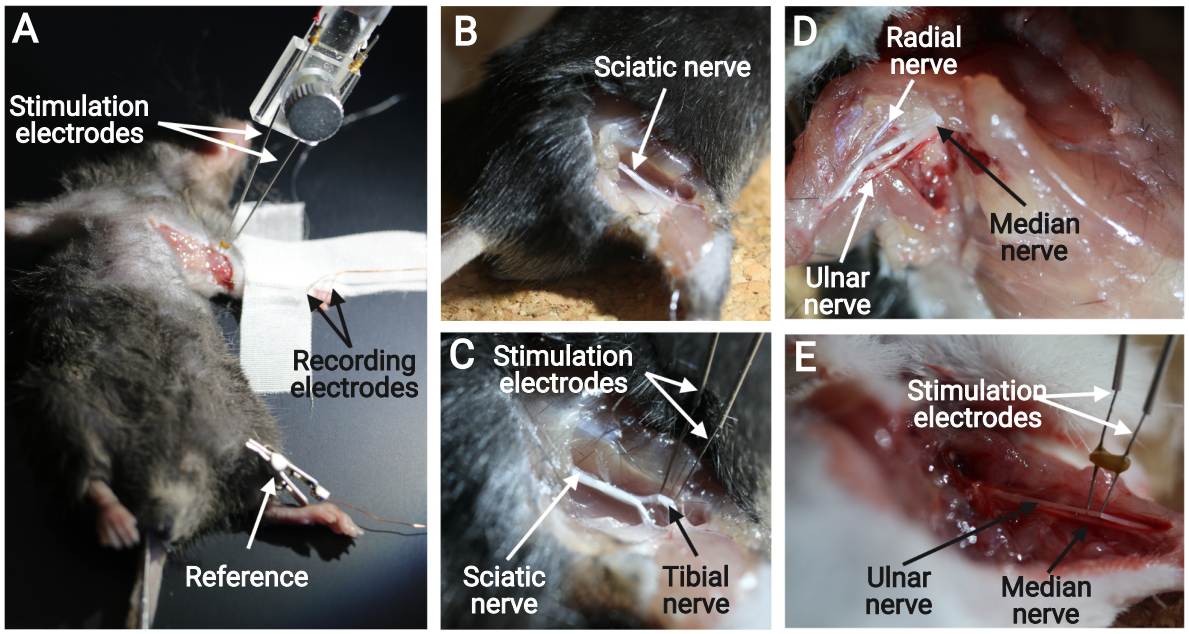

Figure 14 Direct nerve measurement of the M-wave and H-wave. **(A)** Overview of the direct nerve measurement with both hook stimulation electrodes, the recording electrodes within the forepaw, and the reference electrode injected into the hind paw. **(B)** After skin and muscle removal the sciatic nerve becomes visible and can be divided into the sciatic and tibial nerve **(C)**. On the forepaw, the radial, median, and the ulnar nerve becomes visible **(D)**. The ulnar nerve can be stimulated with the hook electrode, without stimulation of neighboring nerves **(E)**.

5.4.3 Electrophysiological evaluation of spasticity

Considering only the M-wave alone does not allow an accurate conclusion about the development of spasticity. The M-wave may differ due to the different transcutaneous positioning within stimulated muscle groups since it is not guaranteed that only the ulnar nerve was stimulated. A confirmation of the existence of spasticity in this context can only be made by the increase of the H-wave. To reduce the influence of the positioning, the ratio of H-wave and M-wave (H/M-ratio) was calculated for the evaluation of spasticity. To further evaluate the presence of spasticity, the animals, were stimulated with different frequencies (0.1, 0.5, 1, 2, 5 Hz) to calculate the rate-dependent depression, which is decreased in animals suffering under PSS.

5.5 Histology

5.5.1 Tissue freezing and sectioning

The brains were transferred from the 30% sucrose storage solution to a cryomold, surrounded by embedding media. The tissue was cooled down in isopentane/2-methyl butane to -60°C and longterm stored at -80°C. The brain and spinal cord tissue were cut in a cryostat at -23°C in 20 µm thick slices and stored afterwards at -20°C.

5.5.2 Immunohistochemistry

To visualize glial fibrillary acidic protein (GFAP), an intermediate filament protein in astrocytes and ionized calcium binding adaptor molecule 1 (Iba1), a marker to identify microglia and macrophages, the sections were thawed for 10 min at RT and pre-treated with sodium citrate (10 mM in PBS) for 20 min at 80°C. A border was marked with a DAKO pen around the sections and was washed three times for 5 min in PBS, followed by incubation of the slices for 1 h at RT in blocking solution (BS; 1x PBS + 0.25% Triton X-100 + 5% serum of secondary antibody; Cy3, Cy5, Alexa Flour 488). The slices were incubated 2 h at RT with the primary antibody, diluted in BS, followed by three wash steps with PBS for 5 min each. The secondary antibody was incubated for 2 h at RT under exclusion of light and was washed away three times with PBS for 5 min each. The sections were covered with DAPI containing media and coverslips.

5.5.3 Histochemistry

Nissl

Sections were thawed 10 min and equilibrated in PBS for 10 min, both at RT. They were then incubated in hematoxylin for 2:30 min and briefly rinsed with PBS. Subsequently, the preparations were covered with 75% ethanol-HCl for 3 sec, washed under running tap water, and incubated with 0.1% eosin staining solution for 1:40 min. Dehydration was performed in descending order with three washes each in cuvettes containing 100% ethanol and two washes each in cuvettes containing xylene for 2 min. Finally, brain sections were coverslipped with Entellan under glass coverslips and dried at RT.

Black & Gold

Black & Gold is an aurohalophosphate complex that stains specifically for myelin within CNS. Thereby the tissue can be fixed in formalin or 4% PFA. The Black & Gold staining powder was suspended in saline solution (0.9% NaCl) to a final concentration of 0.3%. The cresyl violet powder was suspended to a final concentration of 0.1% in MilliQ water and glacial acetic acid. For the staining of mouse brain slices the 0.3% Black & Gold and 1%, sodium thiosulfate solution were pre-heated to 60°C. After rehydrating the tissue section in MiiliQ for 2 min, the slides were incubated in the Black & Gold solution at 60°C for 12 min and were rinsed two times in MilliQ water for 2 min. Aftewards the slices were incubated for 3 min in 1% sodium thiosulfate at 60°C and rinsed three times in MilliQ water for 2 min afterwards. After 3 min of incubation in cresyl violet solution at RT, the slices were washed three times in MilliQ water for 2 min followed by dehydrating steps using a series of alcohol concentrations (25%, 50%, 75%). As the last step, the tissue section was covered with Entellan mounting medium under a coverslip.

5.5.4 Data evaluation

Due to the longitudinal and multimodal data collection, as well as a large number of different researchers, we had developed a cloud-based database for all experiments [196]. With this decentralized database, access is possible at any time and from anywhere, which allows cooperative work on shared data sets with collaboration partners. This database, together with in-house developed analysis tools for MRI data, as well as for histological data, served as objective and reproducible analysis of in vivo, as well as ex vivo data (Figure 15). During my PhD thesis I was involved in the establishment of the database and the evaluation of the analysis tools AIDAmri [194] and AIDAhisto [195] as manual rater, and provided the respective experimental data. To quantify the cell number in each brain area according to the Allen Brain Reference Atlas (ARA), histological sections were analyzed using AIDAhisto (Figure 15). All figures in this thesis, unless otherwise noted, were created using BioRender (BioRender.com).

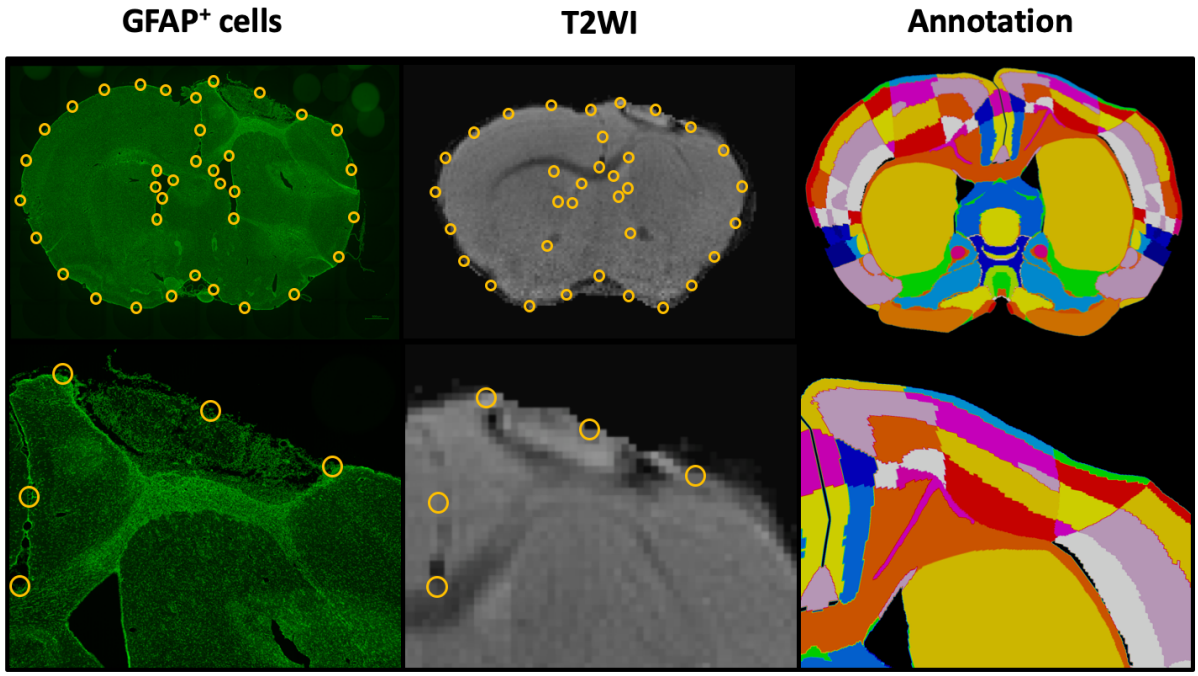

Figure 15 Atlas-based landmark registration of histological staining for astrocytes (GFAP positive cells) to T2-weighted MRI (T2WI) result in region-wise annotation. Using Image J (Fiji), points were made on the microscopic section as well as on the T2WI image. Using landmark registration, both images were registered based on the Allen Brain Reference Atlas, and the individual regions were annotated.

Behavior and electrophysiological measurement were analyzed using a two-way ANOVA, followed by Tukey comparison (GraphPad Software, Version 8.4.3, GraphPard Software, La Jolla, USA). Statistical significance between groups was marked with a and compared to baseline or at the respective time point with an *. A $p<0.05$ was marked with */#, $p<0.01$ with **/##, and a $p<0.001$ with ***/###. All data are represented as mean ± SD. A third order polynomial (cubic) curve was used to describe the sensorimotor deficit score.

6 Results

6.1 Establishment of an electrophysiological method to measure post-stroke spasticity

This project aimed to establish a post-stroke spasticity (PSS) model in the mouse since no corresponding animal model existed so far. This model should provide the basis for the investigation of pathological, electrophysiological (Ephys), and sensorimotor behavioral changes that occur during PSS. To differentiate between motor deficits due to local ischemia and those due to PSS, sensorimotor tests were performed together with Ephys examinations.

6.1.1 H-wave measurement improvement

To validate the changes of the H-wave after cortical lesion in the MOp or MOs, and IC, a setup was established based on previous reports [257, 160]. The replication of data provided by Toda et al. [257] and Lee [160] using the same stimulation and recording settings did not lead to the measurement quality as showed in the respective publications, which could not be further optimized (Figure 16 A). Besides better electrical shielding, positioning of the stimulation and recording electrodes, body temperature control, filtering of data as well as sampling rate, and alternative stimulation electrodes were tested. By using a more simplified setup, where the stimulation was no longer done via an external stimulator but directly through the stimulation software, the quality of the data in terms of signal-to-noise was improved. Further, it was possible to better determine the H-wave (Figure 16 B). To provide an overview of repetitive measurements, a MATLAB script was developed by Felix Schmitt (University of Cologne) to automatically extract (Figure 16 C) and average (Figure 16 D) the data. The heterogeneity of individual measurements (Figure 16 C-D), made averaging of the data difficult and the small amplitudes of the H-wave were no longer represented (Figure 16 D).

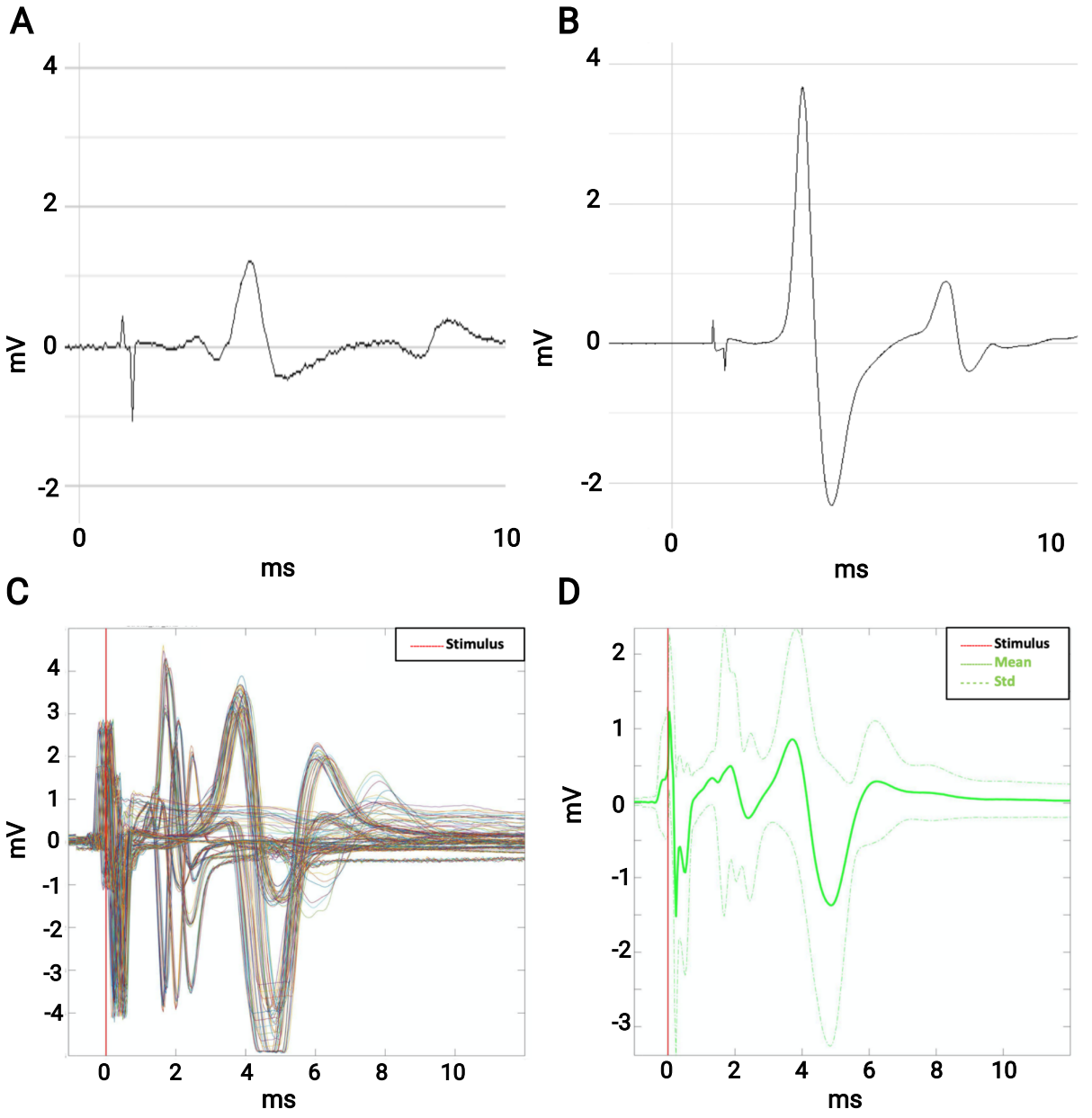

Figure 16 Examples of electrophysiological measurements with different setups. Representative electrophysiological measurements of the M-wave and the H-wave 56 days after stroke within the MOp with the WPI (**A**) and with the iWorx setup (**B**). Overlay of the M-waves and H-waves revealed the individual heterogeneity of the measurements (**C**) and the overlay of the M-wave and H-wave when these results are plotted as average (**D**).

6.1.2 Validation of electrophysiological measurements

To confirm the validity of the longitudinal transcutaneous and direct nerve measurement, the same animals were measured using both techniques sequentially at P56 (transcutaneous first followed by the direct nerve measurement). The respective M-waves, H-waves, and the resulting H/M ratios were then compared (Figure 17). The amplitudes of the M-waves measured transcutaneously and via direct nerve measurement correlate very precisely with each other (Figure 17 A, $p<0.01$). The H-waves obtained by both measurement methods correlate significantly ($p<0.05$, Figure 17 B) and the H/M ratio correlate highly significantly ($p>0.001$, Figure 17 C).
While performing the measurements, it was obvious that the variability in the M-wave was mainly due to the positioning of the electrodes. The comparison of the H/M ratio to the M-wave reveals thereby a lower correlation coefficient (r=0.34) than the H-wave (r=0.83). The spasticity is primarily indicated by a change in the H-wave, which correlates well with the H/M ratio (r=0.83).

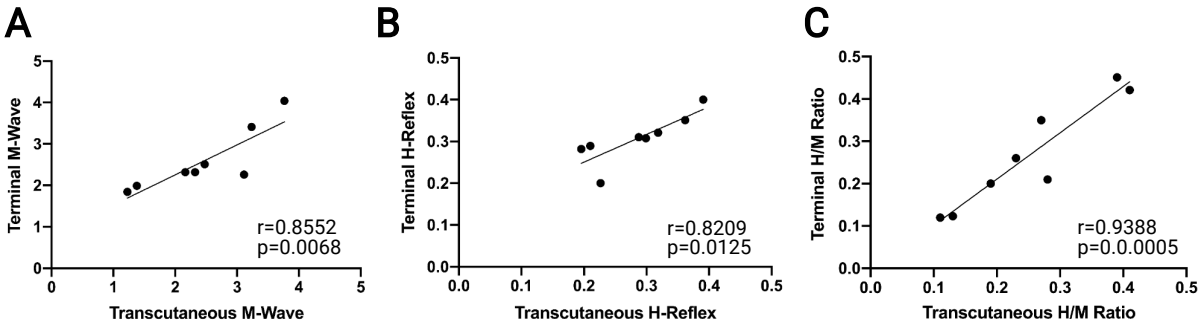

Figure 17 Comparison between transcutaneous and direct nerve measurement. (A) Comparison of the M-Wave amplitude with the transcutaneous and direct nerve measurement method with 0.1 Hz stimulation on P56. **(B)** Comparison of the H-wave amplitude with the transcutaneous and direct nerve measurement method with 0.1 Hz stimulation on P56. **(C)** Comparison of the H/M Ratio with the transcutaneous and direct nerve measurement method with 0.1 Hz stimulation on P56. (r = Pearson correlation coefficients)

The transcutaneous measurement of the M-wave showed an SD of 0.3418, which was significantly different ($p<0.001$) to the direct nerve measurement (0.07422). Also in the H-wave measurement, the direct nerve measurement shows a lower SD (0.1295) than the transcutaneous measurement (0.2521), which was statistically different ($p<0.01$). The H/M then also showed a lower variance ($p<0.01$) in the direct nerve measurement (0.06473) than in the transcutaneous one (0.1261).
The amplitude of the M-wave continuously increased simultaneously the stimulus intensity, whereas the amplitude of the H-wave continuously decreased. The amplitude of the M-wave always remained larger than the amplitude of the H-wave.

6.2 Electrophysiological changes during post-stroke spasticity

M- and H-wave were measured longitudinally with different frequencies (Figure 8) before (baseline) and after photothrombosis (P14, P28, P42, P56) to validate in a further step the rate-dependent depression. After the MOp lesion (Figure 18 A), the transcutaneous measurement was performed on the affected and unaffected forepaw. The measurement of the M-wave showed a maximum amplitude (Mmax) between 2-8 mV in all groups (Figure 18 B), and the H-wave varies between 0.1-0.35 mV during the whole measurement period (Figure 18 C). At all time points, no statistically significant difference between the groups were observed. Similarly, the H/M ratio showed no significant differences at all time points and values varies between 0.05-0.25 in each group (Figure 18 D). For a better overview, only stimulation with 0.1 Hz will be shown in the following.

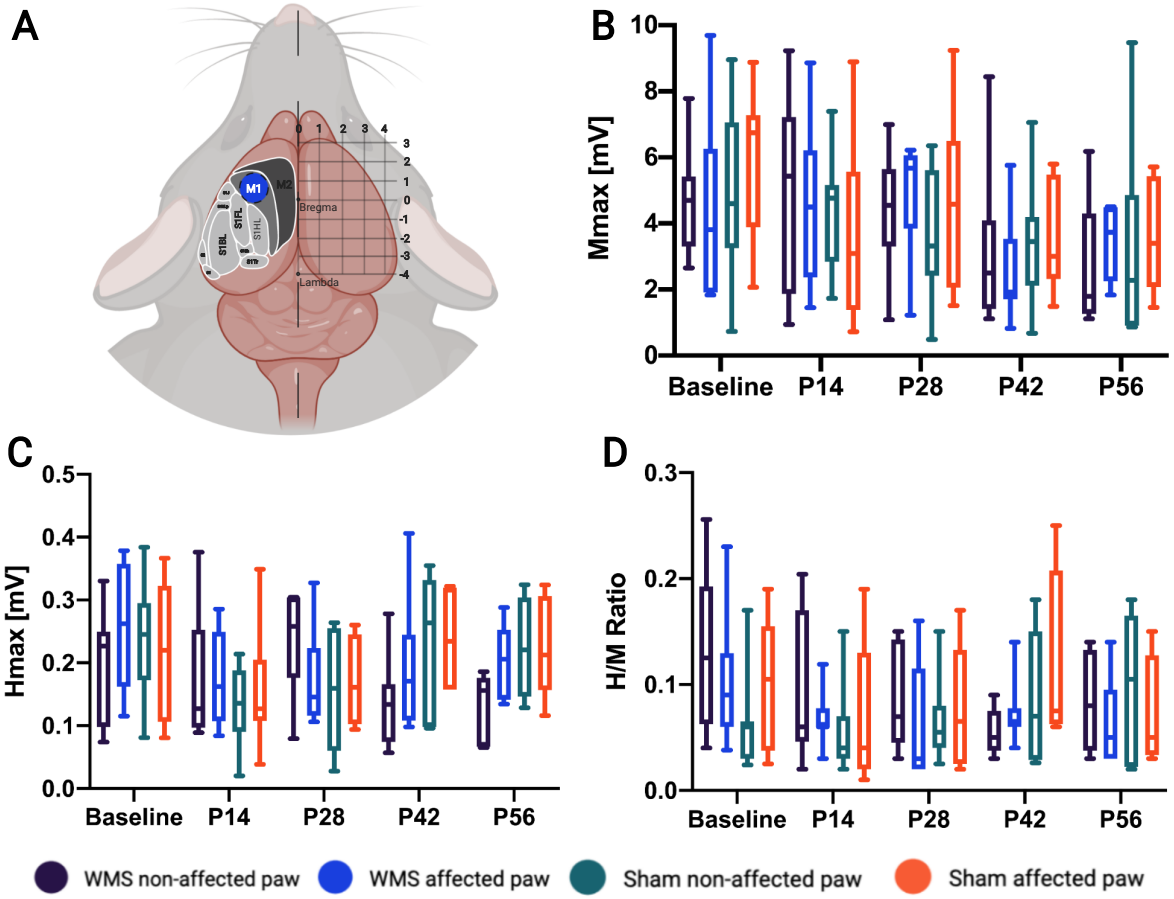

Figure 18 Transcutaneous measurement of the M-wave and H-wave after cortical photothrombosis within the MOp and sham operated animals. **(A)** Coordinates of cortical lesion by photothrombosis within the primary motor cortex (M1). **(B)** Amplitude of the M-wave, **(C)** H-wave after 0.1 Hz stimulation, and the **(D)** H/M ratio. MOp affected and non-affected n=20 each, Sham affected and non-affected n=15 each, 15 technical replicates for each forepaw. Data are shown as mean ± SD.

To verify the transcutaneous measurements of animals with MOp lesions (Figure 19 A), M-wave, H-wave, and H/M ratio were additionally conducted by direct nerve measurement measurements at 14, 28, and 56 days after stroke. The direct nerve measurement of the M-wave at day 14 shows a maximum amplitude of 1-7 mV and at the following recording points (P28 and P56) an amplitude of 1-5 mV (Figure 19 B). The H-wave at the direct nerve measurement varies between 0.01-0.35 and no statistical difference was observed between the stroke and sham animals (Figure 19 C). The H/M ratio showed a ratio of 0.2-0.15 overtime without being statistically significant (Figure 19 D).

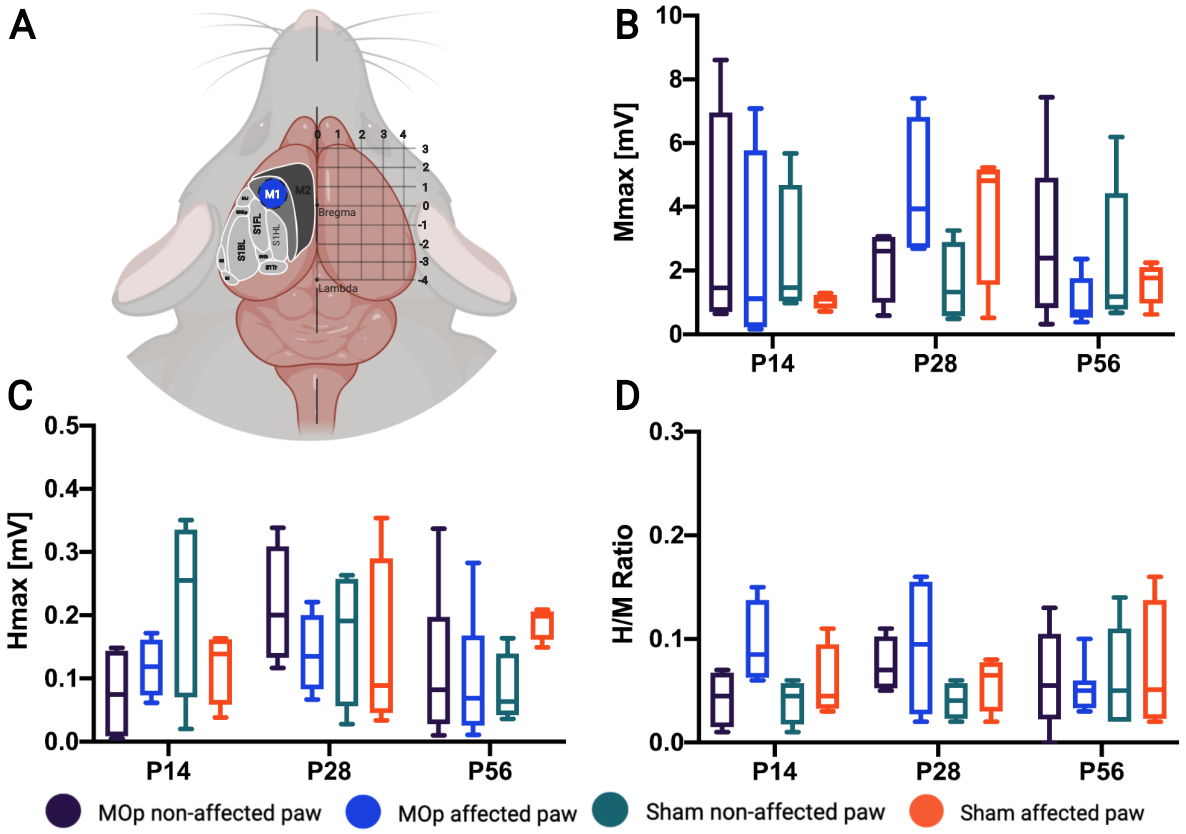

Figure 19 Direct nerve measurement of the M-wave and H-wave after cortical photothrombosis within the MOp and sham-operated animals. **(A)** Coordinates of the cortical lesion by photothrombosis within the primary motor cortex (M1). **(B)** Amplitude of the M-wave, **(C)** H-wave after 0.1 Hz stimulation, and the **(D)** H/M ratio. Stroke=8, Sham=5, 15 technical replicates for each forepaw. Data are shown as mean ± SD.

In the following experiments, cortical photothrombosis was induced within the secondary motor area (MOs, Figure 20 A). Transcutaneous electrophysiological measurements were done in stroke and sham animals as described before at baseline as well as on 14, 28, 42, and 56 days after stroke. Over the entire measurement period, the amplitude of the M-Wave did not change significantly in both, affected and non-affected forepaws of stroke or sham animals (Figure 20 B). The amplitude of the H-wave within the affected forepaw increased already 14 days after stroke and is significantly higher at P42 ($p<0.001$) as well as at P56 ($p<0.001$) than at baseline (Figure 20 C).

A significant increase of the H/M ratio in relation to baseline was observed in the affected forepaw after MOs lesion starting at P14 ($p<0.05$) until P56 ($p<0.001$), whereas all other groups showed no increase of the H/M ratio (Figure 20 D).

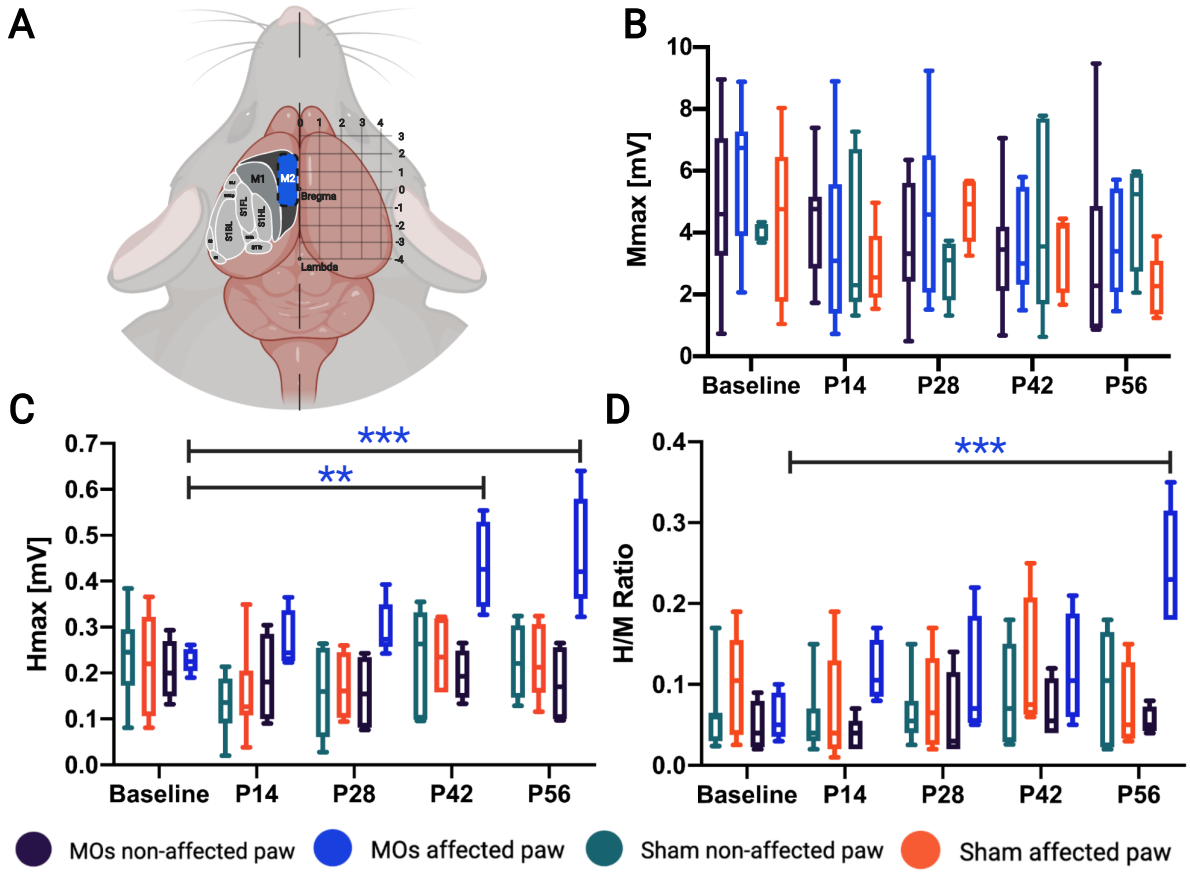

Figure 20 Transcutaneous measurement of the M-wave and H-wave after photothrombosis within the MOs and sham-operated animals. **(A)** Coordinates of the cortical lesion by photothrombosis within the secondary motor cortex (M2). **(B)** Amplitude of the M-wave, **(C)** H-wave after 0.1 Hz stimulation, and **(D)**) H/M Ratio. Stroke=8, Sham=15, 15 technical replicates for each forepaw. Two-way ANOVA, Tukey comparison to baseline: $p<0.05$(*), $p<0.01$(**), $p<0.001$(***).

After photothrombosis within the MOs (Figure 21 A), the M-wave, H-wave, and H/M ratio were measured with the direct nerve method. The M-wave in the stroke and sham group varied between 1-7 mV (Figure 21 B). In the stroke group, an increased H-wave was measured at the affected forepaw, which was higher than the amplitude of the H-wave in the sham group ($p<0.001$, Figure 21 C). The increased H-wave in the forepaw of stroke animals was also reflected in the H/M ratio on P56, compared to the unaffected forepaw and sham group ($p<0.001$, Figure 21 D).

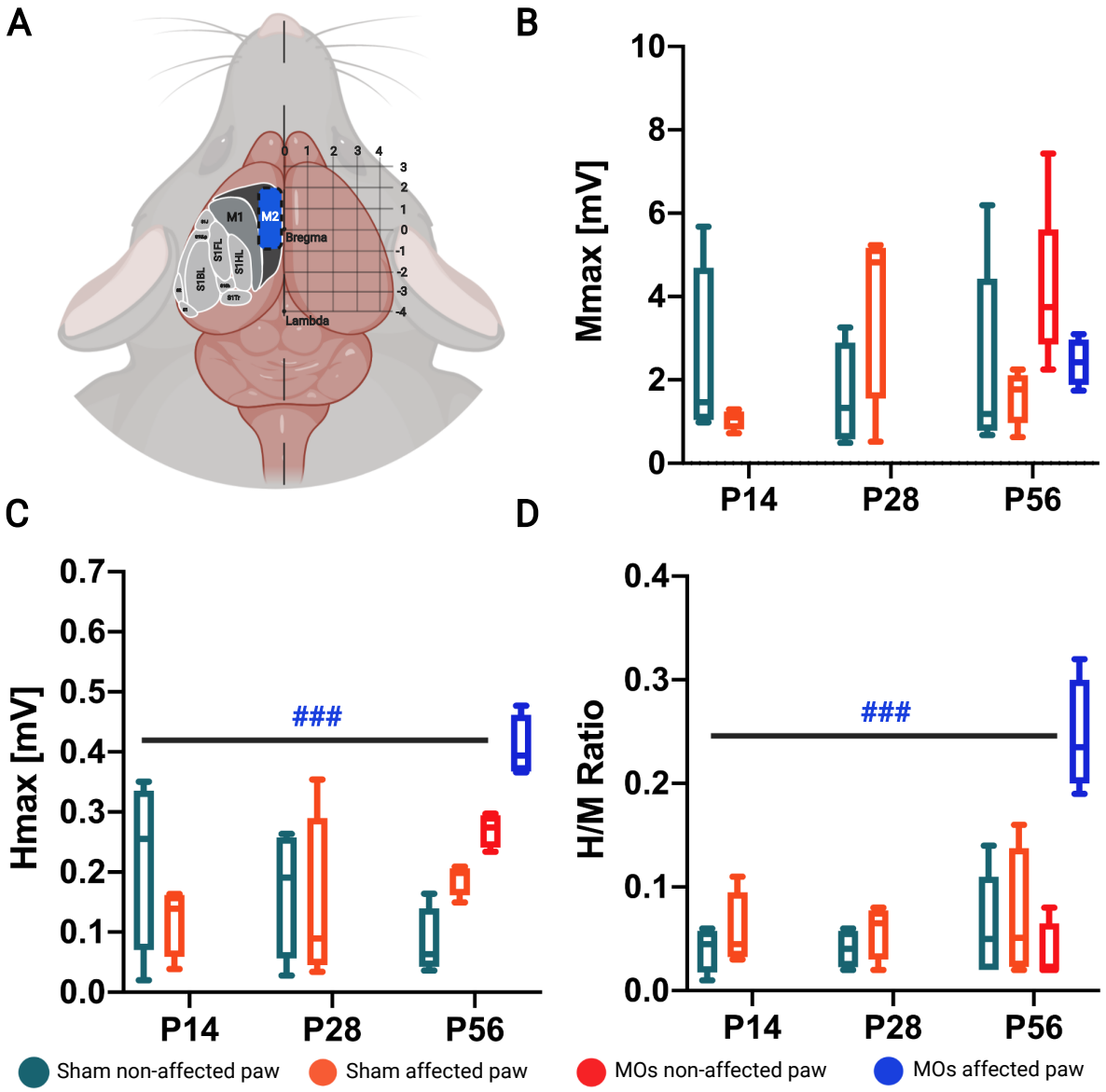

Figure 21 Direct nerve measurement of the M-wave and H-wave after photothrombosis in MOs and sham operated animals. **(A)** Coordinates of cortical stroke lesion within the secondary motor cortex (M2). **(B)** Amplitude of the M-wave, **(C)** H-wave after 0.1 Hz stimulation, and the **(D)** H/M Ratio. Stroke=4, sham=4, 15 technical replicates for each forepaw. Data shown as mean ± SD. Two-way ANOVA, Tukey comparison between groups: $p<0.05$(#), $p<0.01$(##), $p<0.001$(###).

As no increase of the H-wave occurred after a lesion by photothrombosis within the MOp (Figure 18 & Figure 19) and only a minor increase after a lesion within the MOs (Figure 20 & Figure 21) on P56, an alternative stroke model was explored to damage the majority of ascending and descending motor tracts. As a result, internal capsule strokes (ICS) were induced, using a modified photothrombosis (Figure 11). After ICS, there was no significant change in the amplitude of the M-wave at baseline, and 14, 28, 42, and 56 days after stroke (Figure 22 B). As early as P28, the amplitude of the H-wave increased in the affected forepaw compared to the unaffected paw of the same group ($p=0.0684$, Figure 22 C). The measured H-wave after ICS in the affected forepaw further increased at P42 and was significantly higher compared to the sham group ($p<0.001$). At P56, the H-wave was significantly increased compared to the non-affected paw after ICS ($p<0.001$) and to the sham group ($p<0.001$). In the H/M ratio, the increase of the H-wave in relation to the M-wave was already observed 14 days after ICS ($p=0.0344$), and increased continuously until P56 ($p<0.001$, Figure 22 D).

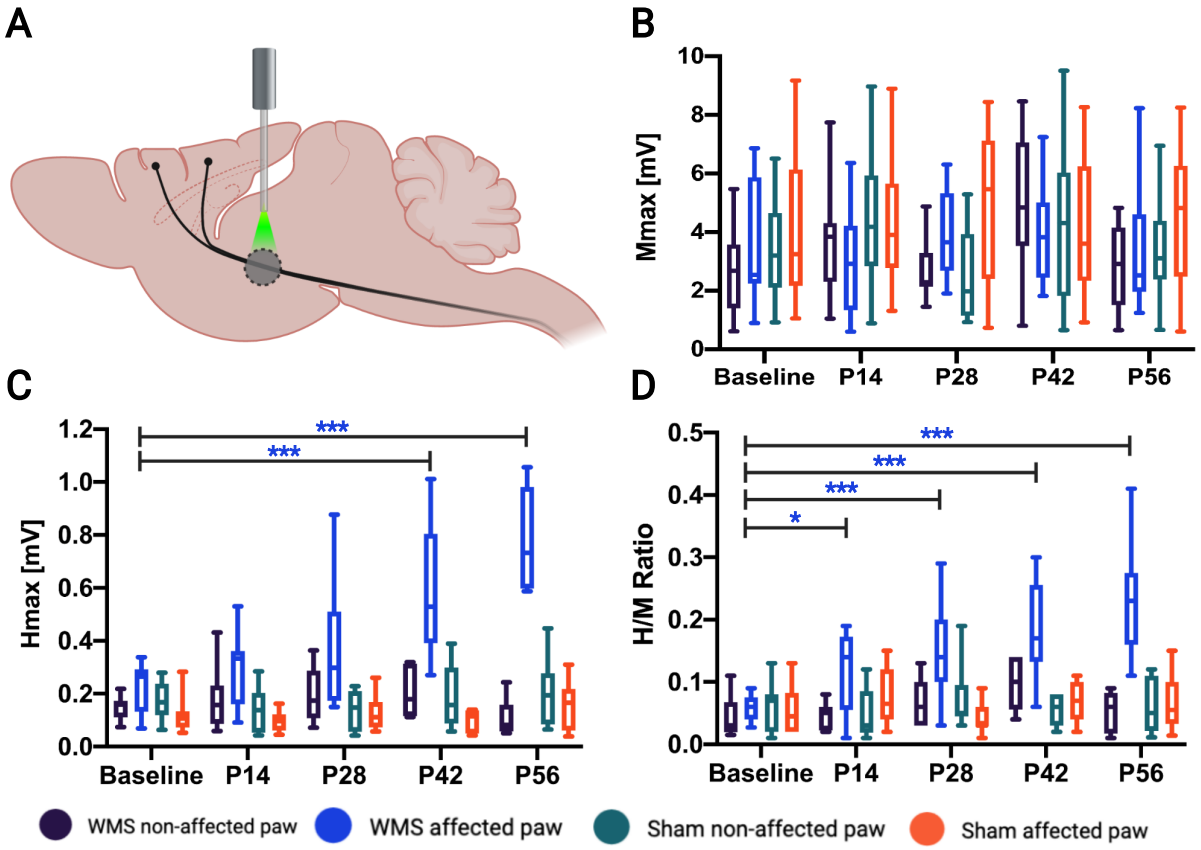

Figure 22 Transcutaneous measurement of the M-wave and H-wave after internal capsule stroke and sham operated animals. (A) Direct nerve measurement of the M-wave **(B)**, H-wave with 0.1 Hz stimulation **(C)** and **(D)** the H/M Ratio. Stroke=11, sham=12, 15 technical replicates for each forepaw. Data shown as mean ± SD. Two-way reapeated ANOVA, Tukey comparison to baseline: $p<0.05$(*), $p<0.01$(**), $p<0.001$(***).

The direct nerve measurement at P28 and P56, respectively, showed a M-wave between 2-7 mV at P28 and 1-3 mV at P56 (Figure 23 B). Measurement of the H-wave at the affected forepaw at P28 showed a significant increase compared to the non-affected forepaw ($p<0.001$) and to the sham group (sham non-affected forepaw $p<0.0001$, sham affected forepaw $p<0.001$, Figure 23 C). At P56, the H-wave of the affected forepaw in the stroke group was strongly increased compared to the non-affected forepaw, as well as against the sham group ($p<0.001$). The increase of the H-wave was also reflected in the H/M ratio, which at P28 was significant to the non-affected forepaw according to ICS ($p<0.05$) as well as to the sham group (non-affected forepaw $p<0.001$, affected forepaw $p=0.01$, Figure 23 D).

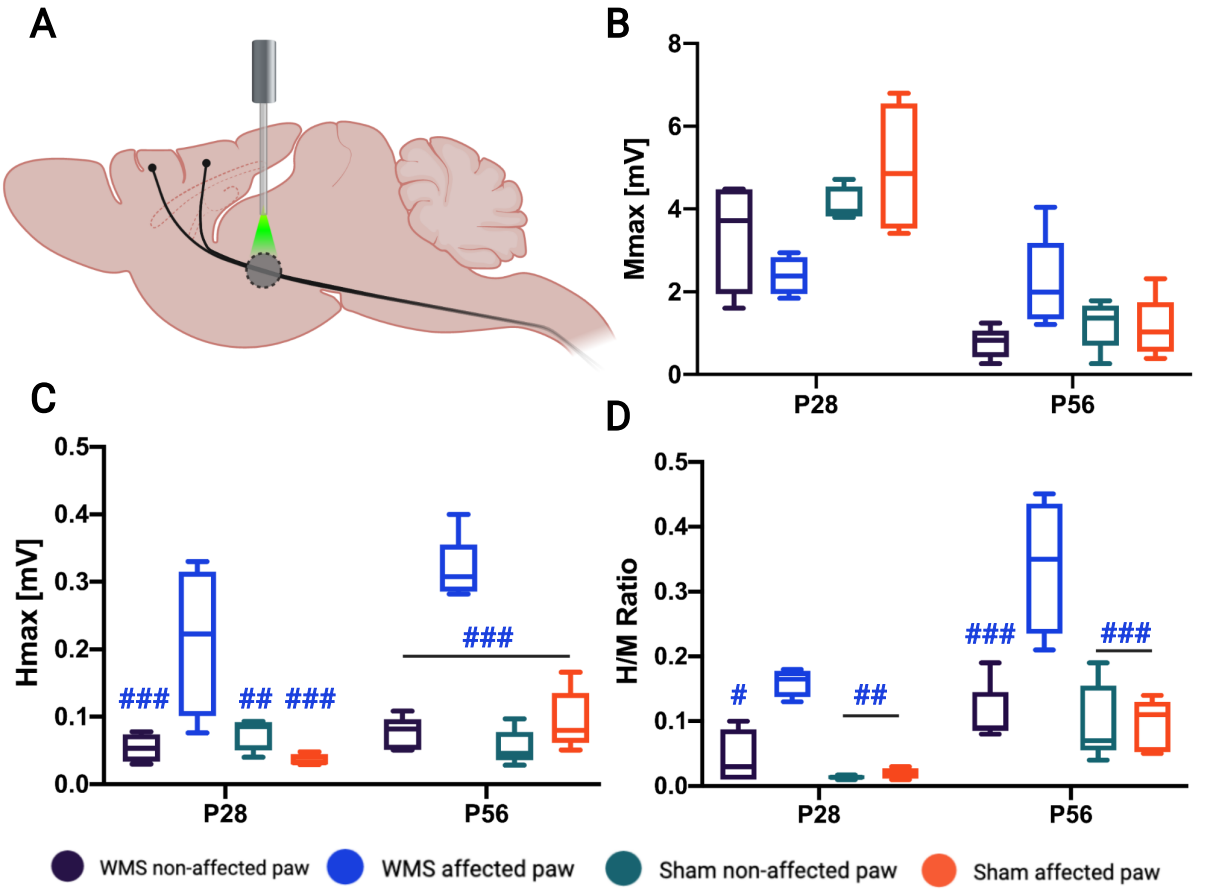

Figure 23 Direct nerve measurement after ICS and sham operated animals. **(A)** Transcutaneous electrophysiological measurement of the M-wave **(B)**, H-wave with 0.1 Hz **(C)**, and **(D)** the H/M Ratio. ICS affected and non-affected on P28 n=4 and on P56 n=5 each. Sham affected and non affected n=4 on P28 and n=5 on P56 each, 15 technical replicates for each forepaw. Data shown as mean ± SD. Two-way ANOVA, Tukey comparison between groups: $p<0.05$(#), $p<0.01$(##), $p<0.001$(###).

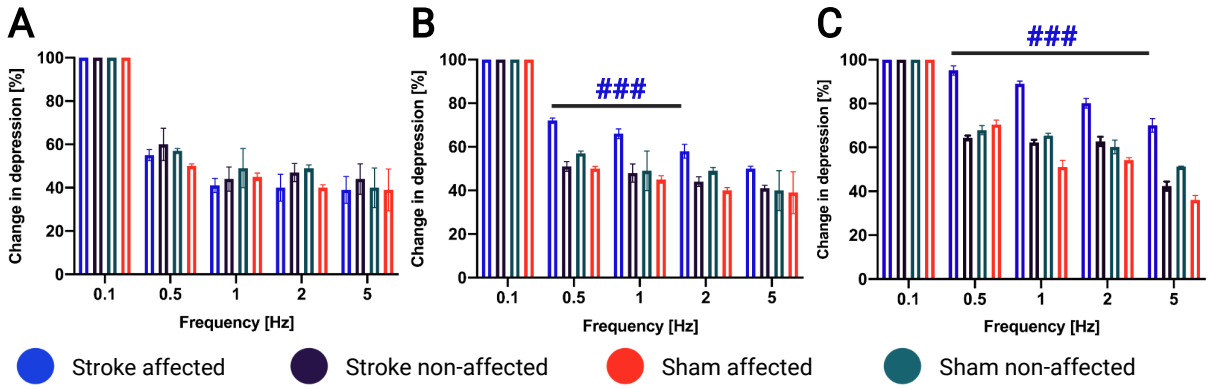

Figure 24 Changes of rate-dependent depression 56 days after photothrombosis within the MOp, MOs or internal capsule. Transcutaneous stimulation with different frequencies revealed different rate-dependent depression of the H-wave 56 days after photothrombosis in the MOp (**A**), or MOs (**B**), and ICS (**C**). MOp=11/sham=8, MOs=8/sham=8, ICS=12/sham=11, 15 technical replicates for each forepaw. Data shown as mean ± SD. Two-way ANOVA, Tukey comparison between groups: $p<0.05$(#), $p<0.01$(##), $p<0.001$(###).

In addition to the H/M ratio, the rate-dependent depression (RDD) was calculated from measurements at different frequencies (0.1, 0.5, 1, 2, 5 Hz), which leads to a frequency-dependent suppression of the H-wave in healthy animals. All values were normalized to 0.1 Hz to validate the percent change in the RDD. As shown in Figure 24 A, photothrombosis within the MOp 56 days after lesion does not lead to any changes in RDD compared with the non-affected forepaw or sham-operated animals. The lesion within the secondary motor area leads to a significantly decreased depression of the RDD at 0.5, 1, and 2 Hz ($p<0.001$), which is no longer detectable at a frequency of 5 Hz (Figure 24 B). 56 days after ICS, a lower frequency-dependent suppression of the H-wave was measured within the affected forepaw ($p<0.001$, Figure 24 C).
To further evaluate the amount of reduced RDD after ICS, direct nerve measurements were further evaluated 28 and 56 days after Figure 25. It was found that in animals with ICS the H-wave was significantly increased compared to the sham group on P28 ($p<0.01$/$p<0.001$) and on P56 ($p<0.001$). A reduced RDD at direct nerve measurement stimulation with 0.1 Hz (Figure 25 A), 0.5 HZ (Figure 25 B), 1 Hz (Figure 25 C), 2 Hz (Figure 25 D), and 5 Hz (Figure 25 E) revealed the severity of internal capsule stroke and the loss of inhibitory circuits.

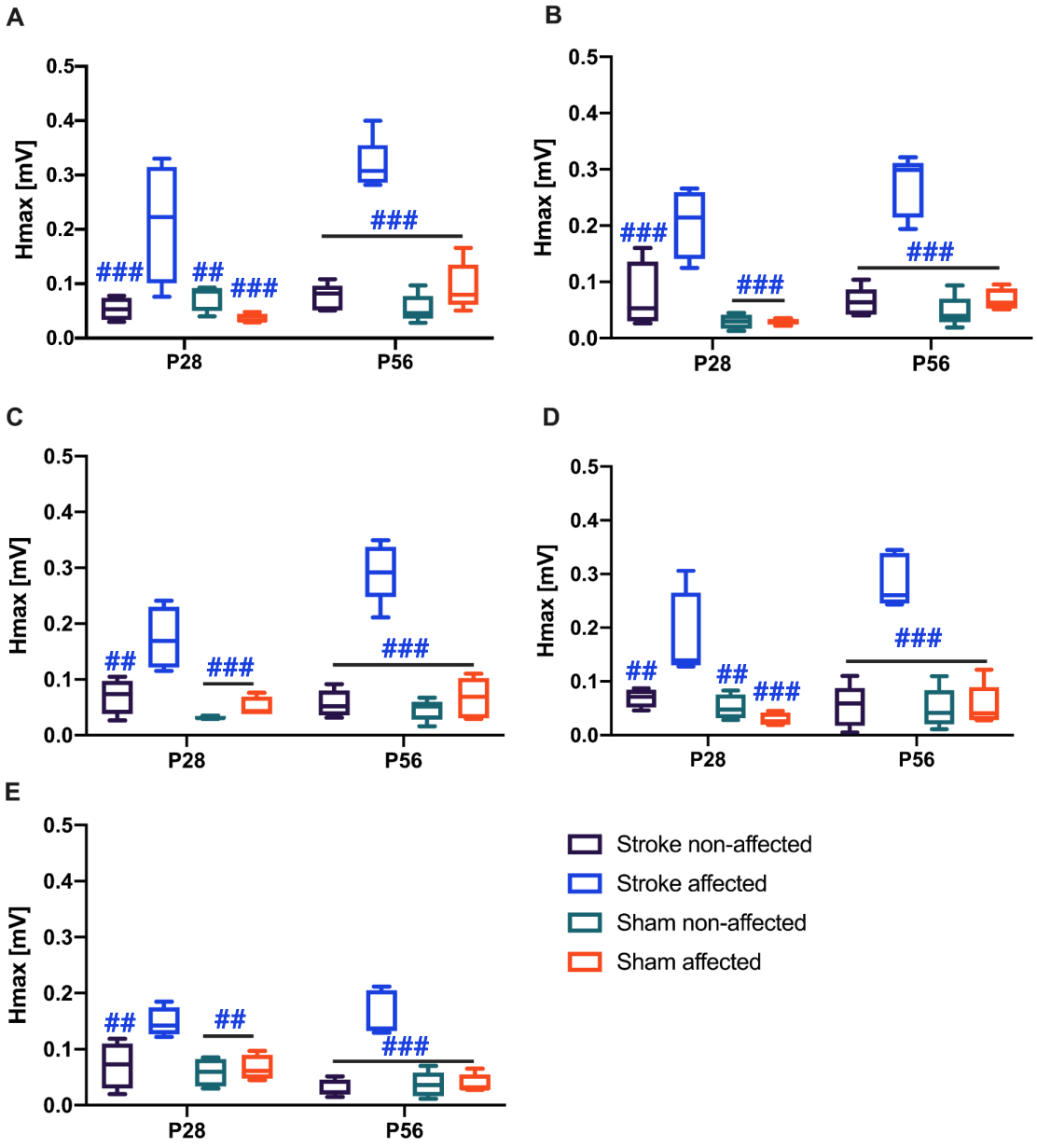

Figure 25 Decreased rate-dependent depression after internal capsule stroke. Direct nerve measurement of H-wave at 28 and 56 after internal capsule stroke. Animals were stimulated at 0.1 Hz (**A**), 0.5 Hz (**B**), 1 Hz (**C**), 2 Hz (**D**), and 5 Hz (**E**), respectively. This revealed that the RDD in the forepaw after internal capsule stroke was lower than in the control groups. ICS=5, Sham=5, 15 technical replicates for each forepaw. Data are shown as mean ± SD. Two-way ANOVA, Tukey comparison between groups: $p<0.05$(#), $p<0.01$(##), $p<0.001$(###).

6.3 Behavioral changes after cortical and subcortical stroke

These results were in part already published in:

Aswendt, Pallast, Wieters et al., Translational Stroke Research, "Lesion Size - and Location-Dependent Recruitment of Contralesional Thalamus and Motor Cortex Facilitates Recovery after Stroke in Mice" (2020)

The results of the quantitative electrophysiological measurements provided strong evidence that spasticity occurs in MOs and internal capsule stroke but not after MOp lesions. The following analysis of sensorimotor behavior tests was done with the aim to establish a portfolio of sensitive measurement methods in the acute and chronic phase after stroke and to evaluate if signs of post-stroke spasticity can be differentiated to motor impairments.

6.3.1 Strokes in MOp and MOs show analogous sensorimotor changes

In a first set of experiments, the influence of lesion size was evaluated by applying the small & large stroke protocol Table 2, and sensorimotor deficit were measured with the rotating beam (Figure 26 A), cylinder test (Figure 26 B), and grid walk test (Figure 26 C) additional to other behavior tests Figure 42. The animals with large strokes had a higher deficit than the small stroke group as measured by hind limb drops ($p<0.001$, Figure 26 A), paw drags ($p<0.01$, Figure 26 B), and foot faults ($p<0.001$, Figure 26 C).

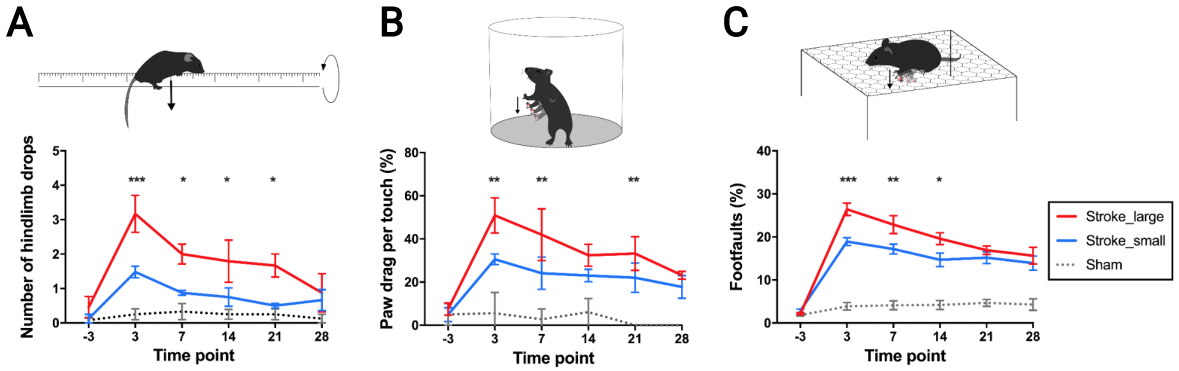

Figure 26 Behavioral deficits after small & large photothrombosis protocols compared to sham animals. (**A**) Number of hindlimb drops during the rotating beam, (**B**) percentage of paw drags of the affected paw during cylinder test, and (**C**) number of foot faults of the affected forepaw during the grid walk test. Stroke=4, sham=4. Data are shown as mean ± SEM. Two-way ANOVA, Tukey comparison between groups at the same time point shown as $p<0.05$(*), $p<0.01$(**), and $p<0.001$(***)

In comparison, the animals that received the small stroke protocol showed an increase of hind limb drops, which was no longer different from the sham group at P21 and the large stroke group at P28 (Figure 26 A). In the cylinder test, a significant difference between small and large stroke was detected at P3, P7, and P21 (Figure 26 B). All post-stroke time points were significantly different between the stroke and sham animals. The animals with a small stroke indicate after the initial deficit of P3 only a small degree of recovery compared to the large stroke group. The number of foot faults in the grid walk test also revealed a deficit in sensorimotor function in the small stroke group, which also remained relatively constant from 3 days after photothrombosis until P28 (Figure 26 C). In the animals with large stroke, after the initial deficit at P3, a continuous reduction of foot faults was observed, whereby at P3 ($p<0.001$), P7 (<0.01), and P14 ($p<0.05$) a distinction was possible between the small and large stroke group.

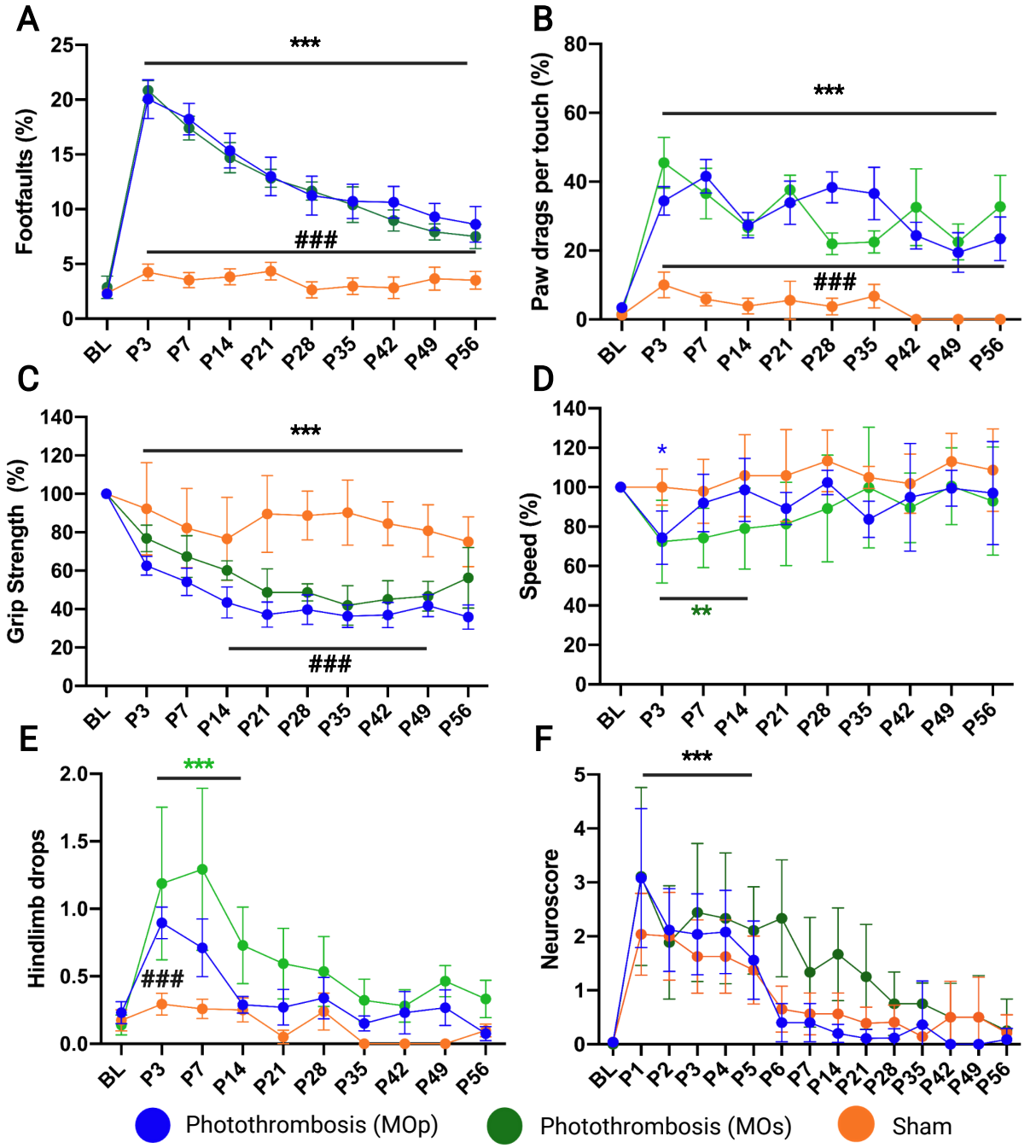

Figure 27 Behavioral changes after photothrombosis within MOp or MOs. (**A**) Number of foot faults in the grid walk test, and (**B**) paw drags during cylinder test over the observation period of 56 days after cortical lesion. (**C**) Development of the grip strength. Changes of speed (**D**) and (**E**) hindlimb drops during the rotating beam test. (**F**) Neuroscore to assess neurological and motor deficits after cortical photothrombosis. Data are shown as mean ± SD. MOp=30, MOs=9, sham=17. Two-way ANOVA, Tukey comparison: significant differences between groups (#) and time points (*) were shown as $p<0.05$ (#/*), $p<0.01$ (##/**), $p<0.001$ (###/***).

To further evaluate the effects of lesion location, the large cortical lesion within the MOp was compared with a lesion in the MOs (Table 2). Independent on the lesion location and despite a continuous improvement over time, the functional deficit, i.e. the number of foot faults in the grid walk test, was significantly increased until P56 compared to baseline and sham, respectively ($p<0.001$, Figure 27 A). Further sensorimotor deficits appeared based on paw drags per touch in the cylinder test (Figure 27 B). At P3 and P7, the MOp as well as the MOs stroke group showed a significantly increased number of paw drags compared to baseline ($p<0.001$). A significant difference between the stroke and the sham group was observed from P3 to P56 ($p<0.001$). With the grip strength test, a delayed development of deficit, compared to the sham group, was measured in stroke animals only from P14 to P49 ($p<0.001$, Figure 27 C). The strength of the sham-operated animals decreased not significantly over the entire observation period and reached 80% at P56. Compared to baseline, the grip strength of the MOp and MOs animals decreased significantly ($p<0.001$) continuously until P21 and remains relatively constant at about 50% from P21 to P56 (P3-P56, $p<0.001$, Figure 27 C). During the rotating beam test, there was a significant decrease in velocity within the MOp at P3 ($p<0.05$, Figure 27 D) and in the MOs group at P3-P14 ($p<0.01$). In the rotating beam a significant increase in hindlimb drops was observed in animals with a lesion within the MOp as well as MOs compared to the sham group at P3 ($p<0.001$, Figure 27 D), as well as at P3 and P7 to baseline ($p<0.001$). The neuroscore after lesion of the MOp as well as MOs increased to 3 at P1 until P5 to a neuroscore of 2, and decreased to almost 0 in the MOp stroke group until P6. The MOs stroke group needed until P56 to reach a comparable low neuroscore ($p<0.001$, Figure 27 F).

6.3.2 Strokes within the internal capsule result in severe impairment of sensorimotor properties

In addition to the cortical stroke models, sensorimotor behavior was characterized for animals with a internal capsule stroke (Figure 28). In the grid walk test, the stroke group showed a significantly increased number of foot faults from P3 to P56 compared to the baseline ($p<0.001$) and the sham group ($p<0.001$, Figure 28 A). After ICS, the sensorimotor properties are impaired immediately after the lesion as shown by the number of paw drags per touch during the cylinder test (Figure 28 B). In the cylinder test the number of paw drags per touch was significantly increased in the stroke group until P21 (P3 $p<0.001$, P7 $p<0.05$, P14 $p<0.01$, P21 $p<0.05$). The grip strength decreased after ICS as well as after sham surgery until P35 and further stabilized at approx. 80% in the sham group and approx. 50% in the stroke group (Figure 28 C). The grip strength in the ICS group decreased significantly from P14 to P56 compared to baseline ($p<0.001$) and reached lower values that the sham group only at P56 ($p<0.001$, Figure 28 C). In the rotating beam test, a significant reduction in velocity occurred over the entire observation period (Figure 28 D). During the rotating beam, an increased number of hindlimb drops up to P7 was detected in the animals with an ICS ($p<0.001$, Figure 28 E), which differed from the sham group at P3 ($p<0.001$). The neuroscore was significantly increased in the stroke group until P7 ($p<0.001$, Figure 28 F) and in the sham group until P5 ($p<0.001$) and the both group were thereby distinguishable until P2 ($p<0.05$).

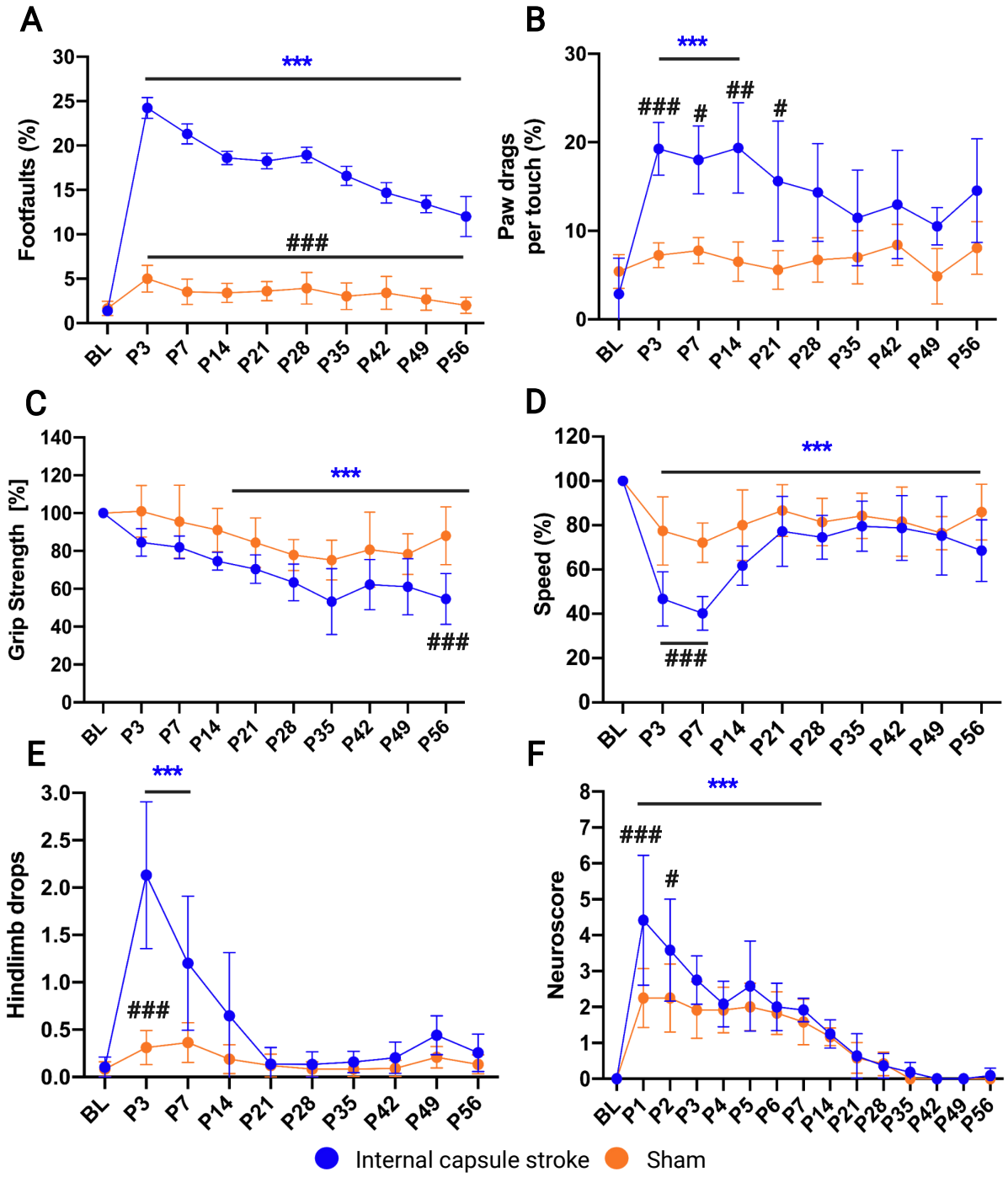

Figure 28 Behavioral changes after internal capsule stroke. (**A**) Number of foot faults in the grid walk test and (**B**) paw drags during cylinder test over the observation period of 56 days after internal capsule stroke.(**C**) Development of the grip strength. Changes of speed (**D**) and (**E**) hindlimb drops during the rotating beam test. (**F**) Neuroscore to assess neurological and motor deficits after ICS. Data are shown as mean ± SD. ICS and sham each n=12. Two-way ANOVA, Tukey comparison: significant differences between groups (#) and time points (*) were shown as $p<0.05$ (#/*), $p<0.01$ (##/**), $p<0.001$ (###/***).

6.3.3 Comparison of test sensitivity for motor deficits

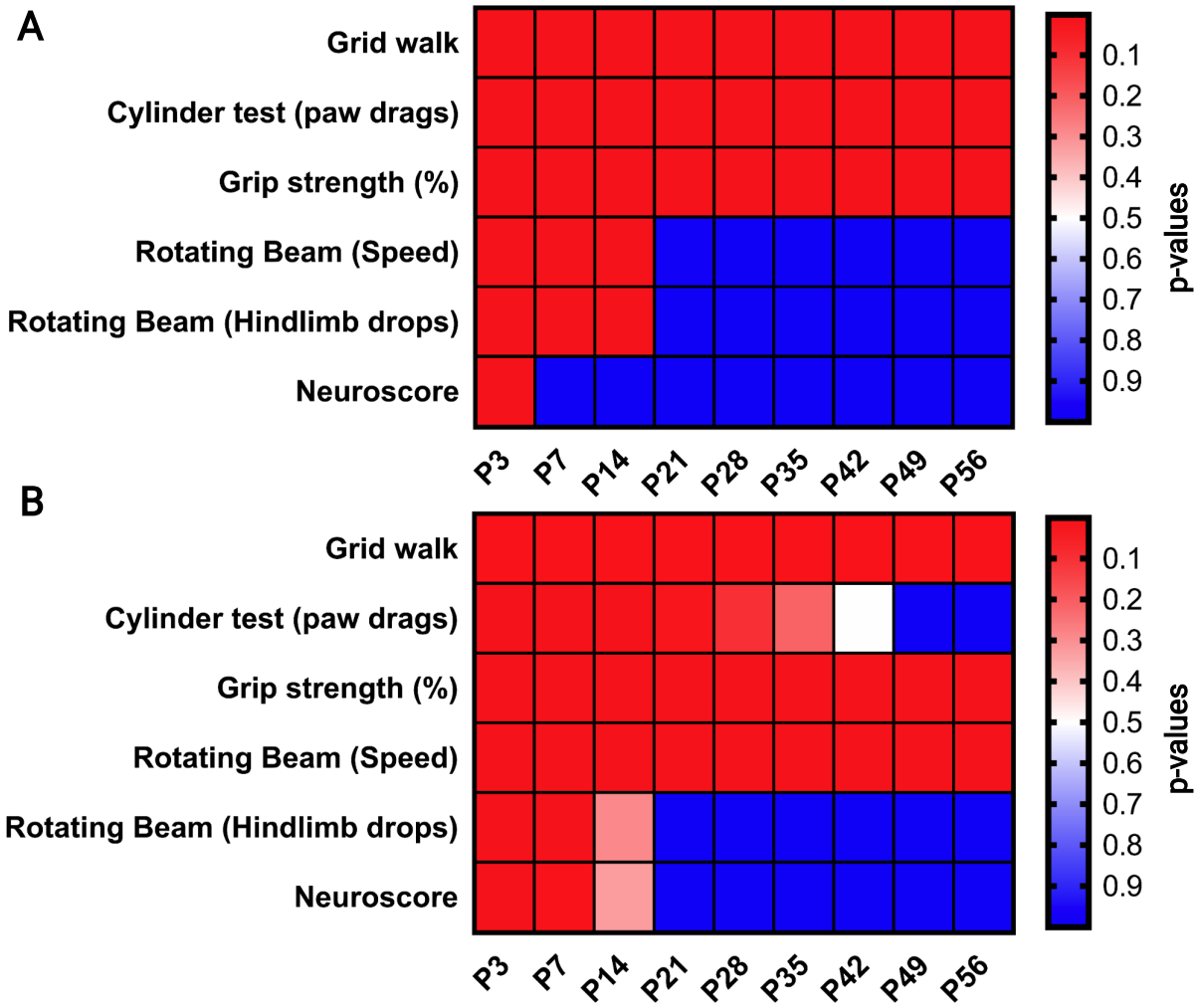

Figure 29 Sensitivity of behavioral tests after cortical and internal capsule stroke. (**A**) Sensitivity of the performed behavioral tests after cortical lesion by photothrombosis and (**B**) after ICS over 56 days after lesion. Sensitivity is described by the p-values of the statistically significant difference from baseline during behavior tests. Two-way ANOVA, Tukey comparison.

6.3.4 Correlation between behavior and electrophysiology

To further evaluate if spasticity is a relevant parameter affecting the sensorimotor deficits measured with the various behavior tests, the H/M ratio was correlated to the behavioral deficits, measured with the grid walk test, cylinder test and grip strength 56 days after stroke (Figure 30). Thereby the different stroke locations like in the primary motor area (Figure 30 A), secondary motor area (Figure 30 B) and internal capsule (Figure 30 C) were correlated with sensorimotor changes in the individual behavioral tests.

In animals with a internal capsule stroke, there was no correlation between the increased H-wave and the grid walk or grip strength data. However, the paw drags during the cylinder test correlated with the H-wave (r=0.73 Figure 30 A). After photothrombosis within the MOp, a small correlation between H/M ratio and paw drags in the cylinder test (r=0.64, p<0.05) were observed, but otherwise showed no correlation between grid walk test and grip strength (Figure 30 B). In contrast, photothrombosis in the MOs 56 days after induction leads to an increase in H-wave, which correlates negatively with grip strength (r=-0.67, p<0.01, Figure 30 C). This correlation is also reflected between the H/M ratio and grip strength (r=-0.71, p<0.01). However, the increase in H-wave did not show a statistical significant correlation with foot faults during the grid walk test (r=-0.42).

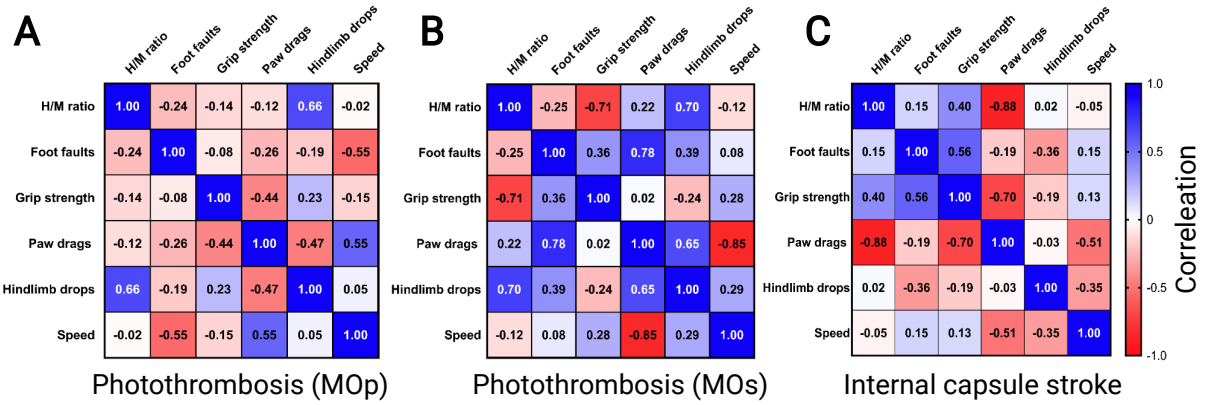

Figure 30 Correlation between behavior and electrophysiological changes after cortical and internal capsule stroke. Correlation, calculated with the Pearson correlation coefficient, between H-wave and behavioral changes 56 days after photothrombosis within the MOp (**A**), MOs (**B**), or ICS (**C**). (MOp=12, MOs=8, ICS=11).

The sensorimotor deficit score was used to assess behavioral changes in animals that did not develop spasticity or PSS during long-term observation. Animals that developed PSS due to ICS were found to recover worse than animals that developed PSS due to a lesion within the MOs (Figure 31 A). The groups differed from each other throughout the observation period (p<0.001). After a reduction of the deficit until P21 in both groups, animals with a ICS as well as a lesion within the MOs described a plateau phase until P42, after which the ICS did not recover significantly. The group with a lesion within the MOs showed further recovery from P42 to P56. In contrast, the animals that did not develop PSS during the observation period (Figure 31 B) showed better sensorimotor recovery.

Moreover, in animals without PSS the recovery progressed also at later time points, i.e. from P21 to P42. In animals with PSS (Figure 31 A), no significant difference between animals with MOs and ICS lesion can be observed, whereby the animals with a MOp lesion recover faster and differ from the MOs and ICS group significantly (P7-P42 $p<0.001$, P49-P56 $p<0.05$). The reduction between the animals that developed PSS after MOs or ICS was significantly different ($p<0.001$) from the recovery of the animals that did not develop PSS after strokes in the MOp, MOs or IC.

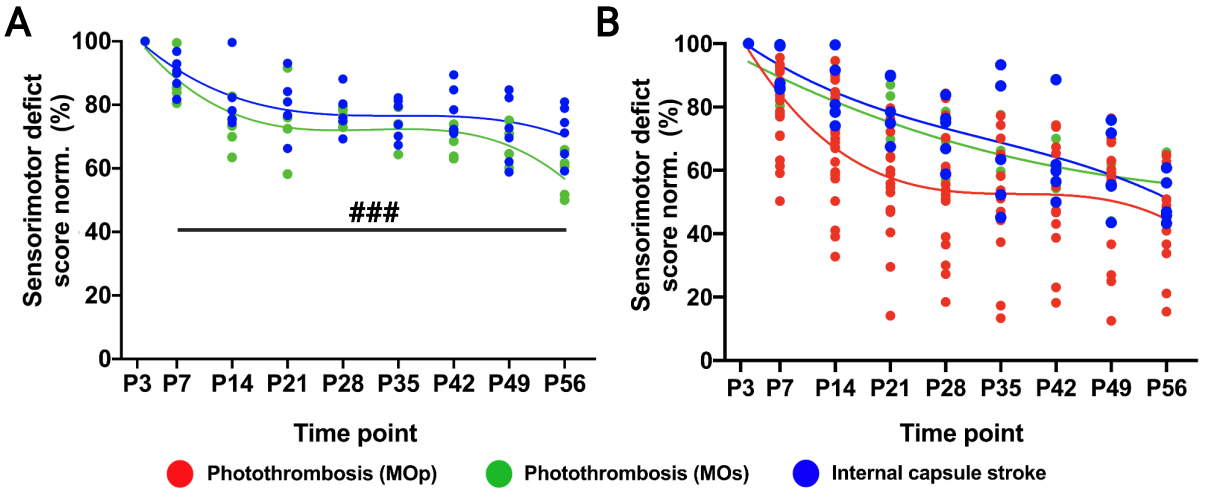

Figure 31 Sensorimotor deficit score of animals with PSS and without PSS after cortical or internal capsule stroke. (**A**) The sensorimotor deficit score was used to evaluate all animals with spasticity after a lesion within the MOs or internal capsule and their sensorimotor development. It can be seen that the animals recover worse after a ICS lesion than the animals with a lesion within the MOs. When the animals are further differentiated into PSS at P56 and (**B**) without PSS at P56 after MOp, MOs and ICS lesion, a different recovery is seen in the respective groups. (With PSS: MOs=6; ICS=8; Without PSS: MOp=28, MOs=3, ICS=4).

6.4 Structural changes after cortical and internal capsule stroke

Incidence map of lesion location and lesion size at day 1 and 7 after small and large photothrombosis protocol (Figure 32 A & D). To quantify the areas affected by the lesion, the affected regions seen in the T2 weighted images (T2WI) on days 1 and 7, as well as the histological on day 28 after photothrombosis were registered on the ARA. The localization within the small and large stroke group is homogeneous (Figure 32 A & D) and mainly affects only cortical regions and only to minor extent areas of the corpus callosum, striatum or hippocampus.

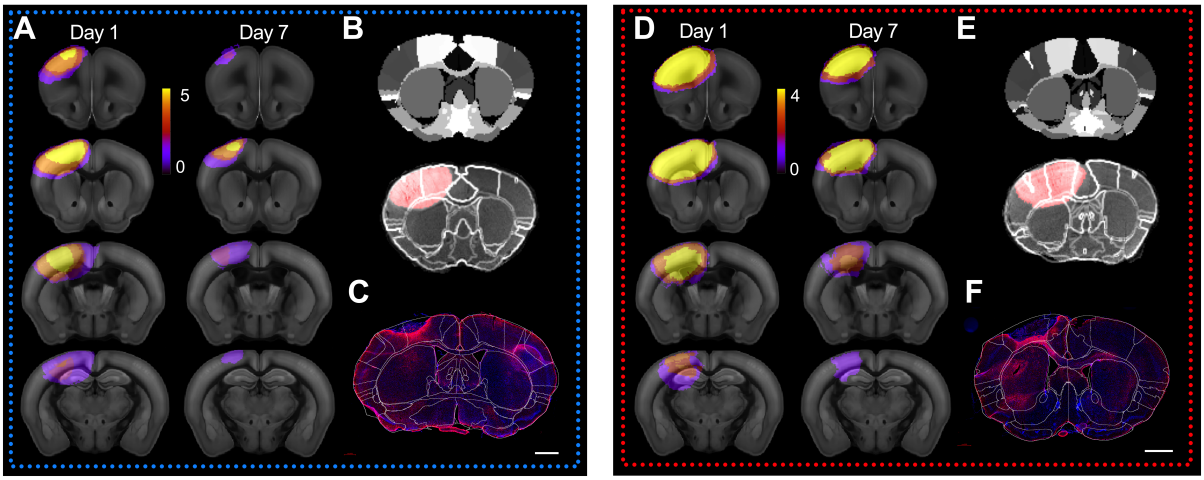

Figure 32 Incidence map of lesion location for two photothrombosis protocols resulting in small (blue) and large (red) lesions. (**A, D**) Stroke masks based on T2WI were averaged and plotted on the ARA **(B, E)**. The images show the maximum extent of the ischemic lesion 1 and 7 days after cortical photothrombosis. For further analysis of the long-term reactive astrogliosis brain sections after small (**C**) and large stroke (**F**) were landmark-based registered to the ARA (GFAP, red; DAPI, blue; Scale bar: 1 mm).

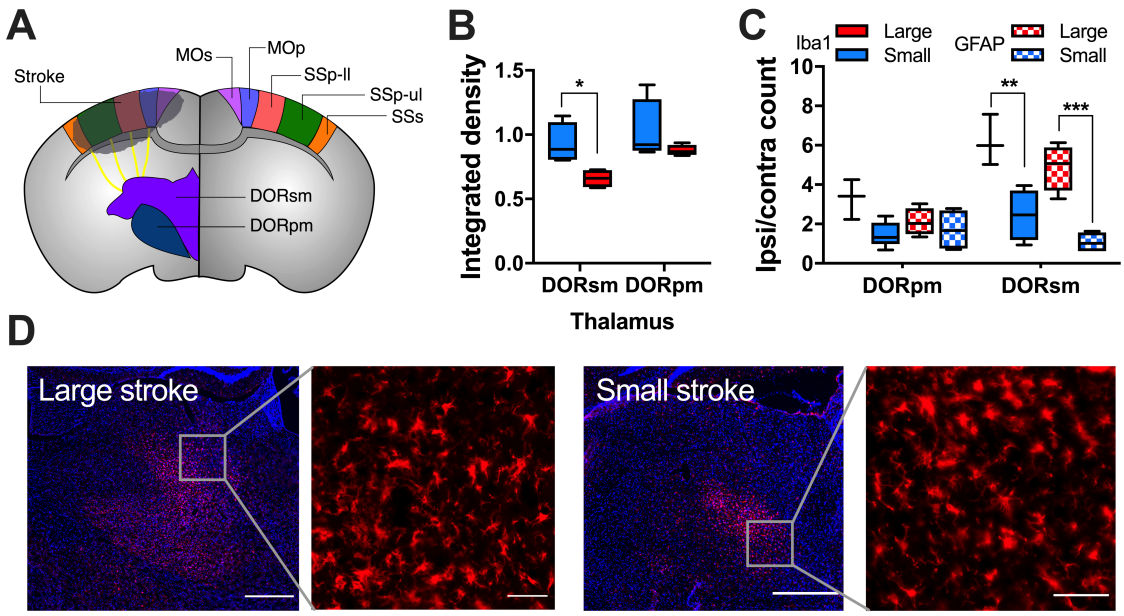

Figure 33 Secondary neurodegeneration after small & large cortical photothrombosis. (**A**) Thalamocortical fiber tracts between the sensory and motor cortex (MOp, MOs, SSp-ul/ll, and SSs) to the related parts of the thalamus (DORsm and DORpm). (**B**) Integrated density as the ratio between ipsilateral/contralateral for signal intensity and normalized to the region size for DORsm and DORpm. (**C**) Quantification for Iba1 and GFAP positive cells within the thalamus (DORsm and DORpm) 28 days after stroke. (**D**) Representative immunofluorescence microscopy of coronal sections of the thalamus (red, Iba1$^+$; blue, DAPI; Scale bar: 500 µm and 50 µm).

The Figure 33 A shows a selection of thalamocortical fiber tracts between the sensorimotor cortex (MOs, MOp, SSP ll/ul/ul, SSs) and the respective areas of the thalamus (DORsm and DORpm). After a small and large cortical stroke, secondary neurodegeneration progresses to different extents in the respective animals. This can be determined by the integrated density (ratio ipsilateral/contralateral for signal intensity normalized to the region size) measured in the T2WI (Figure 33 B). In the DORsm of animals with a small stroke, the integrated density is lower than in animals with a large stroke. Also within the DORpm, a higher integrated density is measurable in animals with a small stroke than in animals with a large stroke, but this is not statistically significant.

To further evaluate the effects of secondary neurodegeneration, Iba$^+$ (microglia/macrophages) and GFAP$^+$ (astrocytes) were quantified within the DORpm and DORsm and the ipsilateral side was related to the contralateral side (Figure 33 C). Within the DORpm there is no significant difference in Iba1$^+$ and GFAP$^+$ cells between the groups. In contrast, animals with a large stroke within DORsm show a significantly increased number of astrocytes and microglia/macrophages compared to the small stroke group. (Figure 33 D shows representative immunofluorescence microscopy images of coronal sections of the thalamus (red, Iba1$^+$; blue, DAPI; Scale bar: 500 µm and 50 µm).

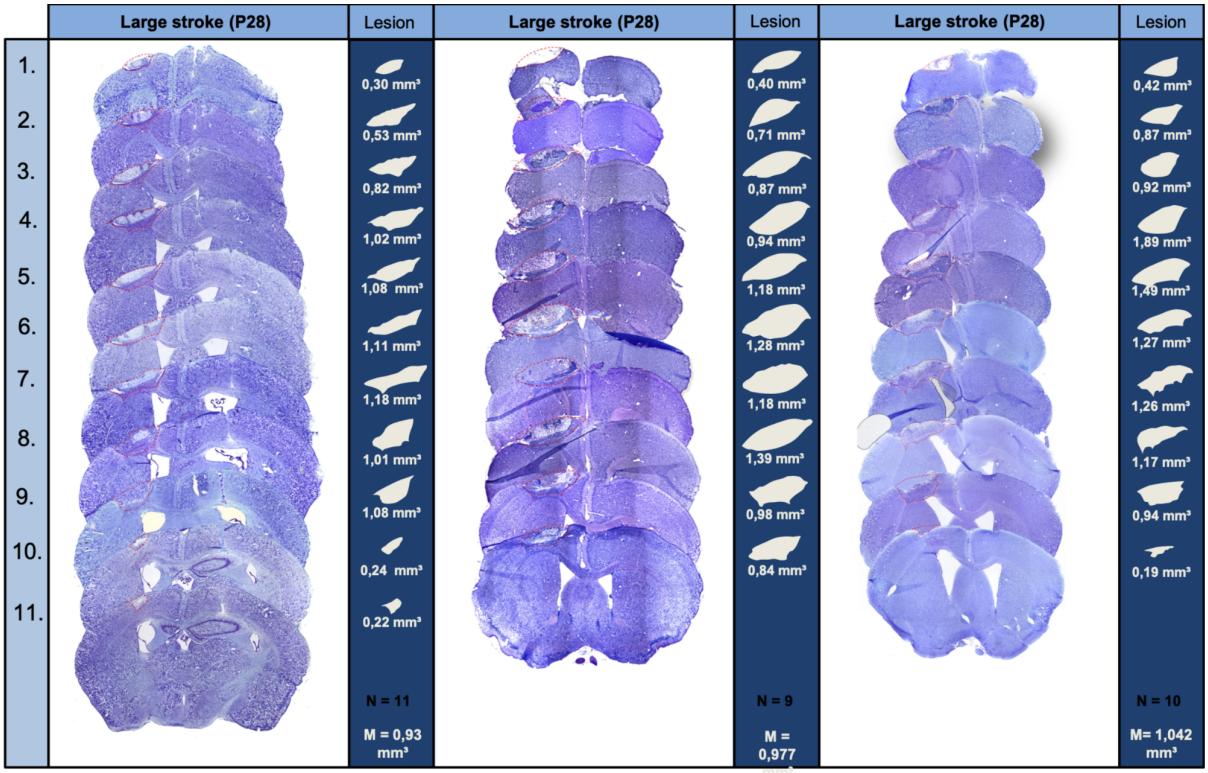

Figure 34 Exemplary nissl brain stainings 28 days after large photothrombotic stroke. Lesions are outlined with red dashed circles in each section. Lesion volumes in mm^3 were indicated from each section and how many sections were included for each calculation (N). M is the mean value of the lesion volumes in mm^3 per animal. (Nissl stainings and microscopy were performed by Alina Jakobs during an internship in the Aswendt laboratory in 2019)

To further evaluate lesion size 28 days after application of the large photothrombosis protocol, every fifth section with a lesion was stained with nissl (Figure 34). For each section, a stroke mask was drawn and lesion size was calculated. In addition, the total number of sections used (N) and the average lesion size (M) were calculated. It can be seen that the lesion size 28 days after the large stroke differs only marginally.

Looking at the lesion size of animals with small stroke using nissl staining (Figure 35) at different time points (P7, P14, P21, P28), it can be seen that within the first 7 days there is a swelling of the lesion (M = 2.02 mm^3) and with time it becomes smaller until the lesion on day 28 is only 0.19 mm^3 in size.

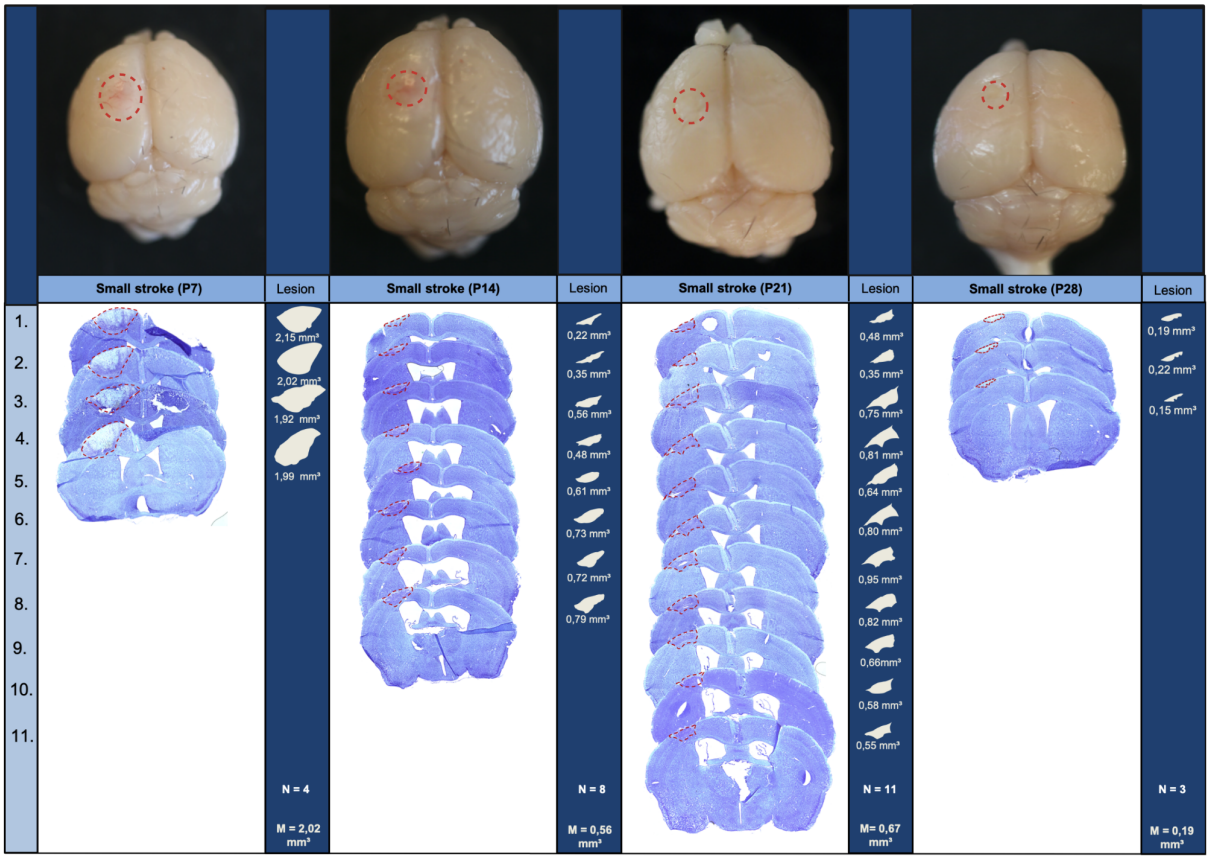

Figure 35 Nissl stainings on different time points after small stroke. Nissl staining 7, 14, 21, and 28 days after small photothrombosis protocol. Lesions are outlined with red dashed circles in each section. Lesion volumes in mm^3 were indicated from each section and how many sections were included for each calculation (N). M is the mean value of the lesion volumes in mm^3 per experimental animal. (Nissl stainings and microscopy were performed by Alina Jakobs during an internship in the Aswendt laboratory in 2019.)

To validate the structural changes after cerebral ischemia, animals received injections of biotinylated dextran amine (BDA) into the contralesional thalamus 21 days after stroke. The ipsilesional BDA injection was used to visualize the thalamo-cortical connection to the areas affected by the stroke. The injections mainly marked the polymodal association cortex related part of the thalamus (DORpm) and less the sensory-motor cortex related part of the thalamus (DORsm) (Figure 36 A, $p<0.001$). To get a more precise statement about the distribution of the BDA from the DORpm within the contralesional hemisphere, these were normalized to the ipsilesional hemisphere (Figure 36 B). The fluorescence intensity in the target regions of the thalamus (SSp-upper limb, MOp, MOs) varied strongly and was highest in the contralesional MOp (Figure 36 C, $p<0.001$). The performed injections thus provided the basis for further injections (e.g. recombinant adeno-associated virus) to visualize the structural changes after cortical lesion in the contralesional thalamus (Figure 36 D).

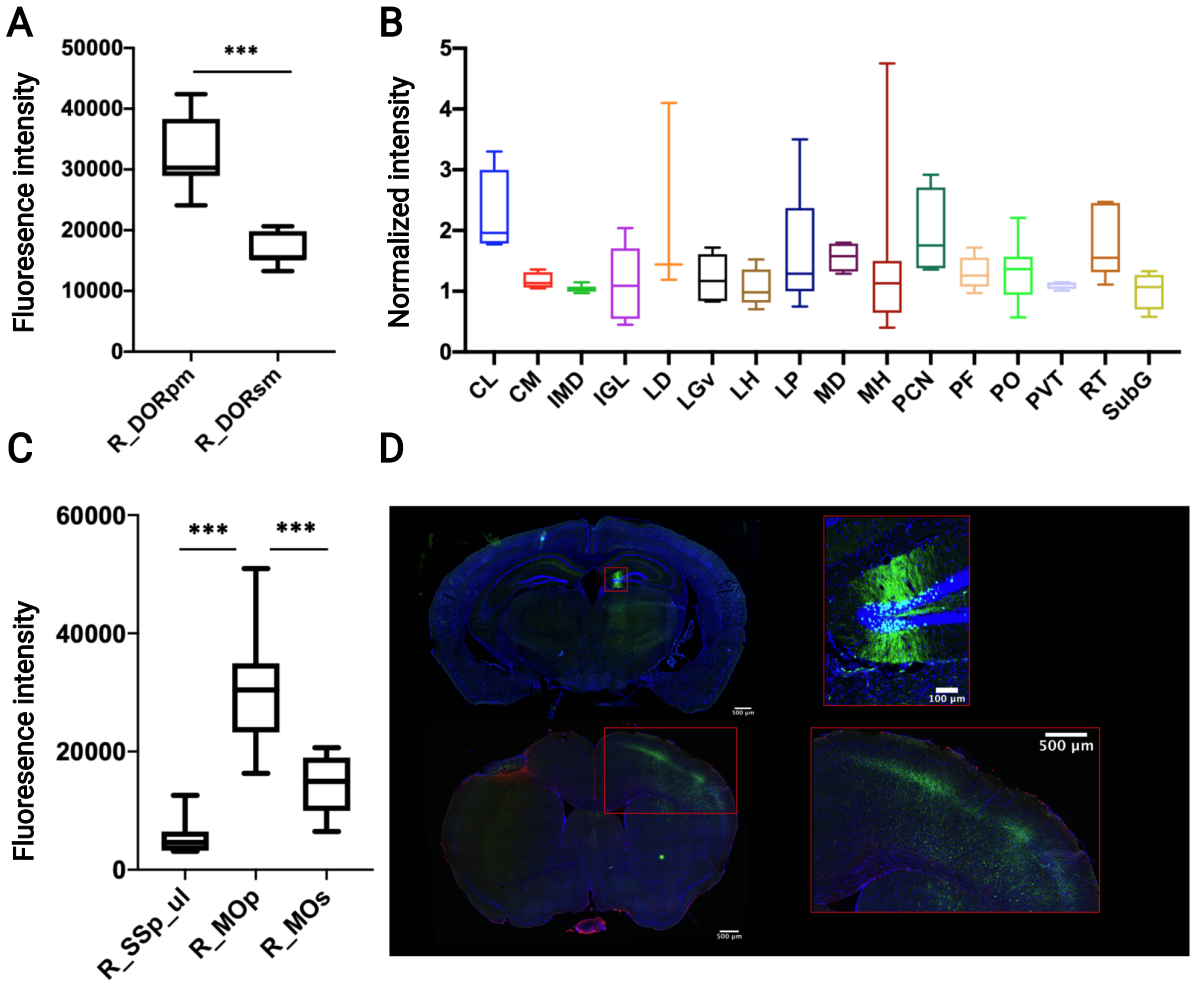

Figure 36 BDA injection into the contralesional thalamus reveal target regions like the SSp-ul, MOp, and MOs. (**A**) Comparison of the fluorescence intensity after BDA injection into the contralesional thalamus (DORpm and DORsm). (**B**) Comparison of DORpm subregion fluorescence intensity after normalization to the the ipsilesional hemisphere. (**C**) Fluorescence intensity of the target regions SSp-ul, MOp, and MOs after BDA injection into the contralesional thalamus. (**D**) Representative slices of the BDA distribution within the hippocampus (upper panel) and striatum (lower panel). Stainings and microscopy were performed by Veronika Fritz during her bachelor thesis in the Aswendt laboratory in 2019.) n=9, data shown as mean ± SD. One-way ANOVA, Tukey comparison between groups: $p<0.05$ (*), $p<0.01$ (**), $p<0.001$ (***).

Injection of tdTomato-labeled rAAV within the MOp (Figure 37 A) stains layer 5 pyramidal neurons. Further posteriorly, the transhemispheric connection across the corpus callosum (Figure 37 B) and further posteriorly across the striatum can be seen (Figure 37 C). The further descending pathways then run over parts of the thalamus (PO and VPM), as well as the zona incerta and internal capsule (Figure 37 D & E) until they run over the pons (Figure 37 F) to the spinal cord.

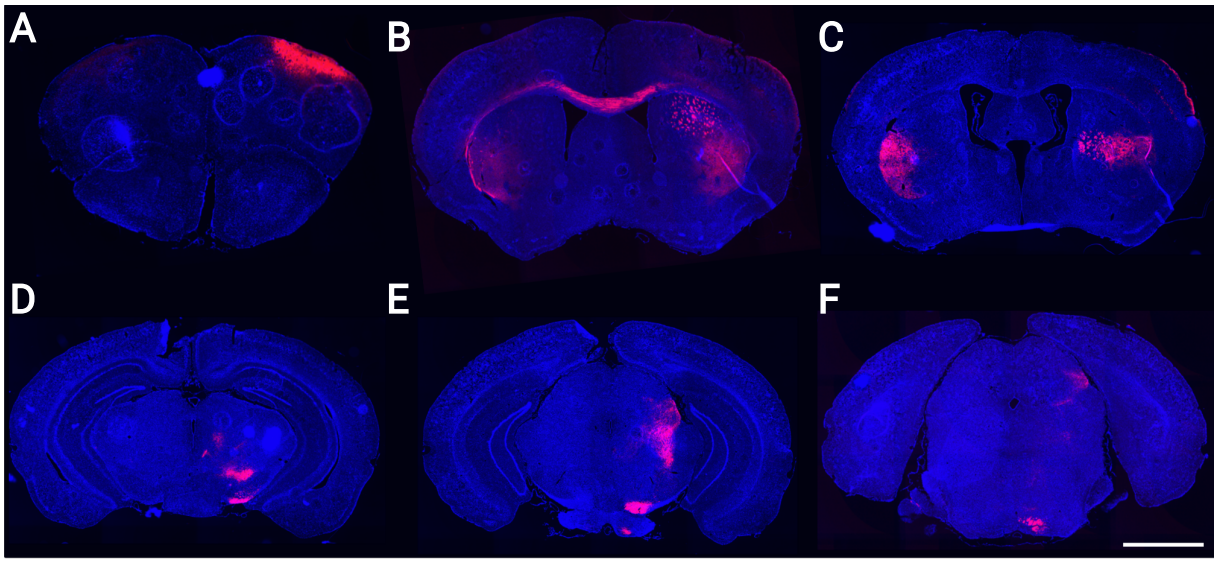

Figure 37 rAAV injection into the MOp of Emx1-Cre mouse. Injection of a tdTomato-labeld rAAV into the MOp (**A**) with subsequent transhemispheric connection across the corpus callosum (**B**) and on posteriorly through the striatum (**C**) via the thalamus (**D & E**) to the pons (**F**).

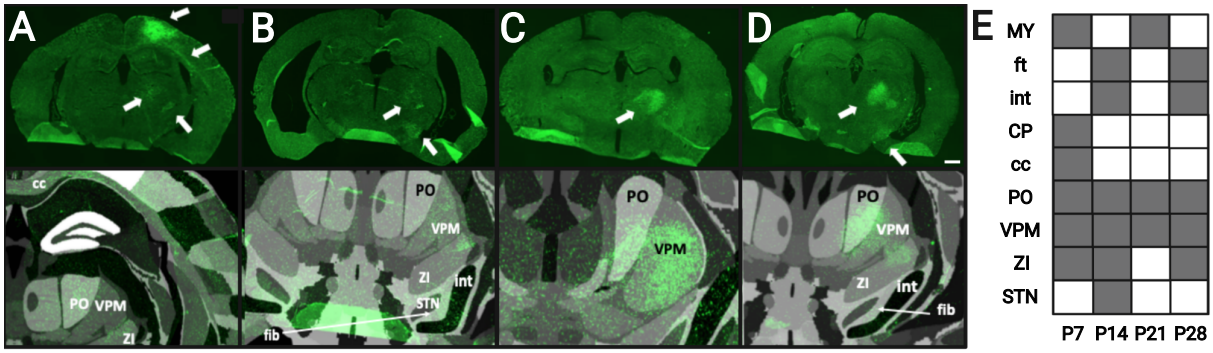

Figure 38 Iba1 staining reveal increased microglia/macrophages activation in remote areas from the ischemic lesion within the MOp. Overlay of histological sections (upper panel) and the Allen Brain Reference Atlas (lower panel) show the local distribution of microglia/macrophages 7 (**A**), 14 (**B**), 21 (**C**), and 28 (**D**) weeks after cortical lesion in the MOp. Increased numbers of microglia/macrophages were found in the posterior complex (PO) and ventral posteromedial nucleus of the thalamus (VPM), zona incerta (ZI), internal capsule (int), fiber tracts (ft), medulla (MY), corpus callosum (cc), caudoputamen (CP), and subthalamic nucleus (STN) regions. Thereby, an increase of microglia/macrophages can be seen on different days after photothrombosis (**E)**). Stainings and microscopy were performed by Mayan Baues during an internship in the Aswendt laboratory in 2018.

After a lesion within the MOp by photothrombosis, an increased number of microglia/macrophages can be detected in more remote areas by Iba1 staining (Figure 38). An increased number of Iba1$^+$ cells within the posterior complex of the thalamus (PO) and ventral posteromedial nucleus of the thalamus (VPM) can be observed at all time points (P7, P14, P21, P28; Figure 38 E). Within the zona incerta (ZI), the number of Iba1$^+$ cells is increased at P7, P14, and P28. There is an accumulation immediately at the lesion (Figure 38 A) as well as in other remote areas like the thalamus (PO/VPM), which becomes more intense over time (Figure 38 C & D). Regions such as the corpus callosum (cc) and caudoputamen (CP) showed an increase of microglia/macrophages only 7 days after photothrombosis (Figure 38 A & E).

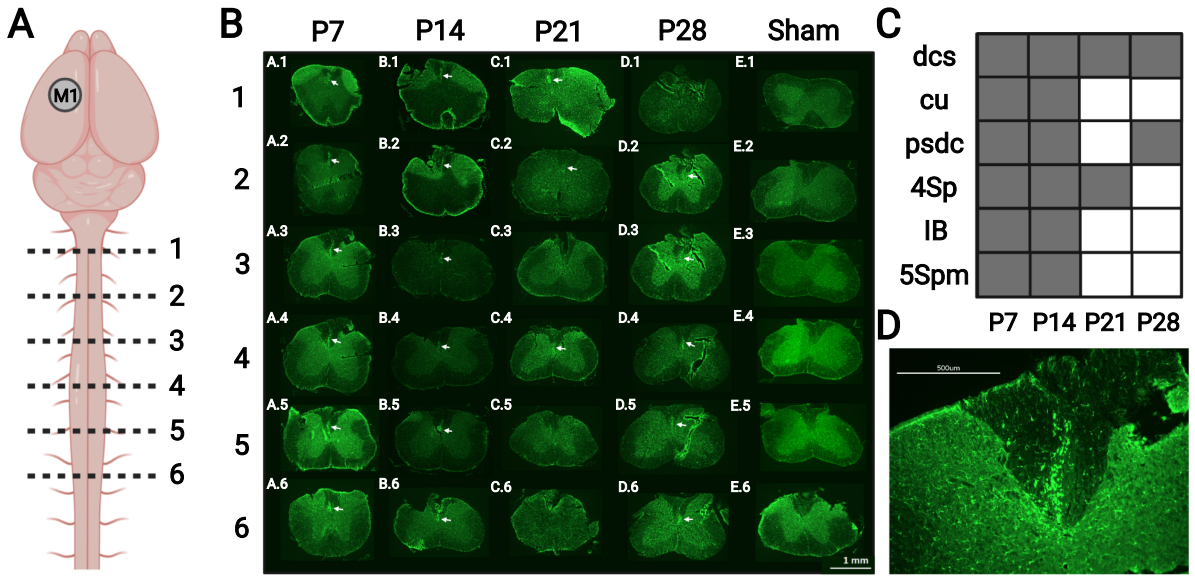

Figure 39 Time series of microglia activation in the spinal cord after photothrombosis in the primary motor cortex. (**A**) Scheme of visualized spinal cord segments. (**B**) Iba1 stainings of different segments of the spinal cord, after 7, 14, 21, and 28 days revealed local accumulations (white arrows) of microglia/macrophages compared to sham animals. (**C**) Quantification of spinal cord areas with increased microglia activation at different time points. (**D**) Exemplary spinal cord section 7 days after cortical lesion with increased amount of Iba1$^+$ cells within the dcs, 5Spm, and psdc. Stainings and microscopy were performed by Mayan Baues during an internship in the Aswendt laboratory in 2018.

In addition to quantifying secondary neurodegeneration in the brain (Figure 39), it was also analyzed in the spinal cord. To follow the time course of microglia/macrophages activation, spinal cord sections were visualized in different sections using Iba1 staining (Figure 39 A). In the time course (P7, P14, P21, and P28) after photothrombosis within the primary motor area, an increased number of Iba1$^+$ cells within the spinal cord was observed at all time points whereas no activation of microglia/macrophages was seen in sham-operated animals (Figure 39 B). Over time, an increased number of Iba1$^+$ cells can be found within the dorsal corticospinal tract (Dcs) at all time points (Figure 39 C). Within the cuneate fasciculus (cu), postsynaptic dorsal column pathway (psdc), internal basilar nucleus (IB), and lamina 5 of the spinal grey (5SpM), increased cell number of Iba1$^+$ is seen only within the first 14 after cortical lesion. Only at P21 within the lamina 4 of the spinal grey (4sP) and at P28 within the psdc an increased number of Iba1$^+$ can still be found. As an example, an increased number of Iba1$^+$ cells within the dcs, psdc, and 5Spm is shown in Figure 39 D.

The quantification of lesion size and the determination of affected regions according to small and large photothrombosis protocol was performed by registration on the Allen brain reference atlas. In Figure 40 A, lesion mapping is shown for days 1 and 7 (based on T2WI) and day 28 (based on histology). 100% of the animals have a lesion within the MOp on days 1 and 7, and 80% on day 28. On day 1 and 7, 100-80% of the animals have a lesion within the primary somatosensory area (barrel field, nose, lower limb, upper limb, mouth, and unassigned). On day 1, the lesion affects the striatum (STRd) and medial forebrain bundle system (mfbs) in both 100% and the hippocampus (HIPP) to 40% after small and 75% after large stroke. 7 days after the small stroke, these areas are only affected to 20%, in contrast to the large protocol where these areas are still affected to 100% (STRd, cc, mfbs) or 25% (HIPP). The lesion in the large protocol extends to the corpus callosum (cc) on day 1 and 7, whereas in the small protocol the cc is affected in 100% of the animals, but only 20% on day 7. Areas such as the supplemental somatosensory area (SSs) are only affected on day 1 (20-50%), but also the lesion within the primary somatosensory area (trunk) is only measurable on days 1 and 7 and no longer on day 28. To quantify the number of affected brain regions on day 1 and 7 after stroke, T2WI was used (Figure 40 B). This revealed that the cc is only affected to 30-40% in both models. In contrast, the primary somatosensory area unassigned (SSp un), upper limb (SSp ul), and lower limb (SSp ll) are almost 100% affected on day 1 in both stroke protocols. On day 7, the infarct area in the small protocol is significantly reduced in all primary somatosensory areas, whereas the percentage infarct area in the large stroke is significantly reduced not only in the SSP-un. The infarct area within the MOs and MOp decreases significantly from day 1 to day 7 in the small stroke and remains the same in the large stroke on day 7 as on day 1. The percent infarct area in the MOs and MOp differs significantly within the different protocols during both time points (Figure 40 B).
To compare the two stroke protocols at day 1 and 7 by T2WI with the lesion determination at day 28 by histology, the left Y-axis in (Figure 40 C) represents the lesion volume (T2WI) and the right Y-axis the histological lesion area. The lesion volumes of the small and large strokes on days 1 and 7 as well as the lesion area on day 28 differ significantly from each other ($p<0.001$). For a more detailed examination of the infarct size on P28, based on GFAP histology, the regions SSp-ul, MOs, and MOp were examined more detailed (Figure 40 D). Here, the infarct area between small and large strokes within the MOp was found to be significantly different ($p<0.01$). In contrast, the SSp ul and MOs regions showed no significant differences between the two stroke protocols.

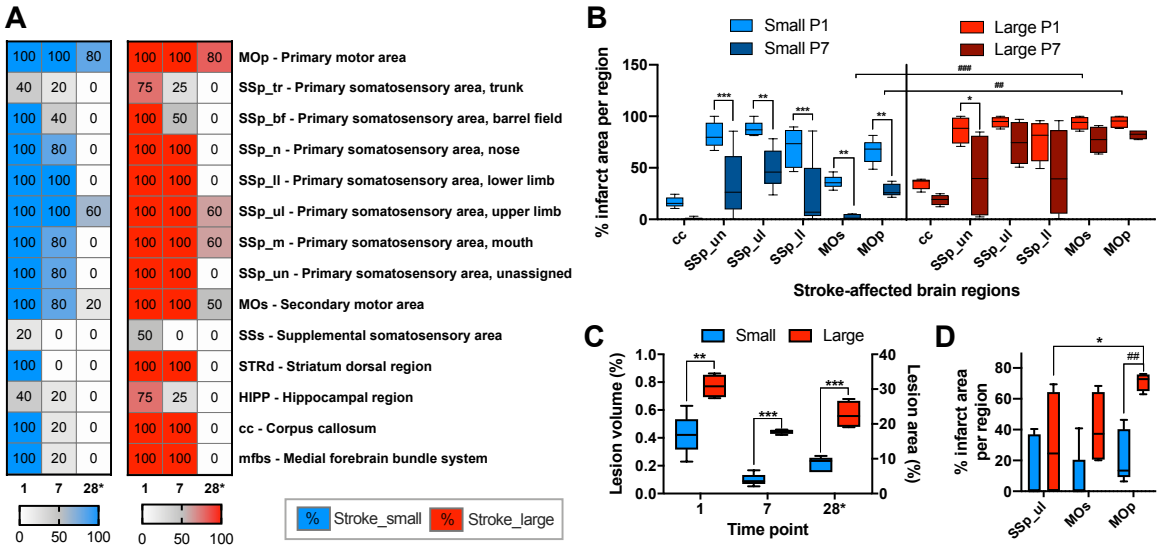

Figure 40 Quantification of lesion location and volume after small & large photothrombosis protocols. (**A**) Illustrates the in vivo lesion mapping 1 and 7 days as well as ex vivo after 28 days in a heat map for small strokes (blue) and large strokes (red). The selection of regions displays which brain atlas region were within the stroke mask on days 1 and 7 (MRI) and day 28 (histology). (**B**) MRI was used to measure the percent infarct size of the corpus callosum (cc), primary somatosensory (SSp) unassigned (un)/upper limb (ul)/lower limb (ll), and secondary/primary motor area (MOs and Mop) on day 1 and 7 after stroke. (**C**) T2WI was used to determine percent lesion size (left Y-axis) at day 1 and 7, and percent lesion size by histology for GFAP (right Y-axis). (**D**) Based on GFAP histology, percent infarct size was determined in the regions for primary somatosensory (upper limb), as well as the secondary and primary motor area (MOs and Mop). Small stroke=5, large stroke=4, sham=4. Two-way ANOVA, Tukey comparison: significant differences between groups (#) and time points (*) were shown as $p<0.05$ (#/*), $p<0.01$ (##/**), $p<0.001$ (###/***).

To visualize the lesion after induction of ICS, myelin was stained using Black & Gold at different sectional levels 56 days after stroke induction (Figure 41). It was found that the lesion is locally very limited and only visible at about 1 mm posterior to Bregma. It can be seen that the lesion has mainly destroyed the internal capsule, but the surrounding tissue is largely intact.

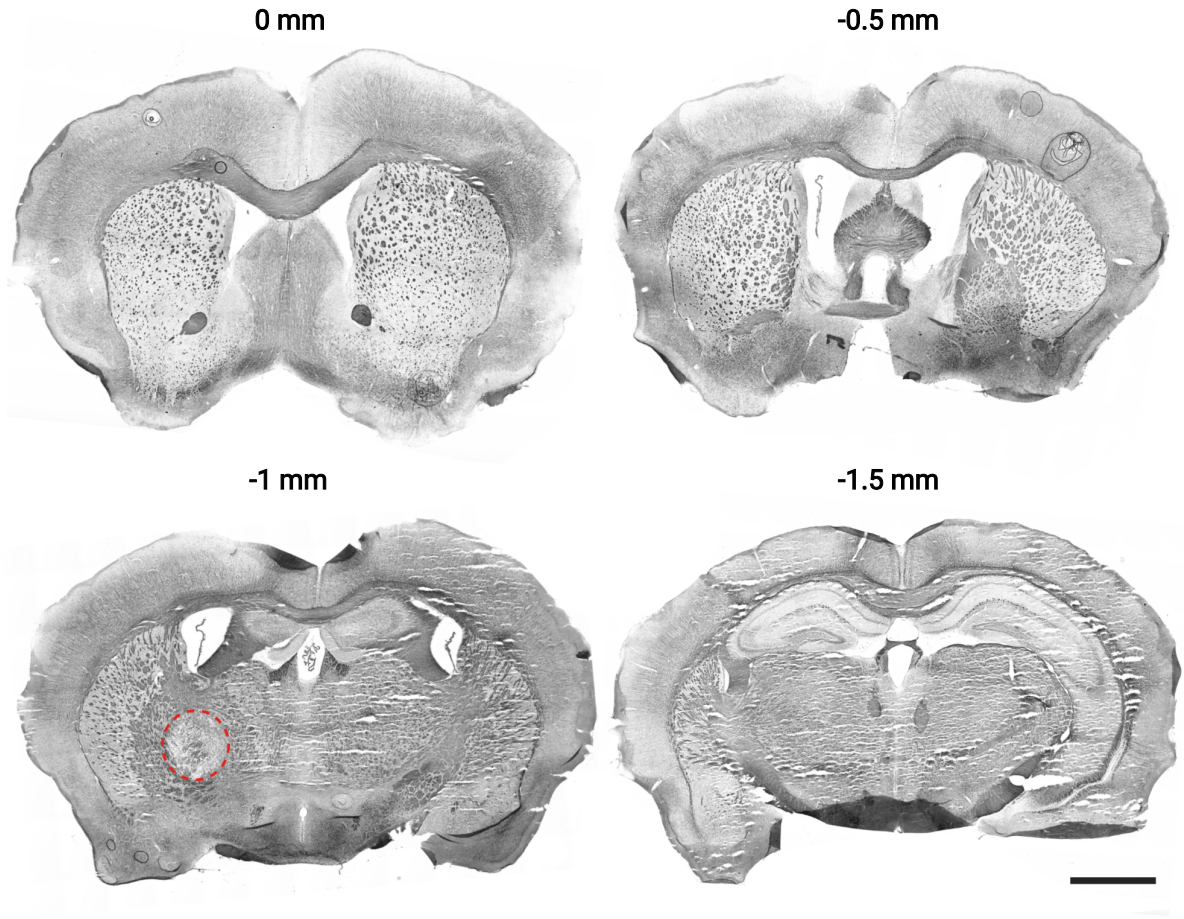

Figure 41 Black & Gold staining after internal capsule stroke. Black & Gold staining on the level of bregma (0 mm), 0.5 mm, 1 mm, and 1.5 mm posterior to visualize the myelin sheaths and the local lesion (red dashed circle) within the internal capsule 1 mm posterior to bregma. Scale bar: 2 mm

7 Discussion

7.1 Mouse models of post-stroke spasticity

In approximately 35% of stroke patients, PSS represents one of the major impairments related to stroke affecting the ability to work and all activities of daily living. Experimental models of stroke in rodents during the last decades, fueled our understanding of stroke pathophysiology, novel thrombolytic treatments in the acute phase, and molecular mechanism of the recovery phase. In contrast to the long and successful history of experimental stroke, the rodent models of PSS are sparse, insufficiently characterized, and have limited translational success [275]. Motivated by this gap in stroke studies, this thesis focused on the development of a reliable post-stroke spasticity model in the mouse and investigated the effects of cortical and internal capsule stroke on electrophysiological changes and sensorimotor behavior in the affected fore limb.

Factors that must be considered when simulating disease in animal models are the absence of comorbidities that lead to stroke in patients (diabetis mellitus, hypertension, obesity) and have a crucial effect on the impact and recovery after stroke. Unfortunately, most disease models still ignore these factors, as well as age in most cases [177], which may also explain the limited number of neuroprotective agents and therapies from animal models to patients [80]. The inclusion of age, as well as the simulation of comorbidities, is considered in more and more models, but mostly only single comorbidities are induced, and this in young male mice, which strongly limits their translation to patients [82]. In addition to the lack of comorbidities, the influence of surgery on the validity of animal models must also be considered. The most common and also used here gas anesthetic isoflurane opens the blood-brain barrier [254], has neuroprotective properties [280], and leads to smaller stroke volumes [168]. Besides, isoflurane affects blood pressure, cerebral blood flow, and metabolism, which may explain some of the better recoveries compared to patients.

To date, however, neither the Endothelin-1 (ET-1) nor the middle cerebral artery occlusion model (MCAO) has specifically induced or measured PSS, and the internal capsule stroke model demonstrated here fills this gap. The ICS model represents a way to induce PSS with no intraoperative as well as low long-term mortality (3.3%), and high reproducibility. Cortical photothrombosis, with its simple application, accuracy, and high reproducibility, represents a well-established model for inducing local cortical strokes.

It is ideal to induce small cortical strokes, whereby the size of the lesion can be manipulated by the amount of Rose Bengal, laser intensity, radiation duration, and size of the illuminated area (Figure 32). Photothrombosis is not usually used to occlude or break only one artery as it usually happens in human strokes, but induces lesions in more superficial vessels, which results in selective interruption of blood in the areas exposed to light. The direct laser radiation through the dura mater does not cause any damage on the irradiated vessels [246] and can be performed without craniotomy and even in freely moving mice [285] without distortion by anesthesia, whereby the animals rapidly recover from surgery with a high survival rate of nearly 100% in our hands.
Because of the use of light guides similar to those used for optogenetic stimulation, these studies can be used to better validate the extent of invasiveness of this type of implantation [147]. Other models that induce stroke within the white matter are based on intracerebral injection of endothelin-1 (ET-1) into the corpus callosum [3] and to local destruction of nerve fibers. In contrast to the ET-1 model or larger stroke models such as the MCAO [47], the internal capsule stroke model described here can specifically induce a local lesion in the internal capsule without destroying its surrounding tissue (Figure 41). To date, motor deficits following a lesion within the internal capsule in the mouse model are poorly described or motor testing needs to be adapted for this type of injury [57]. Data of white mater stroke pathophysiology and motor impairments mostly based on the injection of ET-1 into the corpus callosum [3], which does not lead to a permanent blood flow but results in reperfusion after approximately 3h in the opposite to the internal capsule stroke model presented here, which induce a permanent occlusion. In line with the motor impairments in the internal capsule stroke model (Figure 28), experiments in rats receiving ET-1 into the posterior part of the internal capsule showed a motor deficit in the rotarod, corner test, grid walk, and grip strength test [29]. One point to consider when translating the internal capsule stroke model described here is the different proportion of white matter in rodents (14%) and humans (50%). For this reason, most pre-clinical experiments have been directed toward neuroprotection of gray matter, and the effects of lesions within white matter remain relatively understudied [240].

7.1.1 Lesion location dependent post-stroke spasticity

In a first set of experiments, the aim was to replicated earlier results from Toda et al.[257] and Lee et al. [160] describing PSS in mice with MOp lesions. However, the obtained results with harmonized experimental settings contradict these findings as no PSS was measured (Figure 18 & Figure 19). This may be due to the slightly larger extensive of the lesion within the primary towards the secondary motor area in the earlier studies which could not be directly compared due to the lack of detailed lesion mapping in the previous studies. Unfortunately, all work on the induction of PSS with Toda and Lee has come from one laboratory and no other group has been able to show that PSS can be induced at this rate. Large lesions, such as those caused by MCAO, may induce PSS more rapidly or lead to more severe PSS due to the degree of destruction of brain areas, but this possibility has not yet been demonstrated in the mouse model.
Since the lesion within the MOp, as shown by the preliminary work of Toda and Lee, did not result in PSS, the MOs was destroyed by photothrombosis (Figure 10 B), resulting in a late begin of PSS (Figure 20 & Figure 21). But in contrast to animals with a lesion in the MOp, 42 days after a lesion within the MOs, the animals showed an increased H-wave (Figure 18 & Figure 21), which was partly due to the different lesion location but also due to the lesion size, which was twice as large relative to the MOp lesion (Table 2). Moreover, due to neuroplasticity associated with axonal sprouting and synaptogenesis, PSS may be delayed and possibly prevented in the mouse model using this lesion model. One reason for the increase of the H-wave 42 days after photothrombosis in MOs (Figure 20) could be that the secondary neurodegeneration takes so long to degrade the inhibitory neural circuits in the spinal cord that its effect can only be detected at P42.
The secondary motor area is not precisely defined in the mouse, which makes it difficult to compare results from animal experiments with results from patients [22, 261]. First, different names are used besides the here introduced nomenclature MOs and M2, e.g. FOF, PrCm, AGm, shoulder region, second frontal area (Fr2), and dorsomedial prefrontal cortex (dmPFC). The number of different names indicates which functions have already been assigned to the MOs from decision-making to motor learning and sensory perception. Some experiments suggest a homology of the MOs to the frontal eye field, supplementary motor area or premotor cortex in humans. Interestingly, the removal of the MOs causes transient neglect and permanent sensorimotor deficits [64], which is also evident in the behavior of animals after photothrombosis (Figure 27).

To destroy the descending corticospinal tract a novel model for inducing a lesion within the internal capsule was established (Figure 11), which was initially used only in the rat [107, 146] and could not yet be demonstrated for the mouse model before. Due to the cortical lesion by photothrombosis, the MOp and MOs was destroyed up to 70% one day after photothrombosis (Figure 40 D) and for this reason, it is possible that this type of lesion was not sufficient to induce the degeneration of descending pathways in a sufficient manner [139]. The lesion within the MOp might also not lead to direct induction of spasticity (Figure 18 & Figure 19), as there are still enough pyramidal cells intact within the MOp to compensate for the degeneration of descending tracts.

7.1.2 Electrophysiological validation of spasticity

To detect the electrophysiological changes in spasticity after induction of cortical photothrombosis or stroke within the internal capsule, a transcutaneous, like Toda et al. [257] and Lee et al. [160] presented and a self-established direct nerve measurement were used (Figure 14). The M-wave as well as the H-wave measured by transcutaneous and direct nerve stimulation correlate significantly with each other, whereas the measurement by direct nerve stimulation shows less variability (Figure 17).
To compare the two methods, the ratio between the H-wave and M-wave (H/M ratio) was found to give the best results, eliminating variability in the setup, especially due to positioning of the electrodes (Figure 22). Further, the measured amplitudes of the M-waves and H-wave reflect stronger Ia afferent input to their motorneurons or greater intrinsic motorneuron excitability (Figure 22). The magnitude of the amplitude becomes larger the closer the stimulation electrodes are to the nerve [198, 263]. This could explain the lower variance of the measurements in the direct nerve measurement method with fixed minimal distance of the hook electrodes in contrast to the transcutaneous electrodes.
To quantifying the H-wave, care was taken to ensure that the H-wave peak occurred between 6-11 ms after stimulation, which is consistent with the literature in which the H-wave occurs between 6-8 ms [257] and 9.55 $\pm$ 1.55 ms [212] after stimulation. The latency is nerve-specific, as shorter latency after stimulation of 4-6 ms [51] or 5-8 ms [133] were reported for the tibial nerve.

7.1.3 Evaluation of post-stroke spasticity

In addition to the transcutaneous and direct nerve measurement methods shown here, implantable electrodes [226, 50, 202, 260] could also be used for future experiments. It should be noted that current setups only allow recordings of the hind leg (sciatic or tibial nerve), which is due to size limitations and the better surgical accessibility of the sciatic or tibial nerve. However, most behavioral tests measure an altered sensorimotor function of the forepaw and not the hind paw. For this reason, the correlation between sensorimotor deficits and altered electrophysiology due to PSS would be poor. Furthermore, it must be considered that the implantation of electrodes in the forepaw may cause a change or injury of muscle and nerves due to the surgical intervention. On the other hand, it cannot be excluded that the implanted electrodes restrict the mice in their movements, and thus the use of behavioral tests is no longer possible to the full extent. Surface EMG multi-electrodes offer the possibility to minimize the injury of muscle and nerve tissue, but their use is limited to the hind paw.
Another possibility to measure spasticity on an electrophysiological and motor level has been demonstrated by Mekhael et al. [179]. Here, the muscular response was measured after electrical stimulation of the hind paw. However, this procedure could also only be demonstrated on the hind paw and only a muscular response is measured, which cannot provide any information about the sensory changes that may occur in spasticity.

H-wave reveals the integrity of inhibitory circuits

The H-wave represents the best option to validate the complex inhibitory circuits that are altered following cerebral injury. However, the H-wave is generated by a variety of neural circuits that must be taken into account. Due to presynaptic inhibition, the level of H-wave amplitude can be strongly modulated, causing afferent input toward alpha motor neurons to act suppressive on excitatory anterior horn cells [224]. Reciprocal inhibition is also called antagonistic inhibition and describes the inhibition of the ipsilateral antagonist while the agonist is activated [68]. Here, this type of inhibition can be induced directly via the Ia afferent spinal circuits or by higher-level brain centers such as the motor cortex via the corticospinal tract [233]. The purpose of reciprocal inhibition is the optimization of muscle movements because only if antagonists are inhibited, joint movements can be executed correctly [130]. This is relevant for the validation of the H-wave because the contraction of an antagonist of the target muscle modulates the reflex response [233, 93].

Following the protocol of Toda [257], the stimulation intensity was increased from 1-3 mA in 0.1 mA steps in the first experiments. Stimulation at 3 mA led to the maximum amplitude of the H-wave in each case, which is consistent with data from other research groups [198]. It should be noted that a further increase of the stimulation intensity can lead to a decrease of the H-wave [148].
Both transcutaneous and direct nerve H-wave measurements were performed under ketamine / xylazine anesthesia. Xylazine acts as a muscle relaxant and thus could lead to a decrease in the H-wave. Ketamine induces analgesia and a dissociative anesthetic state, but in higher dose also an increase in skeletal muscle tone. To ensure comparability with the only two previous studies on the induction of post-stroke spasticity [257, 160], the same mixture of ketamine / xylazine was used. An alternative would be isoflurane anesthesia, but this also has muscle relaxant effects and no direct comparison to previous studies can be made. For further experiments it should be kept in mind that the H/M-ratio can vary if different muscles are measured because the ratio is typically higher in muscles with a higher proportion of slow-twitch fibers [181, 197]. Another step to further objectify the measurements is the use of a tool to automatically evaluate the M-waves and H-wave amplitudes. Within our laboratory, this was already partly established using a MATLAB script for automated averaging of the single measurements per animal but further work would be necessary to detect the amplitude in M- and H-wave, respectively. Toda et al. [257] and Lee et al. [160] calculated the rate-dependent depression (RDD) to validate PSS after cortical lesion. The RDD measures the decline in the amplitude of the H-wave by repeated increasing frequencies (0.1, 0.5, 1, 2, 5 Hz), the resulting amplitudes is indicative of the functional of the spinal inhibitory system [159]. Thus, if all neural circuits are intact, the amplitude of the H-wave is suppressed equally at all frequencies [224] which was shown before in rat models of spinal cord injury [143] and also in humans [42]. This lack of suppression was demonstrated by RDD (Figure 24) and shows that a lesion within the MOs or the internal capsule can induce PSS. Alternatively, normalization of the H-wave as a percentage on the Mmax has been established [198]. Thereby the stimulation intensity is increased until a maximum of the M-wave is found. Thereupon, stimulation was performed with 10% of this stimulation intensity to obtain a maximum H-wave. However, this method of evaluation is sometimes criticized and the H/M ratio performed here is preferred [115].

7.2 Behavioral changes after cortical and internal capsule stroke

Behavioral tests are essential in addition to neuroimaging and electrophysiological examinations to reliably assess the functional effects of diseases and their therapy [203]. Besides sensorimotor deficits, behavioral tests can be used to measure motivation, anxiety and motor recovery [108]. The behavioral tests used here (Figure 12) have proven to be valid methods to measure motor deficits after cortical lesion (Figure 27), as well as after internal capsule stroke (Figure 28). The behavioral tests used revealed a high sensitivity in the grid walk, grip strength, and cylinder test (Figure 29), which were in line with previous studies [32, 142]. However, it should be noted that the behavioral tests measure sensorimotor changes and do not differentiate between motor impairment and PSS. In patients, the Tardieu scale, Penn spasm frequency scale, Barthel index, and the modified Ashworth scale (MAS) are used. The direct transfer of the MAS to pre-clinical models is not possible on a 1:1 basis, but the neuroscore used here (Figure 27 F & Figure 28 F), modified for cerebral lesions, is a good approximation to the MAS. Using the neuroscore, however, a deficit could only be detected within the first 14 days (Figure 29) after stroke but can also differentiate between the small and large photothrombosis protocols (Figure 42).
Since the behavioral tests performed here (grid walk, rotating beam, cylinder test) were all video-recorded, this allows a better subsequent analysis of the tests using DeepLabCut (DLC, [175]) in which individual body parts are detected by training a deep neural network and kinematic analysis can be performed based on this. DLC has already been trained for rotating beam test and the analysis of grid walk and cylinder test are going to be established in our research group.

7.2.1 Correlation of electrophysiological and behavioral changes during PSS

To complement the electrophysiological observation of PSS (H-wave, H/M ratio), the individual change in sensorimotor behavior was analyzed. A correlation was found between the H-wave and the number of paw drags, which can be explained by the destruction of ascending pathways ending in the somatosensory cortex via the thalamus [3], which also occurs in patients [268].

A side effect of the destruction of the descending pathways is also the slowing of movements and inactivity, which was described by the neurologist Pierre Marie in 1901 [174] and can be seen here in the activity score during the cylinder test (data not shown).
It is also interesting that the grip strength does not correlate with an increase of the H-wave, as it was shown in animals after ET-1 injection [3] and only the H/M ratio showed a small correlation (Figure 30 A). However, it is important to note that in all tests, the sensorimotor properties were measured and not isolated PSS. Therefore, the correlation between the H/M ratio in animals with a lesion within the MOp can be explained primarily by the motor impairments and not by the presence of a PSS (Figure 30 B). However, the lesion within the MOp seems to decrease grip strength, which correlates with the H-wave (r=-0.67) as well as with the H/M ratio (r=-0.71). The grid walk test seems to be good for detecting motor deficit after cortical as well as internal capsule lesion, but it does not measure isolated spasticity (Figure 30).

7.2.2 Limitations of PSS induction and evaluation

In this work the stroke model photothrombosis was used, which induce a artificial lesion, because there is no penumbra and hemorrhagic transformation in the per-lesional cortex [137]. Photothrombosis is triggered in a large number of vessels in the illuminated area, whereas stroke is typically caused by interruption of blood flow within a single direct nerve artery (mostly the MCA). In contrast to the most permanent occlusion of arteries in the photothrombosis model, in a subset of stroke patients, reperfusion occurs spontaneously and may elicit secondary damages. Because the photothrombosis model lacks a penumbra, which is a major target of any neuroprotective agent, the translational impact of this model is limited.
To evaluate the induction of PSS after cortical or internal capsule stroke electrophysiological properties like the M- and H-wave were obtained. Besides the positioning of the stimulation electrodes, the duration of the experiments, and the body temperature might also influence the M-wave as well as H-wave as Denys et al. showed by local cooling of the abductor digiti minimi, resulting in increased amplitudes of muscle and nerve potentials [70]. Here, the transcutaneous, as well as the direct nerve measurement, were kept as short as possible with a measurement duration of approx. 35 min each, and the body temperature was kept as constant as possible by using a feedback-controlled heating pad (Figure 7).

However, individual variance cannot be excluded here, which together with the positioning of the electrodes contributed to the variance within the M-wave. Notably, electrophysiological monitoring after stroke by the direct nerve method would require much higher animal numbers and for these experiments, the transcutaneous measurement is the method of choice with comparable H/M-detection as proven here.
In order to obtain a comprehensive overview of the sensorimotor changes after cortical as well as internal capsule stroke, behavioral tests such as the corner and string pulling test were also evaluated initially. The corner test, which was only intended to measure the altered sensory function or possible unilateral neglect after a stroke, did not prove to be sensitive in our experiments (data not shown), which was the reason why they were not used in the further experiments. Another test that was supposed to measure sensorimotor changes after stroke besides the behavioral tests performed was the string-pulling test [28], which, however, did not prove to be replicable and was therefore not further used.

7.3 Neural circuits of spasticity

Damage to the CST can be measured by different behavioral tests, counting not only the grid walk but also the cylinder test, which has already been shown in a pyramidotomy model where only the CST was damaged [243]. Rodents share some evolutionary similarities but differ in the localization of the CST within the spinal cord [272], showing higher plasticity of the CST compared to humans, making translation to clinical therapy difficult [253, 234]. However, neuroplasticity and the associated regeneration of the animals depend on the structural integrity of the CST, as well as RST [41, 227]. The regeneration after cerebral damage depends on the non-crossed CST fibers in the contralesional hemisphere, which then leads to a reduction of motor deficits [59].
Spasticity is not only related to the pyramidal system. Selective damage to the pyramidal tract at the level of the cerebral peduncle [36] and at the level of the pyramids [231] is not followed by spasticity. Spasticity is due to the loss or reduction of the inhibitory influences conducted by the dorsal reticulospinal tract (RST). Small lesions within the anterior limb of the internal capsule, where the fibers from the premotor areas are located, tend to be associated with spastic hypertonus, whereas those confined to the posterior limb are not [259]. In conclusion, brain lesions cause spasticity when they disrupt the facilitatory corticobulbar fibers, thus leading to the inhibition of the ventromedial reticular formation, from which the dorsal reticulospinal tract takes its origin.

In the ICS performed here, the fibers within the internal capsule were destroyed unspecifically, which means that no clear differentiation can be made between the destruction of the RST and CST. Different to humans, where the CST axons originate from layer 5 pyramidal cells forming the longest axons with direct synaptic connecions with spinal motorneurons, cortical-motorneuronal (CM) connections in mice start to form during but become actively eliminated by Sema6D-PlexA1 signaling during development. Another indication of the crucial role of PlexA1 is the strong expression of PlexA1 in layer 5 in the motor cortex of mice, whereas in humans it is very weak, which may be due to the FEZF2-mediated cis-regulatory elements found only in higher primates [104]. One possible explanation for the different CM connections in comparison to higher primates is that the increase of manual dexterity confers no fitness advantages to quadrupedal animals. In higher primates the CST runs within the ventral and lateral funiculi of the spinal cord, whereas in rodents they run within the dorsal funiculus [111].
Recovery after cortical stroke is mainly caused by thalamo-cortical circuits on the contralesional side [14, 139], whereas the cellular changes in the peri-infarct zone lead to the unaffected hemisphere in the somatotopic region taking over the function of the destroyed brain areas [183]. Plasticity after stroke is mainly caused by potentiating of existing circuits and not necessarily by functional remapping to new circuits [286]. This recruitment of existing circuits, which then take over the function of destroyed brain areas, was shown with electrical stimulation of the motor cortex stimulating the sprouting of the CST and concomitant motor recovery [46].
The comparability to other white matter stroke studies has to be done with caution because most of the studies were performed with the ET-1 model, in which reperfusion occurs after about 3 hours. In the photothrombosis model used here within the internal capsule, however, there is no reperfusion, but a permanent occlusion of the illuminated vessels. In animals that received an ET-1 injection into the white matter, a loss of grip strength was observed similar to this work [57, 3]. Injections into the corpus callosum resulted in a measurable deficit during the grid walk test [241], but the deficit was much greater in this work because injection into the internal capsule rather than the corpus callosum destroyed more descending tracts from the motor cortex as well as ascending thalamocortical tracts.

7.4 Pathophysiological changes after stroke

To obtain a complete picture of the pathophysiology leading to motor and electrophysiological changes after cortical or internal capsule stroke, histological validation is essential. An important indicator for the disease state of an organism is the regulation of GFAP, which is found as intermediate filament protein especially in astrocytes in the CNS. It plays an important role in astrocyte-neuron interaction and cell-cell communication.
Focal ischemia leads to irreversible injuries in a core region and a surrounding penumbra zone with partially reversible damage [13], which becomes part of the ischemic core already after 2 days. Blockage of blood flow leads to the maximum volume of the ischemic core [124] after 3-6 hours and is surrounded by a glial scar formed primarily by astrocytes (Figure 32 C & F). Without any reperfusion the core injury is irreversible and any further therapeutic approach is restricted to the alleviation of the ischemic core. Therefore the highest therapeutic potential is within the first "golden" hour after ischemia, because the volume of the penumbra reached 50%, and afterward the amount of the tissue to be saved decreases, and improvements are only marginal. Induction of cortical strokes by photothrombosis leads to a hyperintensity signal within 24h, which attenuates within 7 days and is not resolvable thereafter (Figure 40 A & D). The primarily formed edema leads to an enlargement of the ischemic core immediately after the stroke, which, however, becomes smaller and smaller over time (Figure 35).
Cortical lesion within the primary motor area results in microglia/macrophages activation in remote brain regions (Figure 33) and spinal cord (Figure 39), with synaptic connections to the cortical lesion. Iba1$^+$ cells mostly were found within the thalamus (DORsm & DORpm; Figure 33 C) and activation in the spinal cord was mainly observed in the dorsal corticospinal tract, cuneate fasciculus, postsynaptic dorsal column pathway, lamina 5 of the spinal grey, internal basilar nucleus, and lamina 4 of the spinal grey (Figure 39).

This activation within mediodorsal white matter and mediodorsal part of the intermediate grey matter of the spinal cord after cerebral lesion correlates with studies in patients [287]. In contrast, no activation of microglia/macrophages was detected within the ventral horn. However, an increased number of Iba1$^+$ cells was detected within the dorsolateral funiculus, which in humans represents the corticospinal tract. With time from 7 days after stroke, activation of microglia/macrophages within dorsal intermediate gray and mediodorsal white matter was observed (Figure 39). This activation within the gray matter could also be observed in humans after stroke [225] and increased activation of Iba1$^+$ cells within the mediodorsal white matter, which contains the corticospinal fibers, can still be seen 4 weeks after stroke. The observed increase of microglia/macrophages in remote areas of cortical strokes, such as the thalamus, is in agreement with the work of Cao et al. who observed the highest concentration of Iba1$^+$ cells 14-28 days after stroke as sign of secondary neurodegeneration [45].

For the visualization of structural changes after cerebral injury, the use of (viral) tracing has become increasingly effective. In a first step, BDA injection was previously used to identify the exact injection site to effectively mark all target regions of the thalamus (Figure 36). In addition to the different projections of the thalamus, the projections of the MOp should also be visualized (Figure 37). The use of BDA here is a spatially limiting method because there is only a limited amount of dye available. However, the BDA is not absent over time [211] and is transported anterograde around 15-20 mm per week. The BDA is primarily taken up by neurons, but no layer-specific uptake can be guaranteed here. For layer-specific labeling, in this case, layer 5, the rAAV and cre-dependent mouse lines used are more specific [187, 219]. The rAAV used here shows better labeling of posterior regions (Figure 37) in addition to a more extensive transhemispheric labeling.

8 Outlook

With this work, the establishment of all the necessary methods for inducing as well as validating post-stroke spasticity in the mouse model was proven. These results open new possibilities to study the mechanisms of post-stroke spasticity and develop urgently needed targeted therapies.

Further improvements of the electrophysiological setup will include a strength gauge to simultaneously measure muscle strength and the H-Reflex. For that purpose, a strength gauge according to the publication of [179] will be built in cooperation with Robin Bayer (Technical Core Facility University Hospital Cologne) and this will be applied according to the different lesion types (MOp, MOs, and ICS). In addition, automated movement and kinematic quantification using DeepLabCut (DLC) will be extended, which will then allow automated evaluation of the grid walk and cylinder test. Our hope for these tests, as well as for the rotating beam, is that the DLC data will give indications of PSS specific movement patterns, which can determine a PSS more clearly than the otherwise collected parameters (foot faults, paw drags, speed, and hindlimb drops) alone as it has been shown in [205].

Due to the severe limitations associated with the COVID-19 pandemic, a large number of viral tracing experiments could not be evaluated. Animals with a lesion in the MOs or the internal capsule received viral tracings with rAAV to quantify connections of the CST/RST that were degraded by secondary neurodegeneration and to correlate with the recorded electrophysiological as well as sensorimotor changes. In addition to classical immunohistochemistry, tissue clearing and subsequent light-sheet fluorescence microscopy (LSFM) will be performed in cooperation with Anna-Sophia Wahl (ETH Zürich), since LSFM is not only able to visualize individual histological sectional planes, but can also show the altered expression of rAAV in the entire CNS.

In addition to the analysis of the viral tracing experiments, ex vivo DTI measurements of the brains after cortical lesions in the MOs as well as after white matter stroke will be performed, which together with the viral tracing will provide a comprehensive picture of the degenerative changes after the individual lesions. To further investigate secondary neurodegeneration after cerebral lesion, the spinal cords of the animals were taken in addition to the brains. To date, no experimental work has demonstrated secondary neurodegeneration after specific cerebral lesions in a mouse model. By establishing a reference atlas for the spinal cord similar to the Allen Brain Reference Atlas, an atlas-based quantification of microglia/macrophages will be performed.

This histological quantification could then also be correlated with the viral tracing experiments if the expression in the spinal cord is sufficient to provide a more complete picture of the processes in the spinal cord. Based on preliminary work in our group that has shown lesion- and location-dependent recruitment [14], investigation of related areas to the lesion would be necessary for further experiments to obtain an all-encompassing picture of secondary neurodegeneration that may end in PSS.
With an observation period of 56 days after stroke, the experiments performed here represent a comparably long experimental time scale. But even longer experiments would be conceivable. As an proof of concept the induction of a PSS using ICS and subsequent suppression of the PSS through local stimulation of brain regions found by LSFM and ex vivo DTI would be a an advantage. These clues could then be the basis for region-specific neuromodulation to ameliorate PSS symptoms, similar to deep brain stimulation in Parkinson's disease.

9 Summary of projects and publications

9.1 Published projects

The following overview should give you an overview about the projects, which were conducted besides the main PhD project. The first part shows the projects that have already been published and the following part presents the projects that are not yet published or what their current status is.

9.1.1 Structural integrity and remodeling underlying functional recovery after stroke

Wieters F. *& Aswendt M.*
Invited perspective - doi: 10.4103/1673-5374.301004

Neural Regeneration Research, published on the 12 December 2020

	Author contribution
Wieters F.	Writing - original draft
Aswendt M.	Writing - original draft

9.1.2 A teaching tool about the fickle p value and other statistical principles based on real-life data

Alawbathani S., Batool M., Fleckhaus J., Hamad S., Hassenrück F., Hou Y., Li X., Salmanton-Garcia J., Ullah S., ***Wieters F.****, Michel C.M.*

Brief communication - doi: 10.1007/s00210-020-02045-3

Naunyn Schmiedebergs Arch Pharmacol, published on the 14 January 2021

Abstract A poor understanding of statistical analysis has been proposed as a key reason for lack of replicability of many studies in experimental biomedicine. A tool based on a commonly used software package was developed that allows using random samples from real data. The tool is described and together with the underlying database is made available. The tool has been tested successfully in multiple other groups of biomedical scientists. It can also let trainees experience the impact of randomness, sample sizes and choice of specific statistical test on measured p values. We propose that live exercises based on real data will be more impactful in the training of biomedical scientists on statistical concepts.

	Author contribution
Alawbathani S.	Resources, writing - review & editing
Batool M.	Resources, writing - review & editing
Fleckhaus J.	Resources, writing - review & editing
Hamad S.	Resources, writing - review & editing
Hassenrück F.	Resources, writing - review & editing
Hou Y.	Resources, writing - review & editing
Salmanton-Garcia J.	Resources, writing - review & editing
Ullah S.	Resources, writing - review & editing
Wieters F.	Resources, writing - review & editing
Michel C.M.	Conceptualization, supervision, writing - original draft

9.1.3 Introduction into spasticity and related mouse models

***Wieters F.**, Weiss Lucas, C., Gruhn M., Büschges A., Fink G.R., Aswendt M.*
Review article - doi: 10.1016/j.expneurol.2020.113491

Experimental Neurology, published on the 29 September 2020

Abstract Although spasticity is one of the most common causes of motor disability worldwide, its precise definition and pathophysiology remain elusive, which to date renders its experimental targeting tricky. At least in part, this difficulty is caused by heterogeneous phenotypes of spasticity-causing neurological disorders, all causing spasticity by involving upper motor neurons. The most common clinical symptoms are a series of rapid muscle contractions (clonus), an increased muscle tone (hypertonia), and augmented tendon reflex activity (hyperreflexia). This muscle overactivity is due to disturbed inhibition of spinal reflexes following upper motor neuron dysfunction. Despite a range of physical and pharmacological therapies ameliorating the symptoms, their targeted application remains difficult. Therefore, to date, spasticity impacts rehabilitative therapy, and no therapy exists that reverses the pathology completely. In contrast to the incidence and importance of spasticity, only very little pre-clinical work in animal models exists, and this research is focused on the cat or the rat spastic tail model to decipher altered reflexes and excitability of the motor neurons in the spinal cord. Meanwhile, the characterization of spasticity in clinically more relevant mouse models of neurological disorders, such as stroke, remains understudied. Here, we provide a brief introduction into the clinical knowledge and therapy of spasticity and an in-depth review of pre-clinical studies of spasticity in mice including the current experimental challenges for clinical translation.

	Author contribution
Wieters F.	Supervision, writing - original draft
Weiss Lucas C.	Writing - review & editing
Gruhn M.	Writing - review & editing
Büschges A.	Writing - review & editing
Fink G.R.	Writing - review & editing
Aswendt M.	Supervision, writing - review & editing

9.1.4 Graph theoretical quantification of white matter reorganization after cortical stroke in mice

Pallast N., ***Wieters F.****, Nill M., Fink G.R., Aswendt M.*

Original resarch article - doi: 10.1016/j.neuroimage.2020.116873

Neuroimage, published on the 15 August 2020

Abstract Stroke is a devastating disease leading to cell death and disconnection between neurons both locally and remote, often resulting in severe long-term disability. Spontaneous reorganization of areas and pathways not primarily affected by ischemia is, however, associated with albeit limited recovery of function. Quantitative mapping of whole-brain changes of structural connectivity concerning the ischemia-induced sensorimotor deficit and recovery thereof would help to target structural plasticity in order to improve rehabilitation. Currently, only in vivo diffusion MRI can extract the structural whole-brain connectome noninvasively. This approach is, however, used primarily in human studies. Here, we applied atlas-based MRI analysis and graph theory to DTI in wild-type mice with cortical stroke lesions. Using a DTI network approach and graph theory, we aimed at gaining insights into the dynamics of the spontaneous reorganization after stroke related to the recovery of function. We found evidence for altered structural integrity of connections of specific brain regions, including the breakdown of connections between brain regions directly affected by stroke as well as long-range rerouting of intra- and transhemispheric connections related to improved sensorimotor behavior.

	Author contribution
Pallast N.	Conceptualization, methodology, validation data curation, writing - original draft
Wieters F.	Investigations, writing - review & editing
Nill M.	Investigations
Fink G.R.	Writing - review & editing
Aswendt M.	Supervision, writing - review & editing

9.1.5 Lesion Size- and Location-Dependent Recruitment of Contralesional Thalamus and Motor Cortex Facilitates Recovery after Stroke in Mice

Aswendt M., Pallast N.*, **Wieters F.***, Nill M., Fink G.R.**, Aswendt M.***
Shared first authorship, **Shared senior authorship
Original research article - doi: 10.1007/s12975-020-00802-3

Translational Stroke Research, published on the 3 March 2020

Abstract Brain lesions caused by cerebral ischemia or hemorrhage lead to a local breakdown of energy homeostasis followed by irreversible cell death and long-term impairment. Importantly, local brain lesions also generate remote functional and structural disturbances, which contribute to the behavioral deficit but also impact the recovery of function. While spontaneous recovery has been associated with endogenous repair mechanisms at the vascular, neural, and immune cell levels, the impact of structural plasticity on sensorymotor dysfunction and recovery thereof remains to be elucidated by longitudinal imaging in a mouse model. Here, we applied behavioral assessments, in vivo fiber tracking, and histological validation in a photothrombotic stroke mouse model. Atlas-based whole-brain structural connectivity analysis and ex vivo histology revealed secondary neurodegeneration in the ipsilesional brain areas, mostly in the dorsal sensorimotor area of the thalamus. Furthermore, we describe for the first time a lesion size-dependent increase in structural connectivity between the contralesional primary motor cortex and thalamus with the ipsilesional cortex. The involvement of the contralesional hemisphere was associated with improved functional recovery relative to lesion size.

	Author contribution
Aswendt M.	Conceptualization, validation, writing - original draft
Pallast N.	Validation, writing - review & editing
Wieters F.	Investigations, validation, writing - review & editing
Baues M.	Investigations
Hoehn M.	Conceptualization, writing - review & editing
Fink G.R.	Writing - review & editing

9.1.6 Atlas-based imaging data analysis tool for quantitative mouse brain histology (AIDAhisto)

Pallast N., ***Wieters F.****, Fink G.R., Aswendt M.*
Original resarch article - doi: 10.1016/j.jneumeth.2019.108394

Journal of Neuroscience Methods, published on the 1 October 2019

Abstract Cell counting in neuroscience is a routine method of utmost importance to support descriptive in vivo findings with quantitative data on the cellular level. Although known to be error- and bias-prone, manual cell counting of histological stained brain slices remains the gold standard in the field. While the manual approach is limited to small regions-of-interest in the brain, automated tools are needed to up-scale translational approaches and generate whole mouse brain counts in an atlas framework. Our goal was to develop an algorithm which requires no pre-training such as machine learning algorithms, only minimal user input, and adjustable variables to obtain reliable cell counting results for stitched mouse brain slices registered to a common atlas such as the Allen Mouse Brain atlas. We adapted filter banks to extract the maxima from round-shaped cell nuclei and various cell structures. In a qualitative as well as quantitative comparison to other tools and two expert raters, AIDAhisto provides accurate and fast results for cell nuclei as well as immunohistochemical stainings of various types of cells in the mouse brain.

	Author contribution
Pallast N.	Conceptualization, validation, writing - initial draft
Wieters F.	Investigations, validation, writing - review & editing
Fink G.R.	Writing - review & editing
Aswendt M.	Conceptualization, validation, writing - initial draft

9.1.7 Processing Pipeline for Atlas-Based Imaging Data Analysis of Structural and Functional Mouse Brain MRI (AIDAmri)

Pallast N., Diedenhofen M., Blascke S. ***Wieters F.****, Wiederman D., Hoehn M., Fink G.R., Aswendt M.*

Original resarch article - doi: 10.3389/fninf.2019.00042

Frontiers in Neuroinformatics, published on the 4 June 2019

Abstract Brain mapping, the correlation of corresponding regions between multiple brains in a standard brain atlas system, is widely used in human MRI. Here, we describe AIDAmri, a novel Atlas-based Imaging Data Analysis pipeline to process structural and functional mouse brain data including anatomical MRI, fiber tracking using diffusion tensor imaging (DTI) and functional connectivity analysis using resting-state functional MRI (rs-fMRI). The AIDAmri pipeline includes automated pre-processing steps, such as raw data conversion, skull-stripping and bias-field correction as well as image registration with the Allen Mouse Brain Reference Atlas (ARA). Following a modular structure developed in Python scripting language, the pipeline integrates established and newly developed algorithms. The raw data is analyzed and results transferred to the ARA coordinate system in order to allow an efficient and highly-accurate region-based analysis.

	Author contribution
Pallast N.	Conceptualization, software, validation, writing - original draft
Diedenhofen M.	Validation, writing - review & editing
Blaschke S.	Validation, writing - review & editing
Wieters F.	Investigations, validation, writing - review & editing
Wiedermann D.	Validation, writing - review & editing
Hoehn M.	Writing - review & editing
Fink G.R.	Writing - review & editing
Aswendt M.	Supervision, conceptualization, writing - original draft

9.1.8 Cloud-based relational database for multimodal animal data

Pallast N., ***Wieters F.****, Nill M., Fink G.R., Aswendt M.*

Original research article - doi: 10.1093/database/bay124

Database (Oxford), published on the 1 January 2018

Abstract Pre-clinical research builds on a large variety of in vivo and ex vivo tools such as non-invasive imaging, microscopy, and analysis of gene expression. To work efficiently with multimodal data and correlate results across scales, it is of particular importance to have easy access to all data points from different specimen, e.g. the magnetic resonance imaging (MRI) data from different time points, and the post-mortem histology. Here, we present a novel cloud-based relational database for multimodal animal data, which operates on commercial software. We have implemented data fields for various pre-clinical features such as MRI, histology and behaviour. The database template is useful for all labs working with laboratory animals and the adaption to specific research projects requires no prior scripting expertise. The database works operating-system independent through the web browser and allows multiple users to work simultaneously. The data entry is monitored and restricted for particular tests according to the user management in order to keep for example users during the experiment blinded for the experimental group. The database improves data accessibility, standardization of data recording and data handling efficiency in pre-clinical research.

	Author contribution
Pallast N.	Conceptualization, software, validation, writing - original draft
Wieters F.	Investigations, validation, writing - review & editing
Nill M.	Investigations
Fink G.R.	Writing - review & editing
Aswendt M.	Supervision, conceptualization, validation, writing - original draft

9.2 Projects and publications in progress

9.2.1 Terminal Hoffmann-Reflex Measurement after Stroke in Mice

Wieters F.* *& Gruhn M.*, Büschges A., Fink G.R., Aswendt M.*
Shared first authorship

Submitted 2021

Abstract After stroke, up to 35% of the patients develop post-stroke spasticity with clinical symptoms, including hypertonia in the corresponding muscles, non-voluntary muscle contractions, and pathologically augmented stretch-reflex. Cellular mechanisms leading to spasticity include an increased excitatory synaptic input from Ia afferent fibers, decreased inhibition of the spinal network and an increased motoneuron excitability. Here, we show a refinement of the evaluation of spasticity with the Hoffmann-Reflex, induced by electrical stimulation of peripheral nerves provides an established method to quantify the loss of inhibitory circuits in the forepaw.

	Author contribution
Wieters F.	Study design, investigations, validation, writing - original draft
Gruhn M.	Study design, investigations, validation, writing - original draft
Büschges A.	Writing - review & editing
Fink G.R.	Writing - review & editing
Aswendt M.	Writing - review & editing

9.2.2 Longitudinal measurement of spasticity after cortical and subcortical stroke in mice

***Wieters F.**, Gruhn M., Ullert J., Fritz V., Götz J., Büschges A., Fink G.R., Aswendt M.*

Experiments & Manuscript in progress

	Author contribution
Wieters F.	Conceptualization, methodology, investigations, validation, writing - original draft
Gruhn M.	Validation, methodology, writing - review & editing
Ullert J.	Investigations
Fritz V.	Investigations
Götz J.	Investigations
Büschges A.	Writing - review & editing
Fink G.R.	Writing - review & editing, funding acquisition
Aswendt M.	Conceptualization, writing - review & editing

9.2.3 Long-term pathology and behavioral deficit after thrombin stroke in mice

***Wieters, F.**, Dzybenko E., Tegtemeier M., Kuschel N., Middleham W.A., El-Amki M., Binder N., Wegener S., Fink G.R., Aswendt M.*

In preparation

	Author contribution
Wieters, F.	Conceptualization, investigations, funding acquisition, writing - writing original draft
Dzyubenko E.	Investigations, writing - review & editing
Tegtemeier, M.	Investigations
Kuschel, N.	Investigations
Middleham, W.A.	Investigations
El-Amki, M.	Investigations
Binder, N.	Investigations
Wegener, S.	Study design, writing - review & editing
Fink, G.R.	Writing - review & editing, funding acquisition
Aswendt, M.	Conceptualization, validation, study design, writing - original draft

9.2.4 Passive extending forces in mouse hip, knee, and ankle affect half of their joint angular ranges used in walking

Hooper S., Guschlbauer C., ***Wieters, F.****, Aswendt M., Büschges A.*

In preparation

	Author contribution
Hooper S.	Study design, conceptualization, investigations, writing - original draft
Guschlbauer C.	Study design, conceptualization, investigations, writing - original draft
Wieters, F.	Investigations, writing - review & editing
Aswendt, M.	Writing - review & editing
Büschges A.	Writing - review & editing

9.2.5 Reactive astrocytes prevent maladaptive plasticity and facilitate recovery after ischemic stroke

Aswendt M., Wilhelmsson U., ***Wieters F.****, Stokowska A., Schmitt F.J., Pallast N., Pablo Y., Mohammed L., Hoehn M., Pekna M., Pekny M.*

Under review 2021

	Author contribution
Aswendt M.	Conceptualization, validation, investigations, writing - original draft
Wilhelmsson U.	Investigations, validation, writing original draft
Wieters, F.	Investigations
Stokoswka A.	Validation, writing - review &editing
Schmitt F.J.	Validation
Pallast N.	Validation
Mohammed L.	Validation
Hoehn M.	Conceptualization, validation, writing - original draft
Pekna M.	Conceptualization, validation, writing - original draft
Pekny M.	Conceptualization, validation, writing - original draft

9.2.6 The gut microbiota is required for physiological brain network connectivity

Green C., Sadler R., Dzikowski L., Aswendt M., Gomez de Agüero M., Diedenhofen M, ***Wieters F.****, Wiedermann D., Liesz A., Hoehn A.*

Experiments & In revision 2021

	Author contribution
Green C.	Conceptualization, validation, investigations, writing - original draft
Sadler R.	Validation, writing review & editing
Dzikowski L.	investigations
Aswendt M.	Investigations
Gomez de Agürero M.	investigations
Diedenhofen M.	Investigations
Wieters, F.	Investigations
Wiedermann D.	validation
Liesz A.	Conceptualization, validation, writing - original draft
Hoehn M.	Conceptualization, validation, writing - original draft

10 Supplemental figures

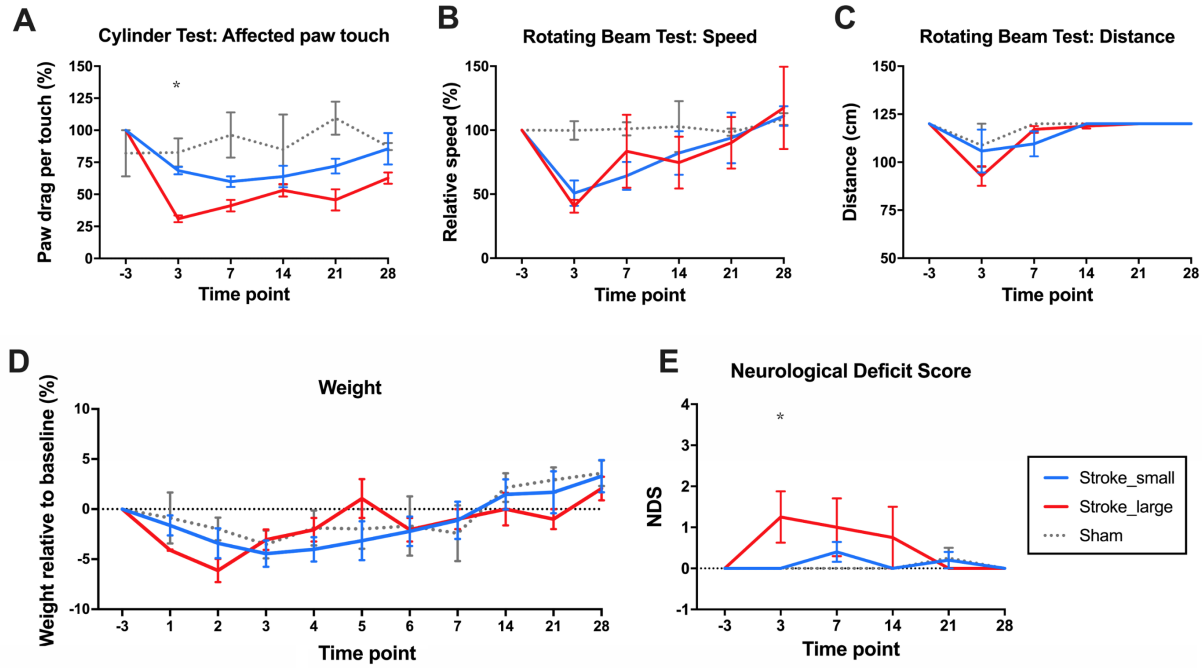

Figure 42 Physiological and behavioral deficits after photothrombosis. (**A**) Paw drags per touch in percent during cylinder test. (**B**) Relative speed and walked distance (**C**) during rotating beam. (**D**) Weight relative to baseline and (**E**) neurological deficit score.

List of Figures

1 Mechanisms during spontaneous recovery after stroke 12
2 Neuroanatomical reorganization after stroke 14
3 Commonly used mouse models of stroke 15
4 Symptoms of spasticity 22
5 Descending pathways of the stretch reflex 25
6 Hoffmann-Reflex as electrophysiological sign for the CNS integrity 29

7 Surgical room for stroke surgeries and electrophysiology 33
8 Schedule for post-stroke spasticity monitoring 35
9 Cortical photothrombosis 36
10 Photothrombosis in the MOp and MOs 37
11 Internal capsule stroke 38
12 Behavior tests 40
13 H-wave measurement for spasticity verification 43
14 Direct nerve measurement on the hind- or forepaw 44
15 Atlas-based landmark registration 47

16 Improvement of EMG measurement 49
17 Correlation between transcutaneous and direct nerve measurement 50
18 Transcutaneous H-wave measurement after lesion within the MOp 52
19 Direct nerve measurement after lesion within the MOp 53
20 Transcutaneous H-wave measurement after lesion within the MOs 54
21 Direct nerve measurement in animals with MOs lesion 55
22 Transcutaneous H-wave measurement after internal capsule stroke 57
23 Direct nerve measurement after internal capsule stroke 58
24 Rate-dependent depression after 56 days after stroke in the MOp, MOs or internal capsule 59
25 Decreased rate-dependent depression after internal capsule stroke 60
26 Behavioral deficits after small & large photothrombotic stroke compared to sham animals 62
27 Behavioral deficits after photothrombosis within the MOp and MOs 63
28 Behavioral changes after internal capsule stroke 66
29 Sensitivity of behavior tests after cortical and internal capsule stroke . . . 67

30 Correlation between behavior tests and electrophysiological properties . . . 68
31 Sensorimotor deficit score 69
32 Lesion mapping for small & large cortical photothrombosis 70
33 Secondary neurodegeneration after small & large cortical photothrombosis 71
34 Nissl staining 28 days after large stroke 72
35 Time series of nissl stainings after small stroke 73
36 BDA injection into the contralesional thalamus 75
37 Viral injection into the MOp in Emx1-Cre mice 76
38 Time series of microglia/macrophages activation in the brain 77
39 Time series of microglia/macrophages activation in the spinal cord 78
40 Quantification of the lesion size and location after cortical photothrombosis. 80
41 Myelin sheet staining with Black & Gold 81

42 Behavioral deficits, weight and neurological deficit scoring after photothrombosis 110

List of Tables

1 Consumables and materials 31
2 Photothrombosis protocols 36

11 Abbrevations

ADL	Activities of daily living
ARA	Allen Brain Reference Atlas
AP	Anteriorposterior
APP	Amyloid precursor protei
ALS	Amytropjic lateral sclerosis
BDA	Biotinylated dextran amine
BS	Blocking solution
CBF	Cerebral blood flow
CM	Cortico-motoneuronal
CNS	Central nervous system
CS	Corticospinal system
CST	Corticospinal tract
CTB	Cholera toxin subunit B
DAPI	4´-6-Diamidino-2-phenylindole
DNA	Deoxyribonucleic acid
DTI	Diffusion Tensor Imaging
DORpm	Thalamus, polymodal association cortex related
DORsm	Thalamus, sensory motor cortex related
DV	Dorsoventral
EMG	Electromyography
GABA	gamma-Aminobutyric acid
GV-SOLAS	Society of Laboratory Animal Science
GFAP	Glial fibrillary acidic protein
GFP	Green flourescent protein

Hip	Hippocampal region
H-Reflex	Hoffmann-Reflex
Hy	Hypothalamus
Hz	Hertz [1/s]
Iba1	Ionized calcium binding adaptor molecule 1
ICS	Internal capsule stroke
IHC	Immunohistochemistry
ip	Intraperitoneal
iv	Intravenous
LANUV	Landesamt für Umwelt, Naturschutz und Verbraucherschutz NRW
LSFM	Light-sheet fluorescence microscopy
LSI	Laser speckle imaging
mA	Milliampere
MAS	Modified Asworth Scale
MCAO	Middle cerebral artery occlusion
MS	Multiple sclerosis
MRI	Magnetic resonance imaging
MOp	Primary motor area
MOs	Secondary motor area
PBS	Phosphate buffered saline
PFA	Paraformaldehyde
PFC	Prefrontal cortex
PSS	Post-stroke spasticity
PT	Photothrombosis
ROS	Reactive oxygen species

rAAV	Recombinant adeno-associated virus
Rbp4	Retinol binding protein 4
RDD	Rate-dependent depression
ROI	Region of interest
RT	Room temperature (20°C)
RPM	Rotation per minute
rtPA	Recombinant tissue-specific plasminogen activator
sc	subcutaneous
SND	Secondary neurodegeneration
SNR	Signal to Noise Ratio
SPAM	Support Programme for Assembly of a database for Spasticity Measurement
SSp-ul	Primary somatosensory area, upper limb
T2WI	T2-weighted imaging
WD	Wallerian degeneration
WT	Wildtype
VST	Vestibulospinal tract

12 Acknowledgement

This work is the result of four years of research at the Department of Neurology at the University Hospital of Cologne in the Neuroimaging and Neuroengineering of Experimental Stroke Group and was funded by the Friebe Foundation.
This PhD thesis would not have been possible without the help and support of many people. First and foremost, I would like to especially thank Markus Aswendt. Thanks to him I enjoyed coming to work every day and without his help and support this work would not have been possible. Thanks to Markus' good networking and his willingness to establish many different and exciting projects, many research questions beyond my research focus could be explored, further rounding out the complexity of my work.
I would especially like to thank Niklas Pallast, without whom the analysis and interpretation of the data would not have been possible. My work was supported by many collaborators, interns and bachelor/master students: Veronika Fritz, Jan Götz, Nicole Kuschel, Mayan Baues, Michele Tetgemeier, Sebastian Kloubert, Leon Scharwächter, Felix Schmitt, Jule Ullert and Alina Jakobs. Thank you for your support, friendship and the great time we had together. Special thanks go to Olivia Käsgen and Marieke Nill, without whom the MRI study and the lengthy behavioral tests would not have been possible.
In addition to my research group, I would especially like to thank Matthias Gruhn for his dedication and indispensable contribution to this work. Without him, the electrophysiological measurements as demonstrated here would not be feasible. I would also like to thank my two tutors Ansgar Büschges and Holger Grüll for their support during my PhD thesis.
Finally, I would like to thank my parents and family, without whom I would not have become the person I am now. Most of all, I would like to thank my father, who has always been a role model for me in every situation in life. One person and a second one little person without whom I cannot imagine my life are my girlfriend Steph and daughter Momo. Without the unselfish care of Steph this work would not have been possible and thanks to Momo my life has been extended by another facet which I would not want to miss anymore.

References

[1] Abdallah, K., Nadeau, F., Bergeron, F., Blouin, S., Blais, V., Bradbury, K. M., Lavoie, C. L., Parent, J.-L. and Gendron, L. [2018]. Adeno-associated virus 2/9 delivery of cre recombinase in mouse primary afferents, *Scientific reports* **8**(1): 1–8.

[2] Ad, P. and Johnson, G. [1999]. Price cim, curless rh, barnes mp, rodgers h. a review of the properties and limitations of the ashworth and modified ashworth scales as measures of spasticity, *Clin Rehabil* **13**(5): 373–383.

[3] Ahmad, A. S., Satriotomo, I., Fazal, J. A., Nadeau, S. E. and Doré, S. [2015]. Optimization of a clinically relevant model of white matter stroke in mice: Histological and functional evidences, *Journal of neurology and neurosurgery* **2**(2).

[4] Ahmed, Z. [2014]. Trans-spinal direct current stimulation alters muscle tone in mice with and without spinal cord injury with spasticity, *Journal of Neuroscience* **34**(5): 1701–1709.

[5] Akay, T. [2014]. Long-term measurement of muscle denervation and locomotor behavior in individual wild-type and als model mice, *Journal of neurophysiology* **111**(3): 694–703.

[6] Akpinar, P., Atici, A., Ozkan, F., Aktas, I., Kulcu, D., Sarı, A. and Durmus, B. [2017]. Reliability of the modified ashworth scale and modified tardieu scale in patients with spinal cord injuries, *Spinal Cord* **55**(10): 944–949.

[7] Albers, G. W., Marks, M. P., Kemp, S., Christensen, S., Tsai, J. P., Ortega-Gutierrez, S., McTaggart, R. A., Torbey, M. T., Kim-Tenser, M., Leslie-Mazwi, T. et al. [2018]. Thrombectomy for stroke at 6 to 16 hours with selection by perfusion imaging, *New England Journal of Medicine* **378**(8): 708–718.

[8] Allison, S., Abraham, L. and Petersen, C. [1996]. Reliability of the modified ashworth scale in the assessment of plantarflexor muscle spasticity in patients with traumatic brain injury., *International journal of rehabilitation research. Internationale Zeitschrift fur Rehabilitationsforschung. Revue internationale de recherches de readaptation* **19**(1): 67–78.

[9] Aloraini, S. M., Gäverth, J., Yeung, E. and MacKay-Lyons, M. [2015]. Assessment of spasticity after stroke using clinical measures: a systematic review, *Disability and rehabilitation* **37**(25): 2313–2323.

[10] Armand, J. [1982]. The origin, course and terminations of corticospinal fibers in various mammals, *Progress in brain research* **57**: 329–360.

[11] Armand, J. and Kuypers, H. [1980]. Cells of origin of crossed and uncrossed corticospinal fibers in the cat, *Experimental brain research* **40**(1): 23–34.

[12] Aske, K. C. and Waugh, C. A. [2017]. Expanding the 3r principles, *EMBO reports* **18**(9): 1490–1492.

[13] Astrup, J., Siesjö, B. K. and Symon, L. [1981]. Thresholds in cerebral ischemia-the ischemic penumbra., *Stroke* **12**(6): 723–725.

[14] Aswendt, M., Pallast, N., Wieters, F., Baues, M., Hoehn, M. and Fink, G. R. [2020]. Lesion size-and location-dependent recruitment of contralesional thalamus and motor cortex facilitates recovery after stroke in mice, *Translational stroke research* pp. 1–11.

[15] Bachmann, L. C., Lindau, N. T., Felder, P. and Schwab, M. E. [2014]. Sprouting of brainstem–spinal tracts in response to unilateral motor cortex stroke in mice, *Journal of Neuroscience* **34**(9): 3378–3389.

[16] Bakheit, A., Maynard, V., Curnow, J., Hudson, N. and Kodapala, S. [2003]. The relation between ashworth scale scores and the excitability of the α motor neurones in patients with post-stroke muscle spasticity, *Journal of Neurology, Neurosurgery & Psychiatry* **74**(5): 646–648.

[17] Balci, B. P. [2018]. Spasticity measurement, *Archives of Neuropsychiatry* **55**(Suppl 1): S49.

[18] Balkaya, M. G., Trueman, R. C., Boltze, J., Corbett, D. and Jolkkonen, J. [2018]. Behavioral outcome measures to improve experimental stroke research, *Behavioural brain research* **352**: 161–171.

[19] Balkaya, M., Kröber, J. M., Rex, A. and Endres, M. [2013]. Assessing post-stroke behavior in mouse models of focal ischemia, *Journal of Cerebral Blood Flow & Metabolism* **33**(3): 330–338.

[20] Baricich, A., Picelli, A., Molteni, F., Guanziroli, E., Eng, B. and Santamato, A. [2016]. Post-stroke spasticity as a condition: a new perspective on patient evaluation, *Functional neurology* **31**(3): 179.

[21] Barlow, S. J. [2016]. Identifying the brain regions associated with acute spasticity in patients diagnosed with an ischemic stroke, *Somatosensory & motor research* **33**(2): 104–111.

[22] Barthas, F. and Kwan, A. C. [2017]. Secondary motor cortex: where 'sensory'meets 'motor'in the rodent frontal cortex, *Trends in neurosciences* **40**(3): 181–193.

[23] Baskin, Y. K., Dietrich, W. D. and Green, E. J. [2003]. Two effective behavioral tasks for evaluating sensorimotor dysfunction following traumatic brain injury in mice, *Journal of neuroscience methods* **129**(1): 87–93.

[24] Bello, S., Krogsbøll, L. T., Gruber, J., Zhao, Z. J., Fischer, D. and Hróbjartsson, A. [2014]. Lack of blinding of outcome assessors in animal model experiments implies risk of observer bias, *Journal of clinical epidemiology* **67**(9): 973–983.

[25] Bennett, D., Sanelli, L., Cooke, C., Harvey, P. and Gorassini, M. [2004]. Spastic long-lasting reflexes in the awake rat after sacral spinal cord injury, *Journal of neurophysiology* **91**(5): 2247–2258.

[26] Bernhardt, J., Hayward, K. S., Kwakkel, G., Ward, N. S., Wolf, S. L., Borschmann, K., Krakauer, J. W., Boyd, L. A., Carmichael, S. T., Corbett, D. et al. [2017]. Agreed definitions and a shared vision for new standards in stroke recovery research: the stroke recovery and rehabilitation roundtable taskforce, *International Journal of Stroke* **12**(5): 444–450.

[27] Biscoe, T. and Fry, J. [1982]. Some pharmacological studies on the spastic mouse., *British journal of pharmacology* **75**(1): 23.

[28] Blackwell, A. A., Banovetz, M. T., Whishaw, I. Q., Wallace, D. G. et al. [2018]. The structure of arm and hand movements in a spontaneous and food rewarded on-line string-pulling task by the mouse, *Behavioural brain research* **345**: 49–58.

[29] Blasi, F., Whalen, M. J. and Ayata, C. [2015]. Lasting pure-motor deficits after focal posterior internal capsule white-matter infarcts in rats, *Journal of Cerebral Blood Flow & Metabolism* **35**(6): 977–984.

[30] Brashear, A., McAfee, A. L., Kuhn, E. R. and Fyffe, J. [2004]. Botulinum toxin type b in upper-limb poststroke spasticity: a double-blind, placebo-controlled trial, *Archives of physical medicine and rehabilitation* **85**(5): 705–709.

[31] Brewer, L., Horgan, F., Hickey, A. and Williams, D. [2013]. Stroke rehabilitation: recent advances and future therapies, *QJM: An International Journal of Medicine* **106**(1): 11–25.

[32] Brooks, S. P. and Dunnett, S. B. [2009]. Tests to assess motor phenotype in mice: a user's guide, *Nature Reviews Neuroscience* **10**(7): 519–529.

[33] Brown, A. and Weaver, L. C. [2012]. The dark side of neuroplasticity, *Experimental neurology* **235**(1): 133–141.

[34] Brown, C. E., Wong, C. and Murphy, T. H. [2008]. Rapid morphologic plasticity of peri-infarct dendritic spines after focal ischemic stroke, *Stroke* **39**(4): 1286–1291.

[35] Brunnstrom, S. [1966]. Motor testing procedures in hemiplegia: based on sequential recovery stages, *Physical therapy* **46**(4): 357–375.

[36] BucY, P. C., Keplinger, J. E. and Siqueira, E. B. [1964]. Destruction of the "pyramidal tract" in man, *Journal of neurosurgery* **21**(5): 385–398.

[37] Burke, D., Wissel, J. and Donnan, G. A. [2013]. Pathophysiology of spasticity in stroke, *Neurology* **80**(3 Supplement 2): S20–S26.

[38] Burridge, J., Wood, D., Hermens, H. J., Voerman, G., Johnson, G., Wijck, F. V., Platz, T., Gregoric, M., Hitchcock, R. and Pandyan, A. [2005]. Theoretical and methodological considerations in the measurement of spasticity, *Disability and rehabilitation* **27**(1-2): 69–80.

[39] Burrows, D. J., McGown, A., Jain, S. A., Felice, M. D., Ramesh, T. M., Sharrack, B. and Majid, A. [2019]. Animal models of multiple sclerosis: From rodents to zebrafish, *Multiple Sclerosis Journal* **25**(3): 306–324. PMID: 30319015.

[40] Bütefisch, C. M., Weβling, M., Netz, J., Seitz, R. J. and Hömberg, V. [2008]. Relationship between interhemispheric inhibition and motor cortex excitability in subacute stroke patients, *Neurorehabilitation and neural repair* **22**(1): 4–21.

[41] Byblow, W. D., Stinear, C. M., Barber, P. A., Petoe, M. A. and Ackerley, S. J. [2015]. Proportional recovery after stroke depends on corticomotor integrity, *Annals of neurology* **78**(6): 848–859.

[42] Calancie, B., Broton, J. G., Klose, K. J., Traad, M., Difini, J. and Ayyar, D. R. [1993]. Evidence that alterations in presynaptic inhibition contribute to segmental hypo-and hyperexcitability after spinal cord injury in man, *Electroencephalography and Clinical Neurophysiology/Evoked Potentials Section* **89**(3): 177–186.

[43] Caleo, M. [2015]. Rehabilitation and plasticity following stroke: Insights from rodent models, *Neuroscience* **311**: 180–194.

[44] Canazza, A., Minati, L., Boffano, C., Parati, E. and Binks, S. [2014]. Experimental models of brain ischemia: a review of techniques, magnetic resonance imaging, and investigational cell-based therapies, *Frontiers in neurology* **5**: 19.

[45] Cao, Z., Harvey, S. S., Chiang, T., Foltz, A. G., Lee, A. G., Cheng, M. Y. and Steinberg, G. K. [2020]. Unique subtype of microglia in degenerative thalamus after cortical stroke, *Stroke* pp. STROKEAHA–120.

[46] Carmel, J. B. and Martin, J. H. [2014]. Motor cortex electrical stimulation augments sprouting of the corticospinal tract and promotes recovery of motor function, *Frontiers in integrative neuroscience* **8**: 51.

[47] Carmichael, S. T. [2005]. Rodent models of focal stroke: Size, mechanism, and purpose, *NeuroRX* **2**(3): 396–409. Animal Models of Neurological Disorders.

[48] Carmichael, S. T. [2016]. The 3 rs of stroke biology: radial, relayed, and regenerative, *Neurotherapeutics* **13**(2): 348–359.

[49] Carmichael, S. T., Kathirvelu, B., Schweppe, C. A. and Nie, E. H. [2017]. Molecular, cellular and functional events in axonal sprouting after stroke, *Experimental neurology* **287**: 384–394.

[50] Carp, J. S., Tennissen, A. M., Chen, X. Y., Schalk, G. and Wolpaw, J. R. [2005]. Long-term spinal reflex studies in awake behaving mice, *Journal of neuroscience methods* **149**(2): 134–143.

[51] Carp, J. S., Tennissen, A. M., Chen, X. Y. and Wolpaw, J. R. [2006]. H-reflex operant conditioning in mice, *Journal of neurophysiology* **96**(4): 1718–1727.

[52] Carter, R. J., Morton, J. and Dunnett, S. B. [2001]. Motor coordination and balance in rodents, *Current protocols in neuroscience* **15**(1): 8–12.

[53] Casals, J. B., Pieri, N. C., Feitosa, M. L., Ercolin, A., Roballo, K., Barreto, R. S., Bressan, F. F., Martins, D. S., Miglino, M. A. and Ambrósio, C. E. [2011]. The use of animal models for stroke research: a review, *Comparative medicine* **61**(4): 305–313.

[54] Chai, C. [1961]. Hereditary spasticity in mice, *Journal of Heredity* **52**(5): 241–243.

[55] Chai, C., Roberts, E. and Sidman, R. L. [1962]. Influence of aminooxyacetic acid, a γ-aminobutyrate transaminase inhibitor, on hereditary spastic defect in the mouse., *Proceedings of the Society for Experimental Biology and Medicine* **109**(3): 491–495.

[56] Chao, O., Pum, M., Li, J.-S. and Huston, J. [2012]. The grid-walking test: assessment of sensorimotor deficits after moderate or severe dopamine depletion by 6-hydroxydopamine lesions in the dorsal striatum and medial forebrain bundle, *Neuroscience* **202**: 318–325.

[57] Chen, W., Xia, M., Guo, C., Jia, Z., Wang, J., Li, C., Li, M., Tang, X., Hu, R., Chen, Y. et al. [2019]. Modified behavioural tests to detect white matter injury-induced motor deficits after intracerebral haemorrhage in mice, *Scientific reports* **9**(1): 1–11.

[58] Cheng, M. Y., Wang, E. H., Woodson, W. J., Wang, S., Sun, G., Lee, A. G., Arac, A., Fenno, L. E., Deisseroth, K. and Steinberg, G. K. [2014]. Optogenetic neuronal stimulation promotes functional recovery after stroke, *Proceedings of the National Academy of Sciences* **111**(35): 12913–12918.

[59] Cirillo, C., Brihmat, N., Castel-Lacanal, E., Le Friec, A., Barbieux-Guillot, M., Raposo, N., Pariente, J., Viguier, A., Simonetta-Moreau, M., Albucher, J.-F. et al. [2020]. Post-stroke remodeling processes in animal models and humans, *Journal of Cerebral Blood Flow & Metabolism* **40**(1): 3–22.

[60] Clarkson, A. N., López-Valdés, H. E., Overman, J. J., Charles, A. C., Brennan, K. and Carmichael, S. T. [2013]. Multimodal examination of structural and functional remapping in the mouse photothrombotic stroke model, *Journal of Cerebral Blood Flow & Metabolism* **33**(5): 716–723.

[61] Colak, G., Filiano, A. J. and Johnson, G. V. [2011]. The application of permanent middle cerebral artery ligation in the mouse, *Journal of visualized experiments: JoVE* (53).

[62] Conte, W. L., Kamishina, H. and Reep, R. L. [2009]. Multiple neuroanatomical tract-tracing using fluorescent alexa fluor conjugates of cholera toxin subunit b in rats, *Nature Protocols* **4**(8): 1157.

[63] Corbett, D., Carmichael, S. T., Murphy, T. H., Jones, T. A., Schwab, M. E., Jolkkonen, J., Clarkson, A. N., Dancause, N., Weiloch, T., Johansen-Berg, H. et al. [2017]. Enhancing the alignment of the preclinical and clinical stroke recovery research pipeline: Consensus-based core recommendations from the stroke recovery and rehabilitation roundtable translational working group, *Neurorehabilitation and Neural Repair* **31**(8): 699–707.

[64] Cowey, A. and Boz^ek, T. [1974]. Contralateral 'neglect'after unilateral dorsomedial prefrontal lesions in rats, *Brain Research* **72**(1): 53–63.

[65] Cramer, S. C. and Crafton, K. R. [2006]. Somatotopy and movement representation sites following cortical stroke, *Experimental brain research* **168**(1-2): 25–32.

[66] Crone, C., Nielsen, J., Petersen, N., Ballegaard, M. and Hultborn, H. [1994]. Disynaptic reciprocal inhibition of ankle extensors in spastic patients, *Brain* **117**(5): 1161–1168.

[67] Cui, L.-l., Golubczyk, D. and Jolkkonen, J. [2017]. Top 3 behavioral tests in cell therapy studies after stroke: difficult to stop a moving train, *Stroke* **48**(11): 3165–3167.

[68] Day, B., Marsden, C., Obeso, J. and Rothwell, J. [1984]. Reciprocal inhibition between the muscles of the human forearm., *The Journal of physiology* **349**(1): 519–534.

[69] Delwaide, P. and Oliver, E. [1988]. Short-latency autogenic inhibition (ib inhibition) in human spasticity., *Journal of Neurology, Neurosurgery & Psychiatry* **51**(12): 1546–1550.

[70] Denys, E. H. [1991]. Aaem minimonograph# 14: The influence of temperature in clinical neurophysiology, *Muscle & Nerve: Official Journal of the American Association of Electrodiagnostic Medicine* **14**(9): 795–811.

[71] Desowska, A. and Turner, D. L. [2019]. Dynamics of brain connectivity after stroke, *Reviews in the Neurosciences* **30**(6): 605–623.

[72] Di Marzo, V. [2007]. The endocannabinoid system for the development of new drugs for spasticity, *Drugs Future* **32**: 341–351.

[73] Dobkin, B. H. and Carmichael, S. T. [2016]. The specific requirements of neural repair trials for stroke, *Neurorehabilitation and neural repair* **30**(5): 470–478.

[74] Drory, V. E., Goltsman, E., Reznik, J. G., Mosek, A. and Korczyn, A. D. [2001]. The value of muscle exercise in patients with amyotrophic lateral sclerosis, *Journal of the neurological sciences* **191**(1-2): 133–137.

[75] du Sert, N. P., Alfieri, A., Allan, S. M., Carswell, H. V., Deuchar, G. A., Farr, T. D., Flecknell, P., Gallagher, L., Gibson, C. L., Haley, M. J., Macleod, M. R., McColl, B. W., McCabe, C., Morancho, A., Moon, L. D., O'Neill, M. J., de Puig, I. P., Planas, A., Ragan, C. I., Rosell, A., Roy, L. A., Ryder, K. O., Simats, A., Sena, E. S., Sutherland, B. A., Tricklebank, M. D., Trueman, R. C., Whitfield, L., Wong, R. and Macrae, I. M. [2017]. The improve guidelines (ischaemia models: Procedural refinements of in vivo experiments), *Journal of Cerebral Blood Flow & Metabolism* **37**(11): 3488–3517.

[76] Eaton, M. [2003]. Common animal models for spasticity and pain., *Journal of Rehabilitation Research & Development* **40**(4).

[77] Edgerton, V. R. and Roy, R. R. [2010]. Spasticity: a switch from inhibition to excitation, *Nature medicine* **16**(3): 270–271.

[78] El Amki, M., Baumgartner, P., Bracko, O., Luft, A. and Wegener, S. [2017]. Task-specific motor rehabilitation therapy after stroke improves performance in a different motor task: translational evidence, *Translational stroke research* **8**(4): 347–350.

[79] Emos, M. C. and Agarwal, S. [2018]. Neuroanatomy, upper motor neuron lesion, *StatPearls [Internet]* .

[80] Endres, M., Engelhardt, B., Koistinaho, J., Lindvall, O., Meairs, S., Mohr, J. P., Planas, A., Rothwell, N., Schwaninger, M., Schwab, M. E. et al. [2008]. Improving outcome after stroke: overcoming the translational roadblock, *Cerebrovascular diseases* **25**(3): 268–278.

[81] Engel, O., Kolodziej, S., Dirnagl, U. and Prinz, V. [2011]. Modeling stroke in mice-middle cerebral artery occlusion with the filament model, *Journal of visualized experiments: JoVE* (47).

[82] Ergul, A., Hafez, S., Fouda, A. and Fagan, S. C. [2016]. Impact of comorbidities on acute injury and recovery in preclinical stroke research: focus on hypertension and diabetes, *Translational stroke research* **7**(4): 248–260.

[83] Esquenazi, A., Albanese, A., Chancellor, M. B., Elovic, E., Segal, K. R., Simpson, D. M., Smith, C. P. and Ward, A. B. [2013]. Evidence-based review and assessment of botulinum neurotoxin for the treatment of adult spasticity in the upper motor neuron syndrome, *Toxicon* **67**: 115–128.

[84] Fang, M. C., Cutler, D. M. and Rosen, A. B. [2010]. Trends in thrombolytic use for ischemic stroke in the united states, *Journal of hospital medicine* **5**(7): 406–409.

[85] Fernando, M., Simpson, J., Matthews, F., Brayne, C., Lewis, C., Barber, R., Kalaria, R., Forster, G., Esteves, F., Wharton, S. et al. [2006]. Mrc cognitive function and ageing neuropathology study group. white matter lesions in an unselected cohort of the elderly: molecular pathology suggests origin from chronic hypoperfusion injury, *Stroke* **37**(6): 1391–1398.

[86] Finnerup, N. [2017]. Neuropathic pain and spasticity: intricate consequences of spinal cord injury, *Spinal Cord* **55**(12): 1046–1050.

[87] Fleuren, J. F., Voerman, G. E., Erren-Wolters, C. V., Snoek, G. J., Rietman, J. S., Hermens, H. J. and Nene, A. V. [2010]. Stop using the ashworth scale for the assessment of spasticity, *Journal of Neurology, Neurosurgery & Psychiatry* **81**(1): 46–52.

[88] Fluri, F., Schuhmann, M. K. and Kleinschnitz, C. [2015]. Animal models of ischemic stroke and their application in clinical research, *Drug design, development and therapy* **9**: 3445.

[89] Foddis, M., Winek, K., Bentele, K., Mueller, S., Blumenau, S., Reichhart N, N., Crespo-Garcia, S., Harnett, D., Ivanov, A., Meisel, A. et al. [2020]. An exploratory investigation of brain collateral circulation plasticity after cerebral ischemia in two experimental c57bl/6 mouse models, *Journal of Cerebral Blood Flow & Metabolism* **40**(2): 276–287.

[90] Francisco, G. E. and McGuire, J. R. [2012]. Poststroke spasticity management, *Stroke* **43**(11): 3132–3136.

[91] Friel, K., Williams, P., Serradj, N., Chakrabarty, S. and Martin, J. [n.d.]. Activity-based therapies for repair of the corticospinal system injured during development. front neurol. 2014; 5: 229.

[92] Frost, S. B., Barbay, S., Mumert, M. L., Stowe, A. M. and Nudo, R. J. [2006]. An animal model of capsular infarct: endothelin-1 injections in the rat, *Behavioural brain research* **169**(2): 206–211.

[93] Funase, K., Imanaka, K., Nishihira, Y. and Araki, H. [1994]. Threshold of the soleus muscle h-reflex is less sensitive to the change in excitability of the motoneuron pool during plantarflexion or dorsiflexion in humans, *European journal of applied physiology and occupational physiology* **69**(1): 21–25.

[94] Gabbott, P. L., Warner, T. A., Jays, P. R., Salway, P. and Busby, S. J. [2005]. Prefrontal cortex in the rat: projections to subcortical autonomic, motor, and limbic centers, *Journal of Comparative Neurology* **492**(2): 145–177.

[95] Gage, G. J., Kipke, D. R. and Shain, W. [2012]. Whole animal perfusion fixation for rodents, *JoVE (Journal of Visualized Experiments)* (65): e3564.

[96] Ganapathy, V., Graham, G. D., DiBonaventura, M. D., Gillard, P. J., Goren, A. and Zorowitz, R. D. [2015]. Caregiver burden, productivity loss, and indirect costs associated with caring for patients with poststroke spasticity, *Clinical interventions in aging* **10**: 1793.

[97] Gill, C., Phelan, J. P., Hatzipetros, T., Kidd, J. D., Tassinari, V. R., Levine, B., Wang, M. Z., Moreno, A., Thompson, K., Maier, M. et al. [2019]. Sod1-positive aggregate accumulation in the cns predicts slower disease progression and increased longevity in a mutant sod1 mouse model of als, *Scientific reports* **9**(1): 1–13.

[98] Gillard, P. J., Sucharew, H., Kleindorfer, D., Belagaje, S., Varon, S., Alwell, K., Moomaw, C. J., Woo, D., Khatri, P., Flaherty, M. L. et al. [2015]. The negative impact of spasticity on the health-related quality of life of stroke survivors: a longitudinal cohort study, *Health and quality of life outcomes* **13**(1): 1–9.

[99] Gorelick, P. B. [2019]. The global burden of stroke: persistent and disabling, *The Lancet Neurology* **18**(5): 417–418.

[100] Gorski, J. A., Talley, T., Qiu, M., Puelles, L., Rubenstein, J. L. and Jones, K. R. [2002]. Cortical excitatory neurons and glia, but not gabaergic neurons, are produced in the emx1-expressing lineage, *Journal of Neuroscience* **22**(15): 6309–6314.

[101] Grefkes, C., Eickhoff, S. B., Nowak, D. A., Dafotakis, M. and Fink, G. R. [2008]. Dynamic intra-and interhemispheric interactions during unilateral and bilateral hand movements assessed with fmri and dcm, *Neuroimage* **41**(4): 1382–1394.

[102] Grefkes, C. and Fink, G. R. [2011]. Reorganization of cerebral networks after stroke: new insights from neuroimaging with connectivity approaches, *Brain* **134**(5): 1264–1276.

[103] Grefkes, C. and Fink, G. R. [2014]. Connectivity-based approaches in stroke and recovery of function, *The Lancet Neurology* **13**(2): 206–216.

[104] Gu, Z., Kalambogias, J., Yoshioka, S., Han, W., Li, Z., Kawasawa, Y. I., Pochareddy, S., Li, Z., Liu, F., Xu, X. et al. [2017]. Control of species-dependent cortico-motoneuronal connections underlying manual dexterity, *Science* **357**(6349): 400–404.

[105] Gupta, A. D., Visvanathan, R., Cameron, I., Koblar, S. A., Howell, S. and Wilson, D. [2019]. Efficacy of botulinum toxin in modifying spasticity to improve walking and quality of life in post-stroke lower limb spasticity-a randomized double-blind placebo controlled study, *BMC neurology* **19**(1): 96.

[106] Hacke, W., Kaste, M., Bluhmki, E., Brozman, M., Dávalos, A., Guidetti, D., Larrue, V., Lees, K. R., Medeghri, Z., Machnig, T. et al. [2008]. Thrombolysis with alteplase 3 to 4.5 hours after acute ischemic stroke, *New England journal of medicine* **359**(13): 1317–1329.

[107] Han, C.-W., Lee, K.-H., Noh, M. G., Kim, J.-M., Kim, H.-S., Kim, H.-S., Kim, R. G., Cho, J., Kim, H.-I. and Lee, M.-C. [2017]. An experimental infarct targeting the internal capsule: histopathological and ultrastructural changes, *Journal of pathology and translational medicine* **51**(3): 292.

[108] Hånell, A. and Marklund, N. [2014]. Structured evaluation of rodent behavioral tests used in drug discovery research, *Frontiers in behavioral neuroscience* **8**: 252.

[109] Hankey, G. J., Jamrozik, K., Broadhurst, R. J., Forbes, S. and Anderson, C. S. [2002]. Long-term disability after first-ever stroke and related prognostic factors in the perth community stroke study, 1989–1990, *Stroke* **33**(4): 1034–1040.

[110] Hass, B. [1994]. The interrater reliability of the original and of the modified ashworth scale for the assessment of spasticity in patients with spinal cord injury, *Spinal Cord* **8**: 441–454.

[111] He, S.-Q., Dum, R. P. and Strick, P. L. [1993]. Topographic organization of corticospinal projections from the frontal lobe: motor areas on the lateral surface of the hemisphere, *Journal of Neuroscience* **13**(3): 952–980.

[112] Heller, A. H. and Hallett, M. [1982]. Electrophysiological studies with the spastic mutant mouse, *Brain research* **234**(2): 299–308.

[113] Hicks, J. M., Taub, E., Womble, B., Barghi, A., Rickards, T., Mark, V. W. and Uswatte, G. [2018]. Relation of white matter hyperintensities and motor deficits in chronic stroke, *Restorative neurology and neuroscience* **36**(3): 349–357.

[114] Hinderer, S. R. and Dixon, K. [2001]. Physiologic and clinical monitoring of spastic hypertonia, *Physical medicine and rehabilitation clinics of North America* **12**(4): 733–746.

[115] Hoch, M. C. and Krause, B. A. [2009]. Intersession reliability of h: M ratio is greater than the h-reflex at a percentage of m-max, *International Journal of Neuroscience* **119**(3): 345–352.

[116] Hodgetts, S. I., Plant, G. W. and Harvey, A. R. [2009]. Chapter 14 - spinal cord injury: experimental animal models and relation to human therapy, *in* C. Watson, G. Paxinos and G. Kayalioglu (eds), *The Spinal Cord*, Academic Press, San Diego, pp. 209–237.
URL: *https://www.sciencedirect.com/science/article/pii/B9780123742476500183*

[117] Hoffman, P. [1910]. Beitrage zur kenntnis der menschlichen: Reflexe mit besonderer berucksichtigung der elektrischen erscheinungen, *Arch F Physiol* pp. 223–256.

[118] Hoffmann, P. [1918]. Uber die beziehungen der sehnenreflexe zur willkurlichen bewegung und zum tonus, *Z. Biol.* **68**: 351–370.

[119] Hofstoetter, U. S., McKay, W. B., Tansey, K. E., Mayr, W., Kern, H. and Minassian, K. [2014]. Modification of spasticity by transcutaneous spinal cord stimulation in individuals with incomplete spinal cord injury, *The journal of spinal cord medicine* **37**(2): 202–211.

[120] Holman, L., Head, M. L., Lanfear, R. and Jennions, M. D. [2015]. Evidence of experimental bias in the life sciences: why we need blind data recording, *PLoS Biol* **13**(7): e1002190.

[121] Holtz, K. A., Lipson, R., Noonan, V. K., Kwon, B. K. and Mills, P. B. [2017]. Prevalence and effect of problematic spasticity after traumatic spinal cord injury, *Archives of physical medicine and rehabilitation* **98**(6): 1132–1138.

[122] Horie, N., Maag, A.-L., Hamilton, S. A., Shichinohe, H., Bliss, T. M. and Steinberg, G. K. [2008a]. Mouse model of focal cerebral ischemia using endothelin-1, *Journal of neuroscience methods* **173**(2): 286–290.

[123] Horie, N., Maag, A.-L., Hamilton, S. A., Shichinohe, H., Bliss, T. M. and Steinberg, G. K. [2008b]. Mouse model of focal cerebral ischemia using endothelin-1, *Journal of neuroscience methods* **173**(2): 286–290.

[124] Hossmann, K.-A. [2012]. The two pathophysiologies of focal brain ischemia: implications for translational stroke research, *Journal of Cerebral Blood Flow & Metabolism* **32**(7): 1310–1316.

[125] Howells, D. W., Porritt, M. J., Rewell, S. S., O'collins, V., Sena, E. S., Van Der Worp, H. B., Traystman, R. J. and Macleod, M. R. [2010]. Different strokes for different folks: the rich diversity of animal models of focal cerebral ischemia, *Journal of Cerebral Blood Flow & Metabolism* **30**(8): 1412–1431.

[126] Hua, Y., Schallert, T., Keep, R. F., Wu, J., Hoff, J. T. and Xi, G. [2002]. Behavioral tests after intracerebral hemorrhage in the rat, *Stroke* **33**(10): 2478–2484.

[127] Hughes, C. and Howard, I. M. [2013]. Spasticity management in multiple sclerosis, *Physical Medicine and Rehabilitation Clinics* **24**(4): 593–604.

[128] Hughes, P., Anthony, D., Ruddin, M., Botham, M., Rankine, E., Sablone, M., Baumann, D., Mir, A. and Perry, V. [2003]. Focal lesions in the rat central nervous system induced by endothelin-1, *Journal of Neuropathology & Experimental Neurology* **62**(12): 1276–1286.

[129] Iadecola, C. [2013]. The pathobiology of vascular dementia, *Neuron* **80**(4): 844–866.

[130] Illert, M. and Kuhtz-Buschbeck, J. [2006]. Motorisches system, *Neuro-und Sinnesphysiologie*, Springer, pp. 94–130.

[131] Ingberg, E., Dock, H., Theodorsson, E., Theodorsson, A. and Ström, J. O. [2016]. Method parameters' impact on mortality and variability in mouse stroke experiments: a meta-analysis, *Scientific reports* **6**(1): 1–19.

[132] Jang, S. H. [2014]. The corticospinal tract from the viewpoint of brain rehabilitation, *Journal of rehabilitation medicine* **46**(3): 193–199.

[133] Jeffrey-Gauthier, R., Piché, M. and Leblond, H. [2019]. H-reflex disinhibition by lumbar muscle inflammation in a mouse model of spinal cord injury, *Neuroscience letters* **690**: 36–41.

[134] Jeong, M., Kim, Y., Kim, J., Ferrante, D. D., Mitra, P. P., Osten, P. and Kim, D. [2016]. Comparative three-dimensional connectome map of motor cortical projections in the mouse brain, *Scientific reports* **6**(1): 1–14.

[135] Jiang, Y.-Q., Zaaimi, B. and Martin, J. H. [2016]. Competition with primary sensory afferents drives remodeling of corticospinal axons in mature spinal motor circuits, *Journal of Neuroscience* **36**(1): 193–203.

[136] Jo, H. M., Choi, B. Y., Chang, C. H., Kim, S. H., Lee, J., Chang, M. C., Son, S. M. and Jang, S. H. [2012]. The clinical characteristics of motor function in chronic hemiparetic stroke patients with complete corticospinal tract injury, *NeuroRehabilitation* **31**(2): 207–213.

[137] Jolkkonen, J., Jokivarsi, K., Laitinen, T. and Gröhn, O. [2007]. Subacute hemorrhage and resolution of edema in rose bengal stroke model in rats coincides with improved sensorimotor functions, *Neuroscience letters* **428**(2-3): 99–102.

[138] Jones, T. A. [2017]. Motor compensation and its effects on neural reorganization after stroke, *Nature Reviews Neuroscience* **18**(5): 267–280.

[139] Jones, T. A. and Adkins, D. L. [2015]. Motor system reorganization after stroke: stimulating and training toward perfection, *Physiology* **30**(5): 358–370.

[140] Jones, T. A. and Schallert, T. [1992]. Overgrowth and pruning of dendrites in adult rats recovering from neocortical damage, *Brain research* **581**(1): 156–160.

[141] Joosten, E. A., Schuitman, R., Vermelis, M. and Dederen, P. [1992]. Postnatal development of the ipsilateral corticospinal component in rat spinal cord: a light and electron microscopic anterograde hrp study, *Journal of Comparative Neurology* **326**(1): 133–146.

[142] Justice, J. N., Carter, C. S., Beck, H. J., Gioscia-Ryan, R. A., McQueen, M., Enoka, R. M. and Seals, D. R. [2014]. Battery of behavioral tests in mice that models age-associated changes in human motor function, *Age* **36**(2): 583–595.

[143] Kakinohana, O., Hefferan, M., Nakamura, S., Kakinohana, M., Galik, J., Tomori, Z., Marsala, J., Yaksh, T. and Marsala, M. [2006]. Development of gaba-sensitive spasticity and rigidity in rats after transient spinal cord ischemia: a qualitative and quantitative electrophysiological and histopathological study, *Neuroscience* **141**(3): 1569–1583.

[144] Karbasforoushan, H., Cohen-Adad, J. and Dewald, J. P. [2019]. Brainstem and spinal cord mri identifies altered sensorimotor pathways post-stroke, *Nature communications* **10**(1): 1–7.

[145] Kaymak, B., Kara, M., Soylu, A. R., Özçakar, L. et al. [2017]. Innervation zone targeted botulinum toxin injections., *European journal of physical and rehabilitation medicine* **54**(1): 100–109.

[146] Kilkenny, C., Browne, W. J., Cuthill, I. C., Emerson, M. and Altman, D. G. [2010]. Improving bioscience research reporting: The arrive guidelines for reporting animal research, *PLOS Biology* **8**(6): 1–5.

[147] Király, B., Balázsfi, D., Horváth, I., Solari, N., Sviatkó, K., Lengyel, K., Birtalan, E., Babos, M., Bagaméry, G., Máthé, D. et al. [2020]. In vivo localization of chronically implanted electrodes and optic fibers in mice, *Nature communications* **11**(1): 1–17.

[148] Knikou, M. [2008]. The h-reflex as a probe: pathways and pitfalls, *Journal of neuroscience methods* **171**(1): 1–12.

[149] Krause, P., Edrich, T. and Straube, A. [2004]. Lumbar repetitive magnetic stimulation reduces spastic tone increase of the lower limbs, *Spinal cord* **42**(2): 67–72.

[150] Krischak, G., Augat, P., Blakytny, R., Claes, L., Kinzl, L. and Beck, A. [2007]. The non-steroidal anti-inflammatory drug diclofenac reduces appearance of osteoblasts in bone defect healing in rats, *Archives of orthopaedic and trauma surgery* **127**(6): 453–458.

[151] Kuo, C.-L. and Hu, G.-C. [2018]. Post-stroke spasticity: a review of epidemiology, pathophysiology, and treatments, *International Journal of Gerontology* **12**(4): 280–284.

[152] Kuraoka, M., Furuta, T., Matsuwaki, T., Omatsu, T., Ishii, Y., Kyuwa, S. and Yoshikawa, Y. [2009]. Direct experimental occlusion of the distal middle cerebral artery induces high reproducibility of brain ischemia in mice, *Experimental animals* **58**(1): 19–29.

[153] Labat-gest, V. and Tomasi, S. [2013]. Photothrombotic ischemia: a minimally invasive and reproducible photochemical cortical lesion model for mouse stroke studies, *Journal of visualized experiments: JoVE* (76).

[154] Lamy, J.-C., Ho, C., Badel, A., Arrigo, R. T. and Boakye, M. [2012]. Modulation of soleus h reflex by spinal dc stimulation in humans, *Journal of neurophysiology* **108**(3): 906–914.

[155] Lance, J. [1990]. What is spasticity?, *The Lancet* **335**(8689): 606.

[156] Lang, C., Bradley, P. M., Jacobi, A., Kerschensteiner, M. and Bareyre, F. M. [2013]. Stat3 promotes corticospinal remodelling and functional recovery after spinal cord injury, *EMBO reports* **14**(10): 931–937.

[157] Lauritzen, M., Dreier, J. P., Fabricius, M., Hartings, J. A., Graf, R. and Strong, A. J. [2011]. Clinical relevance of cortical spreading depression in neurological disorders: migraine, malignant stroke, subarachnoid and intracranial hemorrhage, and traumatic brain injury, *Journal of Cerebral Blood Flow & Metabolism* **31**(1): 17–35.

[158] Lee, K. B., Hong, B. Y., Kim, J. S., Sul, B., Yoon, S. C., Ji, E.-K., Son, D. B., Hwang, B. Y. and Lim, S. H. [2019]. Which brain lesions produce spasticity? an observational study on 45 stroke patients, *PloS one* **14**(1): e0210038.

[159] Lee-Kubli, C. A. and Calcutt, N. A. [2014]. Altered rate-dependent depression of the spinal h-reflex as an indicator of spinal disinhibition in models of neuropathic pain, *PAIN®* **155**(2): 250–260.

[160] Lee, S., Toda, T., Kiyama, H. and Yamashita, T. [2014]. Weakened rate-dependent depression of hoffmann's reflex and increased motoneuron hyperactivity after motor cortical infarction in mice, *Cell death & disease* **5**(1): e1007–e1007.

[161] Lehmann-Horn, F. [2007]. Motorische systeme, *Physiologie des Menschen*, Springer, pp. 143–183.

[162] Levin, M. F., Kleim, J. A. and Wolf, S. L. [2009]. What do motor "recovery" and "compensation" mean in patients following stroke?, *Neurorehabilitation and neural repair* **23**(4): 313–319.

[163] Li, S. [2017]. Spasticity, motor recovery, and neural plasticity after stroke, *Frontiers in neurology* **8**: 120.

[164] Li, S. and Francisco, G. E. [2015]. New insights into the pathophysiology of post-stroke spasticity, *Frontiers in human neuroscience* **9**: 192.

[165] Liebeskind, D. S., Cotsonis, G. A., Saver, J. L., Lynn, M. J., Cloft, H. J., Chimowitz, M. I. and the Warfarin—Aspirin Symptomatic Intracranial Disease (WASID), I. F. [2011]. Collateral circulation in symptomatic intracranial atherosclerosis, *Journal of Cerebral Blood Flow & Metabolism* **31**(5): 1293–1301.

[166] Liu, F. and McCullough, L. D. [2011]. Middle cerebral artery occlusion model in rodents: methods and potential pitfalls, *Journal of Biomedicine and Biotechnology* **2011**.

[167] Lotze, M., Markert, J., Sauseng, P., Hoppe, J., Plewnia, C. and Gerloff, C. [2006]. The role of multiple contralesional motor areas for complex hand movements after internal capsular lesion, *Journal of Neuroscience* **26**(22): 6096–6102.

[168] Lu, H., Li, Y., Bo, B., Yuan, L., Lu, X., Li, H. and Tong, S. [2017]. Hemodynamic effects of intraoperative anesthetics administration in photothrombotic stroke model: a study using laser speckle imaging, *BMC neuroscience* **18**(1): 1–8.

[169] Lundström, E., Terént, A. and Borg, J. [2008]. Prevalence of disabling spasticity 1 year after first-ever stroke, *European journal of neurology* **15**(6): 533–539.

[170] Macrae, I. M. and Allan, S. M. [2018]. Stroke: the past, present and future, *Brain and neuroscience advances* **2**: 2398212818810689.

[171] Macrae, I. M., Robinson, M. J., Graham, D. I., Reid, J. L. and McCulloch, J. [1993]. Endothelin-1-induced reductions in cerebral blood flow: dose dependency, time course, and neuropathological consequences, *Journal of Cerebral Blood Flow & Metabolism* **13**(2): 276–284.

[172] Malhotra, S., Cousins, E., Ward, A., Day, C., Jones, P., Roffe, C. and Pandyan, A. [2008]. An investigation into the agreement between clinical, biomechanical and neurophysiological measures of spasticity, *Clinical rehabilitation* **22**(12): 1105–1115.

[173] Marcantoni, M., Fuchs, A., Löw, P., Kiehn, O. and Bellardita, C. [2019]. Nimodipine prevents the development of spasticity after spinal cord injury, *bioRxiv* p. 639211.

[174] Marie, P. [1901]. Des foyers lacunaires de desintegration et de differents autres etats cavitaires de cerveau, *Rev Med* **21**: 281–298.

[175] Mathis, A., Mamidanna, P., Cury, K. M., Abe, T., Murthy, V. N., Mathis, M. W. and Bethge, M. [2018]. Deeplabcut: markerless pose estimation of user-defined body parts with deep learning, *Nature neuroscience* **21**(9): 1281–1289.

[176] Mazzocchio, R. and Rossi, A. [1997]. Involvement of spinal recurrent inhibition in spasticity. further insight into the regulation of renshaw cell activity., *Brain: a journal of neurology* **120**(6): 991–1003.

[177] McCann, S. K. and Lawrence, C. B. [2020]. Comorbidity and age in the modelling of stroke: are we still failing to consider the characteristics of stroke patients?, *BMJ Open Science* **4**(1).

[178] McGuire, J. R. and Harvey, R. L. [1999]. The prevention and management of complications after stroke, *Physical medicine and rehabilitation clinics of North America* **10**(4): 857–874.

[179] Mekhael, W., Begum, S., Samaddar, S., Hassan, M., Toruno, P., Ahmed, M., Gorin, A., Maisano, M., Ayad, M. and Ahmed, Z. [2019]. Repeated anodal trans-spinal direct current stimulation results in long-term reduction of spasticity in mice with spinal cord injury, *The Journal of physiology* **597**(8): 2201–2223.

[180] Meseguer-Henarejos, A.-B., Sanchez-Meca, J., Lopez-Pina, J.-A. and Carles-Hernandez, R. [2017]. Inter-and intra-rater reliability of the modified ashworth scale: a systematic review and meta-analysis., *European journal of physical and rehabilitation medicine* **54**(4): 576–590.

[181] Messina, C. and Cotrufo, R. [1976]. Different excitability of type 1 and type 2 alpha-motoneurones: The recruitment curve of h-and m-responses in slow and fast muscles of rabbits, *Journal of the neurological sciences* **28**(1): 57–63.

[182] Minassian, A., Radmilovic, M. D., Vogel, S., Diedenhofen, M., Nelles, M., Stoeber, M., Wiedermann, D. and Hoehn, M. [2019]. Cortical tissue loss and major structural reorganization as result of distal middle cerebral artery occlusion in the chronic phase of nude mice, *Scientific reports* **9**(1): 1–11.

[183] Mohajerani, M. H., Aminoltejari, K. and Murphy, T. H. [2011]. Targeted mini-strokes produce changes in interhemispheric sensory signal processing that are indicative of disinhibition within minutes, *Proceedings of the National Academy of Sciences* **108**(22): E183–E191.

[184] Mozaffarian, D., Benjamin, E. J., Go, A. S., Arnett, D. K., Blaha, M. J., Cushman, M., Das, S. R., De Ferranti, S., Després, J.-P., Fullerton, H. J. et al. [2016]. Heart disease and stroke statistics—2016 update: a report from the american heart association, *circulation* **133**(4): e38–e360.

[185] Mukherjee, A. and Chakravarty, A. [2010]. Spasticity mechanisms–for the clinician, *Frontiers in neurology* **1**.

[186] Mülhardt, C., Fischer, M., Gass, P., Simon-Chazottes, D., Guenet, J.-L., Kuhse, J., Betz, H. and Becker, C.-M. [1994]. The spastic mouse: aberrant splicing of glycine receptor β subunit mrna caused by intronic insertion of ll element, *Neuron* **13**(4): 1003–1015.

[187] Nassi, J. J., Cepko, C. L., Born, R. T. and Beier, K. T. [2015]. Neuroanatomy goes viral!, *Frontiers in neuroanatomy* **9**: 80.

[188] Newman, T., Woolley, S., Hughes, P., Sibson, N., Anthony, D. and Perry, V. [2001]. T-cell-and macrophage-mediated axon damage in the absence of a cns-specific immune response: involvement of metalloproteinases, *Brain* **124**(11): 2203–2214.

[189] Nikolova, S., Moyanova, S., Hughes, S., Bellyou-Camilleri, M., Lee, T.-Y. and Bartha, R. [2009]. Endothelin-1 induced mcao: dose dependency of cerebral blood flow, *Journal of neuroscience methods* **179**(1): 22–28.

[190] Nowak, D. A., Grefkes, C., Ameli, M. and Fink, G. R. [2009]. Interhemispheric competition after stroke: brain stimulation to enhance recovery of function of the affected hand, *Neurorehabilitation and neural repair* **23**(7): 641–656.

[191] Orset, C., Macrez, R., Young, A. R., Panthou, D., Angles-Cano, E., Maubert, E., Agin, V. and Vivien, D. [2007]. Mouse model of in situ thromboembolic stroke and reperfusion, *Stroke* **38**(10): 2771–2778.

[192] Ovbiagele, B., Goldstein, L. B., Higashida, R. T., Howard, V. J., Johnston, S. C., Khavjou, O. A., Lackland, D. T., Lichtman, J. H., Mohl, S., Sacco, R. L. et al. [2013]. Forecasting the future of stroke in the united states: a policy statement from the american heart association and american stroke association, *Stroke* **44**(8): 2361–2375.

[193] Ozcakir, S. and Sivrioglu, K. [2007]. Botulinum toxin in poststroke spasticity, *Clinical medicine & research* **5**(2): 132–138.

[194] Pallast, N., Diedenhofen, M., Blaschke, S., Wieters, F., Wiedermann, D., Hoehn, M., Fink, G. R. and Aswendt, M. [2019]. Processing pipeline for atlas-based imaging data analysis of structural and functional mouse brain mri (aidamri), *Frontiers in neuroinformatics* **13**: 42.

[195] Pallast, N., Wieters, F., Fink, G. R. and Aswendt, M. [2019]. Atlas-based imaging data analysis tool for quantitative mouse brain histology (aidahisto), *Journal of neuroscience methods* **326**: 108394.

[196] Pallast, N., Wieters, F., Nill, M., Fink, G. R. and Aswendt, M. [2018]. Cloud-based relational database for multimodal animal data, *Database* **2018**.

[197] Palmieri, R. M., Hoffman, M. A. and Ingersoll, C. D. [2002]. Intersession reliability for h-reflex measurements arising from the soleus, peroneal, and tibialis anterior musculature, *International Journal of Neuroscience* **112**(7): 841–850.

[198] Palmieri, R. M., Ingersoll, C. D. and Hoffman, M. A. [2004]. The hoffmann reflex: methodologic considerations and applications for use in sports medicine and athletic training research, *Journal of athletic training* **39**(3): 268.

[199] Papadopoulos, C. M., Tsai, S.-Y., Cheatwood, J. L., Bollnow, M. R., Kolb, B. E., Schwab, M. E. and Kartje, G. L. [2006]. Dendritic plasticity in the adult rat following middle cerebral artery occlusion and nogo-a neutralization, *Cerebral Cortex* **16**(4): 529–536.

[200] Patejdl, R. and Zettl, U. K. [2017]. Spasticity in multiple sclerosis: contribution of inflammation, autoimmune mediated neuronal damage and therapeutic interventions, *Autoimmunity reviews* **16**(9): 925–936.

[201] Paxinos, G., Franklin, K. and Franklin, K. [2001]. The mouse brain in stereotaxic coordinates. academic, *San Diego* .

[202] Pearson, K., Acharya, H. and Fouad, K. [2005]. A new electrode configuration for recording electromyographic activity in behaving mice, *Journal of neuroscience methods* **148**(1): 36–42.

[203] Pereira, T. D., Shaevitz, J. W. and Murthy, M. [2020]. Quantifying behavior to understand the brain, *Nature neuroscience* pp. 1–13.

[204] Picelli, A., Tamburin, S., Gajofatto, F., Zanette, G., Praitano, M., Saltuari, L., Corradini, C. and Smania, N. [2014]. Association between severe upper limb spasticity and brain lesion location in stroke patients, *BioMed research international* **2014**.

[205] Preisig, D. F., Kulic, L., Krüger, M., Wirth, F., McAfoose, J., Späni, C., Gantenbein, P., Derungs, R., Nitsch, R. M. and Welt, T. [2016]. High-speed video gait analysis reveals early and characteristic locomotor phenotypes in mouse models of neurodegenerative movement disorders, *Behavioural brain research* **311**: 340–353.

[206] Pryce, G., Ahmed, Z., Hankey, D. J., Jackson, S. J., Croxford, J. L., Pocock, J. M., Ledent, C., Petzold, A., Thompson, A. J., Giovannoni, G. et al. [2003]. Cannabinoids inhibit neurodegeneration in models of multiple sclerosis, *Brain* **126**(10): 2191–2202.

[207] Pryce, G., Cabranes, A., Fernández-Ruiz, J., Bisogno, T., Di Marzo, V., Long, J., Cravatt, B., Giovannoni, G. and Baker, D. [2013]. Control of experimental spasticity by targeting the degradation of endocannabinoids using selective fatty acid amide hydrolase inhibitors, *Multiple Sclerosis Journal* **19**(14): 1896–1904.

[208] Puig, J., Blasco, G., Daunis-I-Estadella, J., Thomalla, G., Castellanos, M., Figueras, J., Remollo, S., van Eendenburg, C., Sánchez-González, J., Serena, J. et al. [2013]. Decreased corticospinal tract fractional anisotropy predicts long-term motor outcome after stroke, *Stroke* **44**(7): 2016–2018.

[209] Pundik, S., Falchook, A. D., McCabe, J., Litinas, K. and Daly, J. J. [2014]. Functional brain correlates of upper limb spasticity and its mitigation following rehabilitation in chronic stroke survivors, *Stroke research and treatment* **2014**.

[210] Reep, R. and Corwin, J. [1999]. Topographic organization of the striatal and thalamic connections of rat medial agranular cortex, *Brain research* **841**(1-2): 43–52.

[211] Reiner, A., Veenman, C. L., Medina, L., Jiao, Y., Del Mar, N. and Honig, M. G. [2000]. Pathway tracing using biotinylated dextran amines, *Journal of neuroscience methods* **103**(1): 23–37.

[212] Ren, H., Zhou, R.-L. and Zhou, C.-T. [2012]. Establishment of h reflex model in mice with minimal insult and measurement of nerve conduction velocity, *Sheng li xue bao:[Acta physiologica Sinica]* **64**(4): 469–474.

[213] Renaud, L., Picher-Martel, V., Codron, P. and Julien, J.-P. [2019]. Key role of ubqln2 in pathogenesis of amyotrophic lateral sclerosis and frontotemporal dementia, *Acta neuropathologica communications* **7**(1): 1–11.

[214] Robinson, A. P., Harp, C. T., Noronha, A. and Miller, S. D. [2014]. The experimental autoimmune encephalomyelitis (eae) model of ms: utility for understanding disease pathophysiology and treatment, *Handbook of clinical neurology* **122**: 173–189.

[215] Roome, R. B. and Vanderluit, J. L. [2015]. Paw-dragging: a novel, sensitive analysis of the mouse cylinder test, *Journal of visualized experiments: JoVE* (98).

[216] Rosenblum, W. I. and El-Sabban, F. [1977]. Platelet aggregation in the cerebral microcirculation: effect of aspirin and other agents., *Circulation Research* **40**(3): 320–328.

[217] Rosenzweig, E. S., Brock, J. H., Culbertson, M. D., Lu, P., Moseanko, R., Edgerton, V. R., Havton, L. A. and Tuszynski, M. H. [2009]. Extensive spinal decussation and bilateral termination of cervical corticospinal projections in rhesus monkeys, *Journal of Comparative Neurology* **513**(2): 151–163.

[218] Rosenzweig, S. and Carmichael, S. T. [2015]. The axon–glia unit in white matter stroke: Mechanisms of damage and recovery, *Brain research* **1623**: 123–134.

[219] Rothermel, M., Brunert, D., Zabawa, C., Díaz-Quesada, M. and Wachowiak, M. [2013]. Transgene expression in target-defined neuron populations mediated by retrograde infection with adeno-associated viral vectors, *Journal of Neuroscience* **33**(38): 15195–15206.

[220] Sahrmann, S. A. and Norton, B. J. [1977]. The relationship of voluntary movement of spasticity in the upper motor neuron syndrome, *Annals of Neurology: Official Journal of the American Neurological Association and the Child Neurology Society* **2**(6): 460–465.

[221] Salga, M., Tseng, H.-W., Alexander, K. A., Jose, B., Vaquette, C., Debaud, C., Gatin, L., Genêt, F. and Levesque, J.-P. [2019]. Blocking neuromuscular junctions with botulinum toxin a injection enhances neurological heterotopic ossification development after spinal cord injury in mice, *Annals of physical and rehabilitation medicine* **62**(3): 189–192.

[222] Schaar, K. L., Brenneman, M. M. and Savitz, S. I. [2010]. Functional assessments in the rodent stroke model, *Experimental & translational stroke medicine* **2**(1): 1–11.

[223] Schaechter, J. D., Fricker, Z. P., Perdue, K. L., Helmer, K. G., Vangel, M. G., Greve, D. N. and Makris, N. [2009]. Microstructural status of ipsilesional and contralesional corticospinal tract correlates with motor skill in chronic stroke patients, *Human brain mapping* **30**(11): 3461–3474.

[224] Schieppati, M. [1987]. The hoffmann reflex: a means of assessing spinal reflex excitability and its descending control in man, *Progress in neurobiology* **28**(4): 345–376.

[225] Schmitt, A., Brook, G., Buss, A., Nacimiento, W., Noth, J. and Kreutzberg, G. [1998]. Dynamics of microglial activation in the spinal cord after cerebral infarction are revealed by expression of mhc class ii antigen, *Neuropathology and applied neurobiology* **24**(3): 167—176.

[226] Schulz, A., Walther, C., Morrison, H. and Bauer, R. [2014]. In vivo electrophysiological measurements on mouse sciatic nerves, *Journal of visualized experiments: JoVE* (86).

[227] Schulz, R., Braass, H., Liuzzi, G., Hoerniss, V., Lechner, P., Gerloff, C. and Hummel, F. C. [2015]. White matter integrity of premotor–motor connections is associated with motor output in chronic stroke patients, *NeuroImage: Clinical* **7**: 82–86.

[228] Sehgal, N. and McGuire, J. R. [1998]. Beyond ashworth: Electrophysiologic quantification of spasticity, *Physical medicine and rehabilitation clinics of North America* **9**(4): 949–979.

[229] Sheean, D. G. [2009]. Is spasticity painful?, *European journal of neurology* **16**(2): 157–158.

[230] Shelton, F. d. N., Volpe, B. T. and Reding, M. [2001]. Motor impairment as a predictor of functional recovery and guide to rehabilitation treatment after stroke, *Neurorehabilitation and neural repair* **15**(3): 229–237.

[231] Sherman, S., Koshland, G. and Laguna, J. [2000]. Hyper-reflexia without spasticity after unilateral infarct of the medullary pyramid, *Journal of the neurological sciences* **175**(2): 145–155.

[232] Shimizu, T., Hosaki, A., Hino, T., Sato, M., Komori, T., Hirai, S. and Rossini, P. M. [2002]. Motor cortical disinhibition in the unaffected hemisphere after unilateral cortical stroke, *Brain* **125**(8): 1896–1907.

[233] Shindo, M., Harayama, H., Kondo, K., Yanagisawa, N. and Tanaka, R. [1984]. Changes in reciprocal ia inhibition during voluntary contraction in man, *Experimental Brain Research* **53**(2): 400–408.

[234] Siegel, C. S., Fink, K. L., Strittmatter, S. M. and Cafferty, W. B. [2015]. Plasticity of intact rubral projections mediates spontaneous recovery of function after corticospinal tract injury, *Journal of Neuroscience* **35**(4): 1443–1457.

[235] Simpson, D. M., Patel, A. T., Alfaro, A., Ayyoub, Z., Charles, D., Dashtipour, K., Esquenazi, A., Graham, G. D., McGuire, J. R. and Odderson, I. [2017]. Onabotulinumtoxina injection for poststroke upper-limb spasticity: Guidance for early injectors from a delphi panel process, *PMR* **9**(2): 136–148.

[236] Smania, N., Paolucci, S., Tinazzi, M., Borghero, A., Manganotti, P., Fiaschi, A., Moretto, G., Bovi, P. and Gambarin, M. [2007]. Active finger extension: a simple movement predicting recovery of arm function in patients with acute stroke, *Stroke* **38**(3): 1088–1090.

[237] Sommerfeld, D. K., Eek, E. U.-B., Svensson, A.-K., Holmqvist, L. W. and Von Arbin, M. H. [2004]. Spasticity after stroke: its occurrence and association with motor impairments and activity limitations, *stroke* **35**(1): 134–139.

[238] Souza-Rodrigues, R., Costa, A., Lima, R., Dos Santos, C., Picanco-Diniz, C. and Gomes-Leal, W. [2008]. Inflammatory response and white matter damage after microinjections of endothelin-1 into the rat striatum, *Brain research* **1200**: 78–88.

[239] Sozmen, E. G., DiTullio, D. J., Rosenzweig, S., Hinman, J. D., Bridges, S. P., Marin, M. A., Kawaguchi, R., Coppola, G. and Carmichael, S. T. [2019]. White matter stroke induces a unique oligo-astrocyte niche that inhibits recovery, *Journal of Neuroscience* **39**(47): 9343–9359.

[240] Sozmen, E. G., Hinman, J. D. and Carmichael, S. T. [2012]. Models that matter: white matter stroke models, *Neurotherapeutics* **9**(2): 349–358.

[241] Sozmen, E. G., Kolekar, A., Havton, L. A. and Carmichael, S. T. [2009]. A white matter stroke model in the mouse: axonal damage, progenitor responses and mri correlates, *Journal of neuroscience methods* **180**(2): 261–272.

[242] Spalletti, C., Alia, C., Lai, S., Panarese, A., Conti, S., Micera, S. and Caleo, M. [2017]. Combining robotic training and inactivation of the healthy hemisphere restores pre-stroke motor patterns in mice, *Elife* **6**: e28662.

[243] Starkey, M. L., Barritt, A. W., Yip, P. K., Davies, M., Hamers, F. P., McMahon, S. B. and Bradbury, E. J. [2005]. Assessing behavioural function following a pyramidotomy lesion of the corticospinal tract in adult mice, *Experimental neurology* **195**(2): 524–539.

[244] Stevens, E., Emmett, E., Wang, Y., McKevitt, C. and Wolfe, C. [2017]. The burden of stroke in europe, *London: Stroke Alliance for Europe* pp. 30–125.

[245] Steward, O., Zheng, B., Ho, C., Anderson, K. and Tessier-Lavigne, M. [2004]. The dorsolateral corticospinal tract in mice: an alternative route for corticospinal input to caudal segments following dorsal column lesions, *Journal of Comparative Neurology* **472**(4): 463–477.

[246] Sugimori, H., Yao, H., Ooboshi, H., Ibayashi, S. and Iida, M. [2004]. Krypton laser-induced photothrombotic distal middle cerebral artery occlusion without craniectomy in mice, *Brain Research Protocols* **13**(3): 189–196.

[247] Sunnerhagen, K. S. [2016]. Predictors of spasticity after stroke, *Current physical medicine and rehabilitation reports* **4**(3): 182–185.

[248] Svensson, J., Borg, S. and Nilsson, P. [2014]. Costs and quality of life in multiple sclerosis patients with spasticity, *Acta neurologica Scandinavica* **129**(1): 13–20.

[249] Takeuchi, N. and Izumi, S.-I. [2012]. Noninvasive brain stimulation for motor recovery after stroke: mechanisms and future views, *Stroke research and treatment* **2012**.

[250] Takeuchi, N., Oouchida, Y. and Izumi, S.-I. [2012]. Motor control and neural plasticity through interhemispheric interactions, *Neural plasticity* **2012**.

[251] Tan, A. M., Chakrabarty, S., Kimura, H. and Martin, J. H. [2012a]. Selective corticospinal tract injury in the rat induces primary afferent fiber sprouting in the spinal cord and hyperreflexia, *Journal of Neuroscience* **32**(37): 12896–12908.

[252] Tan, A. M., Chakrabarty, S., Kimura, H. and Martin, J. H. [2012b]. Selective corticospinal tract injury in the rat induces primary afferent fiber sprouting in the spinal cord and hyperreflexia, *Journal of Neuroscience* **32**(37): 12896–12908.

[253] Terashima, T. [1995]. Anatomy, development and lesion-induced plasticity of rodent corticospinal tract, *Neuroscience research* **22**(2): 139–161.

[254] Tétrault, S., Chever, O., Sik, A. and Amzica, F. [2008]. Opening of the blood–brain barrier during isoflurane anaesthesia, *European Journal of Neuroscience* **28**(7): 1330–1341.

[255] Thrift, A. G., Dewey, H. M., Macdonell, R. A., McNeil, J. J. and Donnan, G. A. [2001]. Incidence of the major stroke subtypes, *Stroke* **32**(8): 1732–1738.

[256] Thrift, A. G., Thayabaranathan, T., Howard, G., Howard, V. J., Rothwell, P. M., Feigin, V. L., Norrving, B., Donnan, G. A. and Cadilhac, D. A. [2017]. Global stroke statistics, *International Journal of Stroke* **12**(1): 13–32. PMID: 27794138.

[257] Toda, T., Ishida, K., Kiyama, H., Yamashita, T. and Lee, S. [2014]. Down-regulation of kcc2 expression and phosphorylation in motoneurons, and increases the number of in primary afferent projections to motoneurons in mice with post-stroke spasticity, *PloS one* **9**(12): e114328.

[258] Tohyama, T., Kinoshita, M., Kobayashi, K., Isa, K., Watanabe, D., Kobayashi, K., Liu, M. and Isa, T. [2017]. Contribution of propriospinal neurons to recovery of hand dexterity after corticospinal tract lesions in monkeys, *Proceedings of the National Academy of Sciences* **114**(3): 604–609.

[259] Trompetto, C., Marinelli, L., Mori, L., Pelosin, E., Currà, A., Molfetta, L. and Abbruzzese, G. [2014]. Pathophysiology of spasticity: implications for neurorehabilitation, *BioMed research international* **2014**.

[260] Tysseling, V. M., Janes, L., Imhoff, R., Quinlan, K. A., Lookabaugh, B., Ramalingam, S., Heckman, C. and Tresch, M. C. [2013]. Design and evaluation of a chronic emg multichannel detection system for long-term recordings of hindlimb muscles in behaving mice, *Journal of Electromyography and Kinesiology* **23**(3): 531–539.

[261] Uylings, H. B., Groenewegen, H. J. and Kolb, B. [2003]. Do rats have a prefrontal cortex?, *Behavioural brain research* **146**(1-2): 3–17.

[262] Venkatasubramanian, C., Kleinman, J. T., Fischbein, N. J., Olivot, J.-M., Gean, A. D., Eyngorn, I., Snider, R. W., Mlynash, M. and Wijman, C. A. [2013]. Natural history and prognostic value of corticospinal tract wallerian degeneration in intracerebral hemorrhage, *Journal of the American Heart Association* **2**(4): e000090.

[263] Voerman, G. E., Gregorič, M. and Hermens, H. J. [2005]. Neurophysiological methods for the assessment of spasticity: the hoffmann reflex, the tendon reflex, and the stretch reflex, *Disability and rehabilitation* **27**(1-2): 33–68.

[264] Vollert, J., Schenker, E., Macleod, M., Bespalov, A., Wuerbel, H., Michel, M., Dirnagl, U., Potschka, H., Waldron, A.-M., Wever, K., Steckler, T., van de Casteele, T., Altevogt, B., Sil, A. and Rice, A. S. C. [2020]. Systematic review of guidelines for internal validity in the design, conduct and analysis of preclinical biomedical experiments involving laboratory animals, *BMJ Open Science* **4**(1).

[265] Wahl, A.-S. and Schwab, M. E. [2014]. Finding an optimal rehabilitation paradigm after stroke: enhancing fiber growth and training of the brain at the right moment, *Frontiers in human neuroscience* **8**: 381.

[266] Wahlgren, N., Ahmed, N., Dávalos, A., Ford, G. A., Grond, M., Hacke, W., Hennerici, M. G., Kaste, M., Kuelkens, S., Larrue, V. et al. [2007]. Thrombolysis with alteplase for acute ischaemic stroke in the safe implementation of thrombolysis in stroke-monitoring study (sits-most): an observational study, *The Lancet* **369**(9558): 275–282.

[267] Wang, Q., Ding, S.-L., Li, Y., Royall, J., Feng, D., Lesnar, P., Graddis, N., Naeemi, M., Facer, B., Ho, A. et al. [2020]. The allen mouse brain common coordinate framework: a 3d reference atlas, *Cell* **181**(4): 936–953.

[268] Wang, Y., Liu, G., Hong, D., Chen, F., Ji, X. and Cao, G. [2016]. White matter injury in ischemic stroke, *Progress in neurobiology* **141**: 45–60.

[269] Ward, A. B. [2012]. A literature review of the pathophysiology and onset of post-stroke spasticity, *European journal of neurology* **19**(1): 21–27.

[270] Watson, B. D., Dietrich, W. D., Prado, R. and Green, B. A. [1988]. Photochemically induced vascular thrombosis (photothrombosis): Central nervous system consequences and clinical possibilities, *Neural Development and Regeneration*, Springer, pp. 507–524.

[271] Weiller, C., Ramsay, S., Wise, R., Friston, K. and Frackowiak, R. [1993]. Individual patterns of functional reorganization in the human cerebral cortex after capsular infarction., *Annals of neurology* **33**(2): 181–189.

[272] Welniarz, Q., Dusart, I. and Roze, E. [2017]. The corticospinal tract: Evolution, development, and human disorders, *Developmental neurobiology* **77**(7): 810–829.

[273] Wester, P., Watson, B. D., Prado, R. and Dietrich, W. D. [1995]. A photothrombotic 'ring'model of rat stroke-in-evolution displaying putative penumbral inversion, *Stroke* **26**(3): 444–450.

[274] Wiessner, C., Bareyre, F. M., Allegrini, P. R., Mir, A. K., Frentzel, S., Zurini, M., Schnell, L., Oertle, T. and Schwab, M. E. [2003]. Anti—nogo-a antibody infusion 24 hours after experimental stroke improved behavioral outcome and corticospinal plasticity in normotensive and spontaneously hypertensive rats, *Journal of Cerebral Blood Flow & Metabolism* **23**(2): 154–165.

[275] Wieters, F., Lucas, C. W., Gruhn, M., Büschges, A., Fink, G. R. and Aswendt, M. [2020]. Introduction to spasticity and related mouse models, *Experimental Neurology* p. 113491.

[276] Wils, H., Kleinberger, G., Janssens, J., Pereson, S., Joris, G., Cuijt, I., Smits, V., Ceuterick-de Groote, C., Van Broeckhoven, C. and Kumar-Singh, S. [2010]. Tdp-43 transgenic mice develop spastic paralysis and neuronal inclusions characteristic of

als and frontotemporal lobar degeneration, *Proceedings of the National Academy of Sciences* **107**(8): 3858–3863.

[277] Wissel, J., Manack, A. and Brainin, M. [2013]. Toward an epidemiology of poststroke spasticity, *Neurology* **80**(3 Supplement 2): S13–S19.

[278] Wright, J. and Rang, A. [1990]. The spastic mouse: And the search for an animal model of spasticity in human beings, *Clinical Orthopaedics and Related Research®* **253**: 12–19.

[279] Xerri, C., Zennou-Azogui, Y., Sadlaoud, K. and Sauvajon, D. [2014]. Interplay between intra-and interhemispheric remodeling of neural networks as a substrate of functional recovery after stroke: adaptive versus maladaptive reorganization, *Neuroscience* **283**: 178–201.

[280] Xiong, L., Zheng, Y., Wu, M., Hou, L., Zhu, Z., Zhang, X. and Lu, Z. [2003]. Preconditioning with isoflurane produces dose-dependent neuroprotection via activation of adenosine triphosphate-regulated potassium channels after focal cerebral ischemia in rats, *Anesthesia & Analgesia* **96**(1): 233–237.

[281] Yamanaka, K., Miller, T. M., McAlonis-Downes, M., Chun, S. J. and Cleveland, D. W. [2006]. Progressive spinal axonal degeneration and slowness in als2-deficient mice, *Annals of neurology* **60**(1): 95–104.

[282] Yang, Y., Shi, Y.-Z., Zhang, N., Wang, S., Ungvari, G. S., Ng, C. H., Wang, Y.-L., Zhao, X.-Q., Wang, Y.-J., Wang, C.-X. and Xiang, Y.-T. [2016]. The disability rate of 5-year post-stroke and its correlation factors: A national survey in china, *PLOS ONE* **11**: 1–9.

[283] Yeo, S. S. and Jang, S. H. [2011]. Medullary decussation of the lateral corticospinal tract, *European neurology* **66**(5): 296.

[284] Yoshizaki, S., Yokota, K., Kubota, K., Saito, T., Tanaka, M., Konno, D.-j., Maeda, T., Matsumoto, Y., Nakashima, Y. and Okada, S. [2020]. The beneficial aspects of spasticity in relation to ambulatory ability in mice with spinal cord injury, *Spinal cord* **58**(5): 537–543.

[285] Yu, C.-L., Zhou, H., Chai, A.-P., Yang, Y.-X., Mao, R.-R. and Xu, L. [2015]. Whole-scale neurobehavioral assessments of photothrombotic ischemia in freely moving mice, *Journal of neuroscience methods* **239**: 100–107.

[286] Zeiger, W. A., Marosi, M., Saggi, S., Noble, N., Samad, I. and Portera-Cailliau, C. [2020]. Plasticity after cortical stroke involves potentiating responses of pre-existing circuits but not functional remapping to new circuits, *bioRxiv* .

[287] Zhang, J., Zhang, Y., Xing, S., Liang, Z. and Zeng, J. [2012]. Secondary neurodegeneration in remote regions after focal cerebral infarction, *Stroke* **43**(6): 1700–1705.

[288] Ziv, I., Blackburn, N., Rang, M. and Koreska, J. [1984]. Muscle growth in normal and spastic mice, *Developmental Medicine & Child Neurology* **26**(1): 94–99.

13 Erklärung

Ich versichere, dass ich die von mir vorgelegte Dissertation selbstständig angefertigt, die benutzten Quellen und Hilfsmittel vollständig angegeben und die Stellen der Arbeit - einschließlich Tabellen, Karten und Abbildungen -, die anderen Werken im Wortlaut oder dem Sinn nach entnommen sind, in jedem Einzelfall als Entlehnung kenntlich gemacht habe; dass diese Dissertation noch keiner anderen Fakultät oder Universität zur Prüfung vorgelegen hat; dass sie - abgesehen von unten angegebenen Teilpublikationen - noch nicht veröffentlicht worden ist sowie, dass ich eine solche Veröffentlichung vor Abschluss des Promotionsverfahrens nicht vornehmen werde. Die Bestimmungen dieser Promotionsordnung sind mir bekannt. Die von mir vorgelegte Dissertation ist von Dr. rer. nat. Markus Aswendt betreut worden.
Folgende Studien wurden bereits publiziert:

1. Alawbathani S., Batool M., Fleckhaus J., Hamad S., Hassenrück F., Hou Y., Li X., Salmanton-Garcia J., Ullah S., **Wieters F.**, Michel M.C., "A teaching tool about the fickle *p* value and other statistical principles based on real-life data", *Naunyn-Schmiedeberg´s Archives of Pharmacology* (2021)

2. **Wieters F.** & Aswendt M. "Structural integrity and remodeling underlying functional recovery after stroke", *Neural Regeneration Research* (2020)

3. **Wieters F.**, Weiss Lucas C., Gruhn M., Büschges A., Fink G.R., Aswendt M., "Introduction into spasticity and related mouse models", *Exp. Neurology* (2020)

4. Pallast N., **Wieters F.**, Nill M., Fink G.R., Aswendt M. "Graph theoretical quantification of white matter reorganization after cortical stroke in mice", *Neuroimage* (2020)

5. Aswendt M., Pallast N., **Wieters F.**, Baues M., Hoehn M., Fink G.R., "Lesion Size- and Location-Dependent Recruitment of Contralesional Thalamus and Motor Cortex Facilitates Recovery after Stroke in Mice", *Translational Stroke Research* (2020)

6. Pallast N., **Wieters F.**, Fink G.R., Aswendt M., "Atlas-based imaging data analysis tool for quantitative mouse brain histology (AIDAhisto)", *Journal of Neuroscience Methods* (2019)

7. Pallast N., Diedenhofen M., Blaschke S., **Wieters F.**, Wiedermann D., Hoehn M., Fink G.R., Aswendt M., "Processing Pipeline for Atlas-Based Imaging Data Analysis of Structural and Functional Mouse Brain MRI (AIDAmri)", *Frontiers in Neuroinformatics* (2019)

8. Pallast N., **Wieters F.**, Nill M., Fink G.R., Aswendt M., "Cloud-based relational database for multimodal animal data", *The Journal of Biological Database and Curation* (2018)

9. Müller J., Greiner F.W.J., Zeuner M., Brotzmann V., Schafermann J. **Wieters F.**, Widera D., Sudhoff H.H., Kaltschmidt B., Kaltschmidt C., "1,8-Cineole potentiates IRF3-mediated antiviral response in human stem cells and in an ex vivo model of rhinosinusitis", *Clinical Science* (2016)

Derzeit wurden folgende Studien eingereicht bzw. befinden sich in der Überprüfung:

1. **Wieters F.*** & Gruhn M.*, Büschges A., Fink G.R., Aswendt M., "Terminal Hoffmann-Reflex Measurement after Stroke in Mice", (Jove, Eingereicht, 2021)

2. Aswendt M., Wilhelmsson U., **Wieters F.**, Stokowska A., Schmitt F.J., Pallast N., Pablo Y., Mohammed L., Hoehn M., Pekna M., Pekny M., "Reactive astrocytes prevent maladaptive plasticity and facilitate recovery after ischemic stroke" (Molecular Neurodegeneration, In Überprüfung, 2021)

3. Green C., Sadler R., Dzikowski L., Aswendt M., Gomez de Agüero M., Diedenhofen M, **Wieters F.**, Wiedermann D., Liesz A., Hoehn A., "The gut microbiota is required for physiological brain network connectivity" (Nature Science, In Revision, 2021)

Ich versichere, dass ich alle Angaben wahrheitsgemäß nach bestem Wissen und Gewissen gemacht habe und verpflichte mich, jedmögliche, die obigen Angaben betreffenden Veränderungen, dem Promotionsausschuss unverzüglich mitzuteilen.

Köln, den 19.10.2021

Frederique Wieters